Bulk nanostructured materials from severe plastic deformation

R.Z. Valiev*, R.K. Islamgaliev, I.V. Alexandrov

Institute of Physics of Advanced Materials, Ufa State Aviation Technical University, 12 K. Marx Street, 450000 Ufa, Russian Federation

Contents

* Corresponding author. Tel.: + 7-3472-2334-22; fax: + 7-3472-2334-22.
  E-mail address: valiev@ippm.rb.ru (R.Z. Valiev).

1. Introduction

In recent years, bulk nanostructured materials (NSM) processed by methods of severe plastic deformation (SPD) have attracted the growing interest of specialists in materials science [1]. This interest is conditioned not only by unique physical and mechanical properties inherent to various nanostructured materials, e.g. processed by gas condensation [2,3] or ball milling with subsequent consolidation [4,5], but also by several advantages of SPD materials as compared to other NSM. In particular, SPD methods resulted in overcoming of a number of difficulties connected with residual porosity in compacted samples, impurities from ball milling, processing of large scale billets and practical application of the given materials. The principle of processing of bulk nanostructured materials using SPD methods is an alternative to the existing methods of nanopowder compacting.

It is well known that heavy deformations, for example, by cold rolling or drawing, can result in significant refinement of microstructure at low temperatures [6–9]. However, the structures formed are usually substructures of a cellular type having boundaries with low angle misorientations. At the same time, the nanostructures formed from SPD are ultra fine-grained structures of a granular type containing mainly high angle grain boundaries.[1] Formation of such nanostructures could be realized by SPD methods providing very large deformations at relatively low temperatures under the high pressures imposed [1,10,11]. Special methods of mechanical deformation were developed and used for realization of this principle. These methods are as follows: severe torsion straining under high pressure, equal channel angular pressing and others. It was shown that using SPD methods one can fabricate bulk nanostructured samples and billets out of different metals and alloys including a number of commercial alloys and intermetallics.

The first developments and investigations of nanostructured materials processed using SPD methods were fulfilled by Valiev and his co-workers more than 10

---

[1] SPD materials have often a mean grain size of about 100–200 nm and a grain interior possesses usually some substructure due to a highly distorted crystal lattice. Moreover, the X-ray analysis demonstrates, as a rule, a crystalline size (coherent domains) of about 50 nm. That is why we consider SPD materials as a kind of bulk nanostructured materials.

years ago [12,13]. Recent years are characterized by a sharp increase of different publications on this subject. In spite of this, the authors believe that the most interesting and important discoveries are still waiting for us and this scientific direction will find its further more active development due to unusual properties of the materials processed. Many of these properties are unique and rather interesting for applied and fundamental investigations. The present review deals with achievements and difficulties relating to development and investigations of nanostructured materials processed by severe plastic deformation. The review is based essentially on the results obtained by the authors themselves or their colleagues in the process of joint investigations with many Russian and foreign scientists. References on these works are given below. The authors thank all our friends and colleagues for nice cooperation, discussions and useful remarks. We express special gratefulness also to our colleagues N.F. Yunusova and N.A. Enikeev taking part in preparation of the present manuscript.

2. Methods of severe plastic deformation and formation of nanostructures

Methods of severe plastic deformation should meet a number of requirements which are to be taken into account while developing them for formation of nanostructures in bulk samples and billets. These requirements are as follows. Firstly, it is important to obtain ultra fine-grained structures with prevailing high-angle grain boundaries since only in this case can a qualitative change in properties of materials occur (Section 4). Secondly, the formation of nanostructures uniform within the whole volume of a sample is necessary for providing stable properties of the processed materials. Thirdly, though samples are exposed to large plastic deformations they should not have any mechanical damage or cracks. Traditional methods of severe plastic deformation, such as rolling, drawing or extrusion cannot meet these requirements. Formation of nanostructures in bulk samples is impossible without application of special mechanical schemes of deformation providing large deformations at relatively low temperatures as well as without determination of optimal regimes of material processing. At present the majority of the obtained results are connected with application of two SPD methods: torsion straining under high pressure [10–23] and others and equal channel angular pressing [10,11,13–15,24–31]. There are known some investigations on formation of nano- and submicrocrystalline structures in various metals and alloys by means of multiple forging [32–39].

The present section is devoted to the questions of realization of the SPD methods mentioned above, their modeling and optimal regimes. Data on evolution of initial microstructure and its transformation to a nanostructured state during severe plastic deformation are also considered here.

2.1. SPD techniques and regimes

Torsion straining under high pressure and equal channel angular (ECA)

pressing are the most well-known methods of providing large plastic deformations (with true strains ≥ 10) and formation of nanostructures. Below, these methods are discussed in detail.

2.1.1. Torsion straining under high pressure

Devices, where severe plastic torsion straining (SPTS) was conducted under high pressure, were first used in [40,41]. Their design is a further development of the Bridgeman anvil type device [42]. In the first work these devices were used for investigation of phase transformations during heavy deformation [40] as well as evolution of structure and changes in temperature of recrystallization after large plastic deformations [17,18]. Successful formation of homogeneous nanostructures with high-angle grain boundaries via severe torsion straining [10,12,43] was a very important step allowing one to consider this procedure as a new method of processing of nanostructured materials.

Let us first consider the mechanical aspects of severe torsion straining.

A method of torsion straining under high pressure can be used for fabrication of disk type samples (Fig. 1(a)). An ingot is held between anvils and strained in torsion under the applied pressure (P) of several GPa. A lower holder rotates and surface friction forces deform the ingot by shear. Due to the specific geometric shape of the sample, the main volume of the material is strained in conditions of quasihydrostatic compression under the applied pressure and the pressure of sample outer layers. As a result, in spite of large strain values, the deformed sample is not destroyed.

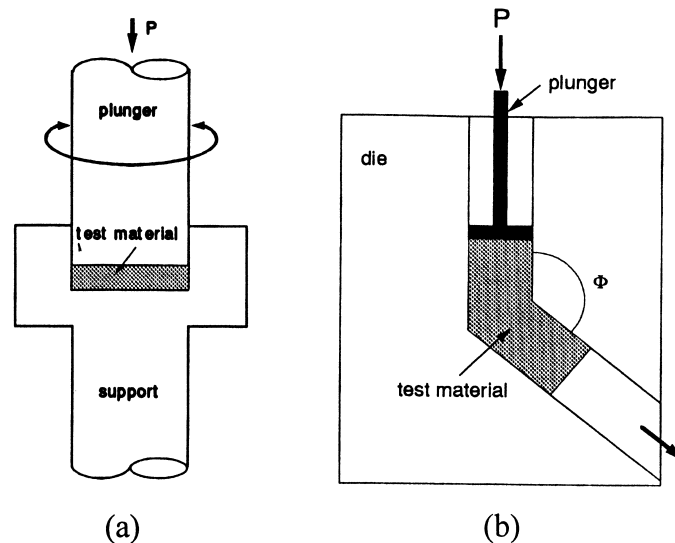Different relationships were used to calculate strain values during torsion

Fig. 1. Principles of SPD methods: (a) torsion under high pressure, (b) ECA pressing.

straining under high pressure. In particular, in [17,41] the true logarithmic strain e was calculated by the equation:

$$e = \ln(\vartheta r / l) \tag{1}$$

where ϑ is the rotation angle in radians, r and l are the radius and thickness of the disk, respectively.

This formula is similar to the Krown equation, which one can use to calculate true strains during tension. However, in the case of tension this formula has a physical background, but in the case of torsion this substantiation is absent. In particular, according to this relationship, the logarithmic torsion strain of samples, 20 mm in diameter and 1 mm thick (five rotations), was 5, that of samples, 10 mm in diameter and 0.2 mm in thick, was 7 at the perimeter of the disk, whereas in the center of all these samples it is equal to zero. At the same time the results of numerous investigations show that after several rotations the deformation by the given mode often results in similar refinement of a microstructure in the center of samples as well and the processed nanostructure is usually homogeneous at the radius of samples. The structural homogeneity of the resulting samples has been confirmed by the uniform distribution of microhardness values measured across each sample.

The following formula is very often used for calculation of the strain value in the considering case as well:

$$\gamma = \frac{2\pi R N}{l}. \tag{2}$$

As known, this formula is used in the case of usual torsion straining for calculation of the shear strain value at the distance R from the axis of the disk type sample. Here, N is the number of rotations, l is the thickness of the sample. To compare the shear strain value during torsion with a strain value during deformation by other schemes, the first value is usually converted to the so-called equivalent strain e_{eq} according to the Mises criterion

$$e_{eq} = \frac{\gamma}{\sqrt{3}} \tag{3}$$

Two remarks are true in respect to Eq. (2) [20]: (1) calculations by this formula have led to the conclusion that the strain value should change linearly from zero in the center of the sample to the maximum value at the ends of its diameter (however, as noted above, this was not confirmed by experiments); (2) during deformation the initial thickness of the sample is reduced by approximately twice under high compression pressure, that is why, the traditional use of l as the initial thickness of the sample underrates the calculated strain values as compared to the true ones.

Both these remarks testify that the strain values calculated by the above equations are only approximately equal to the real strain values. Moreover, the formation of nanostructures during SPD occurs as an effect of both external and

internal stresses (see Section 2.2). At the same time true strain values are not rigidly bounded with values of internal stresses. The formation of a homogeneous structure at the diameter of the sample imposed to severe torsion straining confirms this, though according to Eqs. (1) and (2) a significant refinement of the structure should not occur in the center of the sample. That is why, while studying the evolution of the microstructure during severe torsion straining under high pressure it is more reasonable to consider the number of rotations and not the strain value calculated by the analytical equations. This statement becomes especially important in the case of hard-to-deform and brittle materials where sliding between an anvil and a sample or cracking of the latter is possible. The imposed pressure should be increased to remove these drawbacks. However, these results have additional technological difficulties. There is a necessity to use more strong material for anvils and optimize a die set design.

The samples fabricated by severe torsion straining are usually of a disk shape, from 10 to 20 mm in diameter and 0.2–0.5 mm in thickness. A significant change in the microstructure is observed already after deformation by 1/2 rotation [20], but for formation of the homogeneous nanostructure several rotations are required, as a rule.

Recent investigations also showed that severe torsion straining can be used successfully not only for the refinement of a microstructure but also for the consolidation of powders [21–23,44,45]. It was revealed that during torsion straining at room temperature high pressures equal to several GPa can provide a rather high density close to 100% in the processed disk type nanostructured samples. For fabrication of such samples via severe torsion straining consolidation not only conventional powders but also powders subjected to ball milling can be used.

The SPTS consolidation of nanostructured Ni powder prepared by ball milling [44] can be given as an example. The conducted investigations showed that the density of the fabricated powders is close to 95% of the theoretical density of the bulk coarse-grained Ni. TEM examinations showed the absence of porosity. The mean grain size is very small, it is equal to 17 nm, and, consequently, a large volume fraction of grain boundaries is present. Since grain boundaries have a reduced atomic density the authors assume that the given samples demonstrate a decrease in the theoretical density in the materials with a very small grain size and strong distortions of the crystal lattice (see Section 3). It is also very interesting that the value of microhardness of the Ni samples fabricated by SPTS consolidation is 8.60 ± 0.17 GPa, the highest value of microhardness mentioned in the literature for nanocrystalline Ni.

2.1.2. ECA pressing

The method of ECA pressing realizing deformation of massive billets via pure shear was developed by Segal and co-workers in the beginning of 80s [24,27]. Its goal was to introduce intense plastic strain into materials without changing the cross section area of billets. Due to that, their repeat deformation is possible. In the early 90s the method was further developed and applied as an SPD method

for processing of structures with submicron and nanometric grain sizes [10,13,31]. In these experiments the initial billets with a round or square cross section were cut from rods, from 70 to 100 mm in length. The cross section diameter or its diagonal did not exceed 20 mm, as a rule.

During ECA pressing a billet is multiple pressed through a special die using an ECA facility in which the angle of intersection of two channels is usually 90°. If necessary, in the case of a hard-to-deform material, ECA pressing is conducted at elevated temperatures.
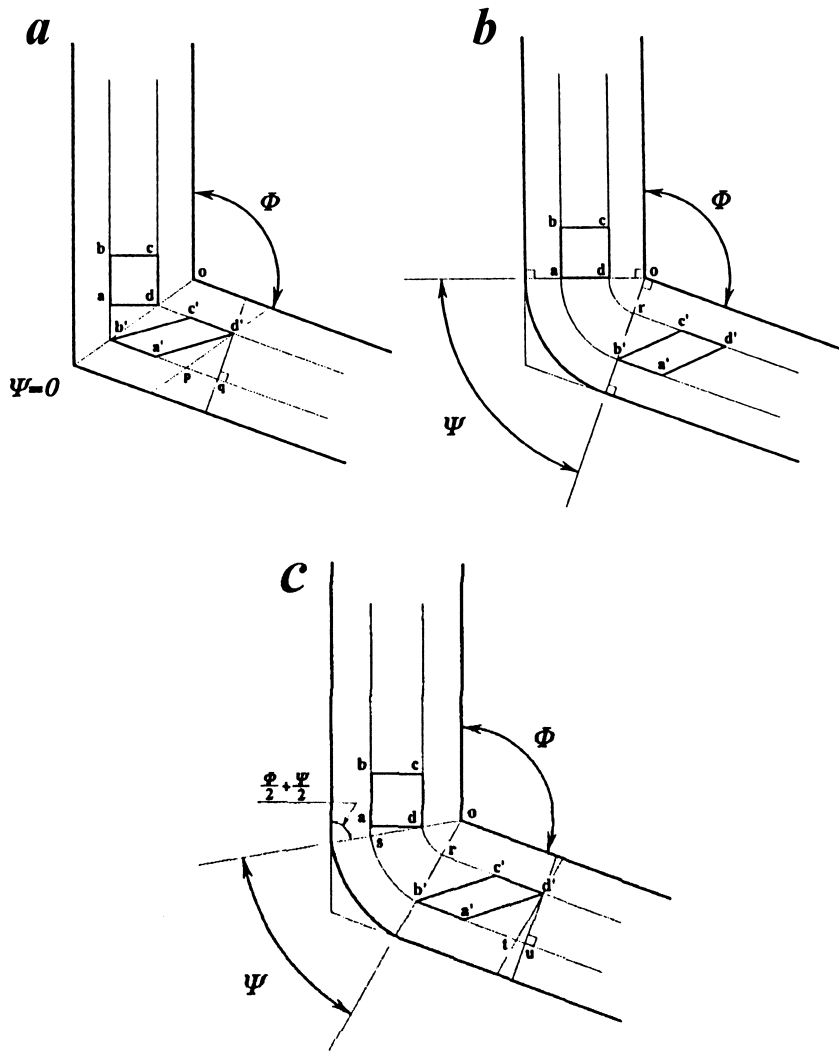
Fig. 2. Principles of ECA pressing: (a) $\psi = 0°$, (b)) $\psi = \pi - \phi$, (c) ψ is between $\psi = 0°$ and $\psi = \pi - \phi$ [25].

When the outer angle $\psi = 0°$, and the inner angle ϕ is arbitrary (see Fig. 2), according to [24] the shear strain value increment at each pass through the channels can be calculated by the equation:

$$\frac{P}{Y} = \Delta\varepsilon_i = 2/\sqrt{3} \times \cot(\phi/2) \tag{4}$$

where P is imposed pressure and Y is the flow stress of the deformed material.

Since during ECA pressing the ingot is pressed through intersecting channels several times, the total strain value is

$$e_N = N \times \Delta e_i, \tag{5}$$

where N is the number of passes.

A more general relationship allowing one to calculate the strain value of the billet during ECA pressing for N passes has the following form [25]:

$$e_N = N\left\{ \frac{2\cot(\phi/2 + \psi/2) + \psi\operatorname{cosec}(\phi/2 + \psi/2)}{\sqrt{3}} \right\} \tag{6}$$

From this relationship it follows that at the frequently used angles, $\phi = 90°$, $\psi = 20°$, each pass corresponds to an additional strain value approximately equal to 1.
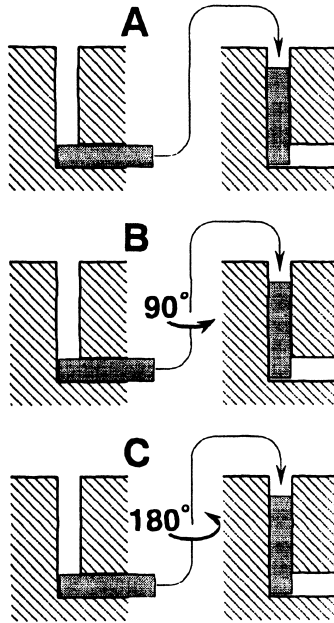

Fig. 3. Versions of ECA pressing: (a) route A, (b) route B, (c) route C [28].

During ECA pressing the direction and number of billet passes through the channels are very important for microstructure refinement. In papers [24,27–30] the following routes of billets were considered (see Fig. 3): orientation of a billet is not changed at each pass (route A); after each pass a billet is rotated around its longitudinal axis through the angle 90° (route B); after each pass a billet is rotated around its longitudinal axis through the angle 180° (route C).

The given routes are distinguished in their shear directions at repeat passes of a billet through intersecting channels. Due to that, during ECA pressing a change in a spherical cell within a billet body occurs.

During ECA pressing in the place of intersection of channels the cell takes a shape of an ellipsoid (Fig. 4(a)). This occurs after the first pass due to pure shear. Further, in the process of route A the following passes result in lengthening of
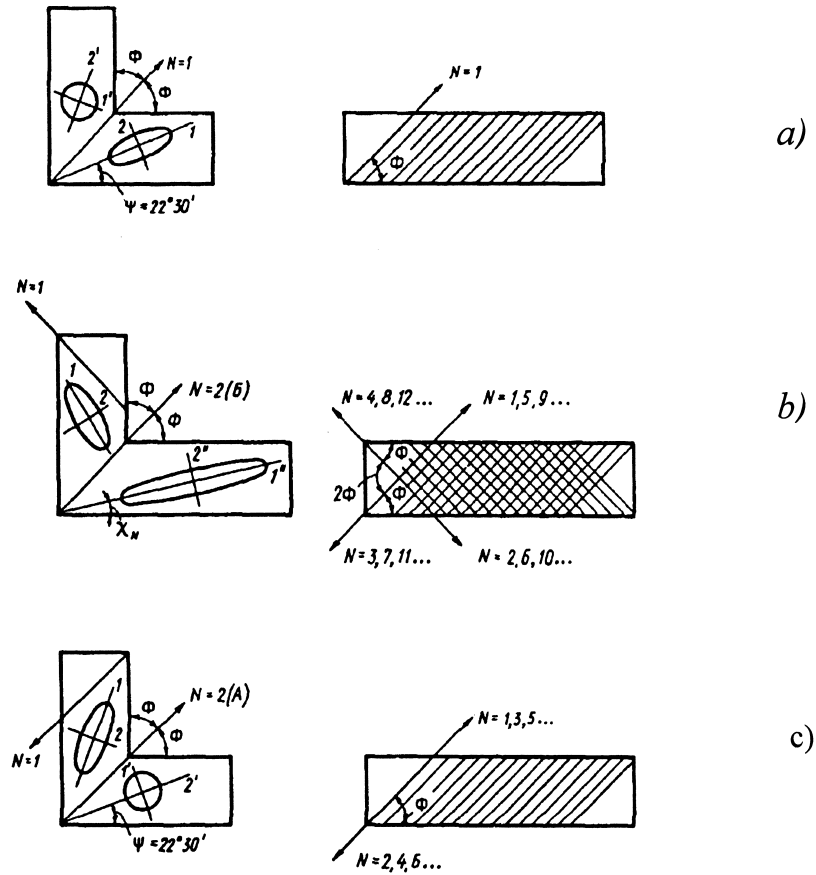

Fig. 4. Regimes of simple shear during ECA pressing: (a) one cycle deforming; (b) route A; (c) route C [27].

axis 1 and the ellipsoid is elongated. At the same time the direction of shear is turned around the axis perpendicular to the longitudinal section of channels through the angle 2ϕ. It is shown in Fig. 4(b).

The repeat pass in the route B leads to a change in the direction of shear and the shear plane is turned through the angle $120°$ (at $2\phi = 90°$) (Fig. 5(b)) [30].

During deformation by route C the repeat pass leads to shear in the same plane but in the opposite direction (Figs. 4c and 5c). The cell again takes a spherical shape.

The application of all three routes results in an increase in values of yield stress and strength of a processed material which after several passes achieve saturation [26]. In the paper [31] it was also shown that the first three passes at ECA pressing of Cu and Ni samples lead to a growth of a strain load. Further, there is a stable stage of strengthening and the load does not almost change.

2.1.3. Multiple forging

One more method of formation of nanostructures in bulk billets is multiple forging developed by Salishchev et al. [32–39]. The process of multiple forging is usually associated with dynamic recrystallization.

The principle of multiple forging (Fig. 6) assumes multiple repeats of a free forging operations: setting-drawing with a change of the axis of the applied strain load. The homogeneity of strain provided by multiple forging is lower than in the
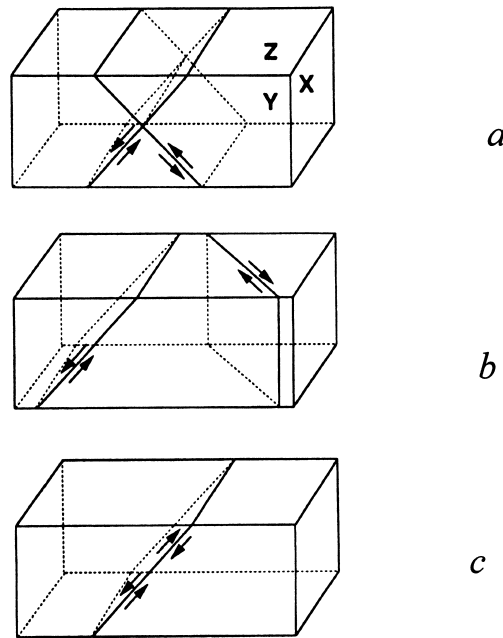

Fig. 5. Directions of shear during ECA pressing according to routes A (a) B (b) C (c) [30].
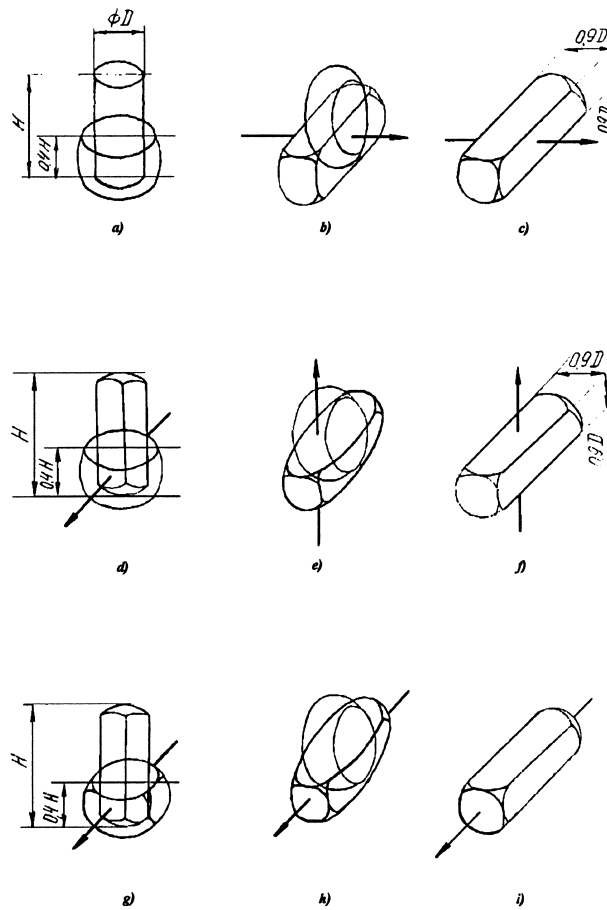
Fig. 6. Principle of multiple forging: (a), (b), (c) — setting and pull broaching along the first axis; (d), (e), (f) — setting and pull broaching along the second axis; (g), (h), (i) — setting and pull broaching along the third axis [32].

case of ECA pressing and torsion straining. However, the method allows one to obtain a nanostructured state in rather brittle materials because processing starts at elevated temperatures and specific loads on tooling are low. The choice of appropriate temperature–strain rate regimes of deformation leads to a minimal grain size.

The method of multiple forging was used for refinement of microstructures in a number of alloys, including pure Ti [38,39], titanium alloys VT8 [32,35], VT30 [33], Ti-6%Al-32%Mo [36,38], magnesium alloy Mg-6%Zr [36], high strength high alloyed nickel base alloys [37,38] and others. The given approach is usually realized over the plastic deformation temperature interval 0.1–0.5 T_{ml} (T_{ml} is the melting temperature). It was shown that hydrogen alloying of two-phase titanium

(a)

(b)
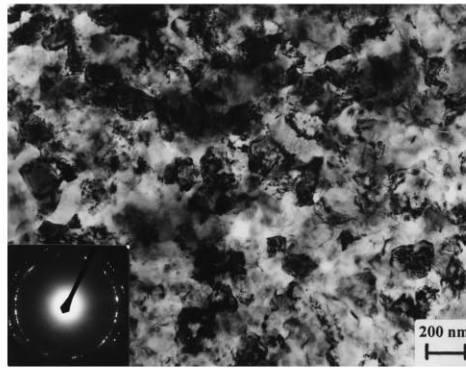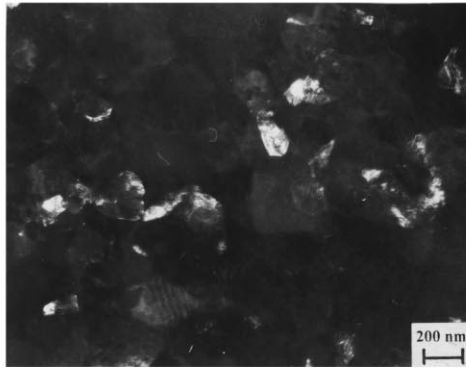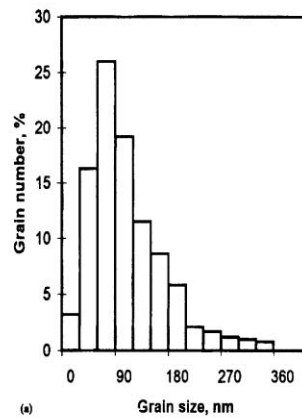
(c)

Fig. 7. Typical TEM micrographs of nanostructured copper, processed by severe torsion straining; (a) bright field image and diffraction pattern; (b) dark field image; (c) histogram of grain size distribution.

alloys not only increases their plasticity and decreases the temperature of deformation but also leads to smaller grain size [46].

Thus, by now, the SPD methods have been actively developed for formation of nanostructures in bulk billets and discs out of different metals and alloys. Nevertheless, the problem of fabrication of massive ingots of a larger dimension having enough homogeneous structure is still very actual (see Section 2.2). The problems of development of new SPD methods are more efficient in terms of their technology, as well as improvement of die-set equipment and processing of low ductile materials, including hard-to-deform ones, where a nanostructured state can be attained, are very urgent too.

2.2. Typical nanostructures and their formation

Methods of severe plastic deformation can provide formation of nanostructures in different materials. However, an obtained grain size and a character of a nanostructure forming depends on the SPD methods applied, processing regimes, phase composition and initial microstructure of a material. Below, are examples of typical nanostructures, discuss procedures of attaining of a minimal grain size in various materials processed by SPD methods and consider data on evolution of the microstructure during intense straining.

By now nanostructures have been obtained in a number of pure metals, alloys, steels and intermetallic compounds via application of different SPD methods.

In pure metals, for example, the application of severe plastic torsion straining can result usually in the formation of ultrafine-grained structure with a mean grain size of about 100 nm and the application of ECA pressing can provide a grain size of 200–300 nm. In Fig. 7 one can see typical nanostructures of copper (99.98%) subjected to SPTS at room temperature (true strain $e = 7$, applied pressure $P = 7$ GPa) which are observed in a transmission electron microscope in bright and dark field images, a corresponding diffraction pattern being shown too [47,48]. It is seen that many grain boundaries are distinct. But, as a rule, they appear not straight, but curved or wavy. There are also grain boundaries with images which are poor and diffraction contrast inside grains is non-homogeneous and often undergoes complex changes. This indicates a high level of internal stresses and elastic distortions of the crystal lattice. Such a complex contrast observed both inside the grains containing lattice dislocations and the grains having no defects testifies that grain boundaries are sources of internal stresses. The azimuthal spreading of spots observed on diffraction patterns also indicates high internal stresses. According to [47,48] the average density of lattice dislocations in SPD copper was about 5×10^{14} m^{-2}. Numerous spots on the diffraction pattern arranged along circles indicate high angle misorientations of neighbouring areas of the crystal lattice. The presence of mainly high angle grain boundaries in the structure of copper subjected to intense straining was also confirmed by direct measurements of misorientations of individual grain boundaries [43], being a very important feature of SPD materials. Histograms of grain size distribution obtained from dark field images [47] showed that the
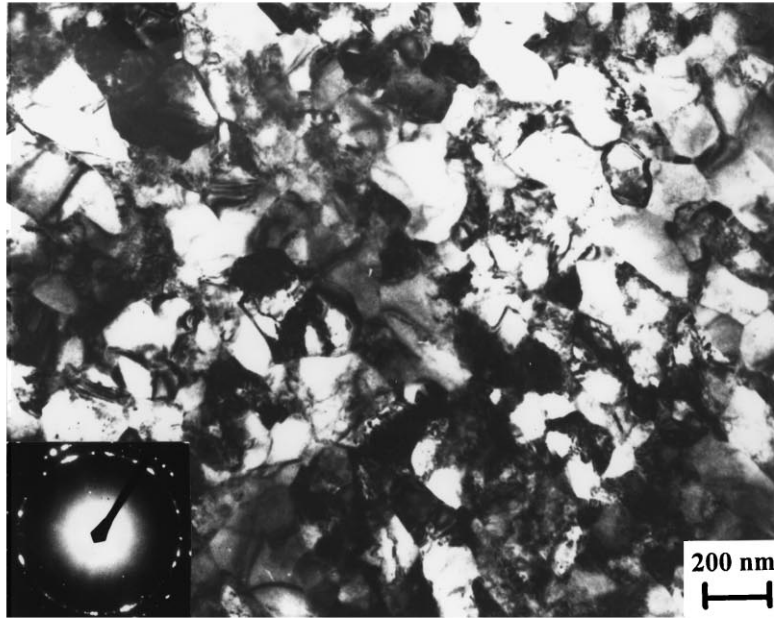
Fig. 8. Typical TEM micrographs of nanostructured copper processed by ECA pressing: (a) route B (see Section 2.1); (b) route C.

structure of SPD copper was characterized by logarithmic normal distribution with a mean grain size of 107 nm (Fig. 7(c)).

Analogous features of the nanostructure are observed in pure nickel exposed to SPTS at room temperature [49]. A smaller grain size of about 80 nm was obtained in samples of Armco-Fe [20] and Ti [50] having bcc and hcp lattices, respectively. However, their nanostructures are characterized by more complex diffraction contrasts attributed to higher internal elastic stresses. Defect structures of materials subjected to SPD will be described in more detail in Section 3.

As shown in papers [31,51], ECA pressing can also lead to formation of equiaxed nanostructures in pure metals. In particular, in Cu (99.97%) subjected to ECA pressing at room temperature (12 passes, route B) the mean grain size was 210 nm (Fig. 8(a)) and the grain size distribution was similar to the logarithmic one [51,52]. At the same time, TEM studies revealed the presence of three types of grains. In small grains, up to 100 nm in size, lattice dislocations were almost absent, in grains of an intermediate size separate chaotically arranged dislocations were observed and in large grains (400–500 nm) formation of subgrains was revealed. The mean density of lattice dislocations inside a grain was 5×10^{14} m^{-2}. Moreover, the type of structure resulted from ECA pressing depends strongly on the route of deformation. For example, during ECA pressing of Cu, in the case of the same number of passes (12), a change in route of a billet from B to C (see Section 2.1) leads to the formation of another type of microstructure — a banded structure, having many low angle grain boundaries (Fig. 8(b)). Recently, this
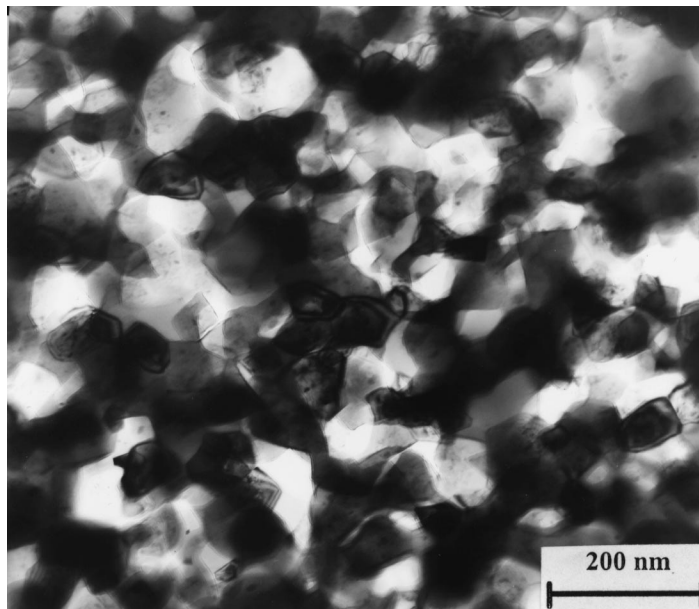

Fig. 9. Two-phase structure of the Zn-22% Al alloy subjected to severe torsion straining at room temperature.
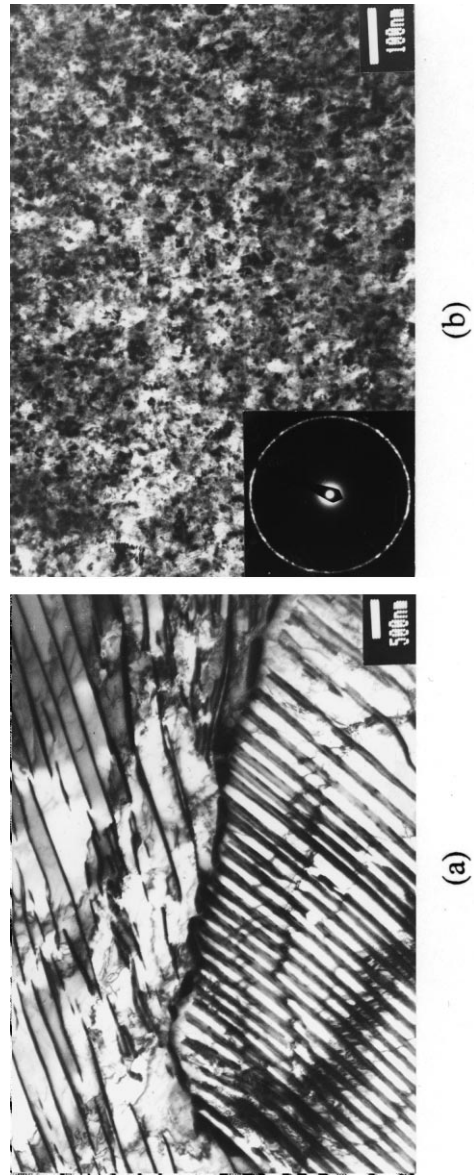
Fig. 10. Structure of the high carbon (1.8%C) steel: (a) in the initial, normalized state; (b) after severe torsion straining at room temperature.

question was investigated in detail during ECA pressing of Al in [30] where it was shown that the homogeneity of the structure, elongation of grains and volume fraction of high angle grain boundaries are determined not only by the strain value but also mainly by the routes of pressing. One should also take into account the possibility of self heating of billets during ECA pressing [53] which exerts a significant influence on formation of the structure as well. In this connection, the fabrication of massive samples with homogeneous nanostructure using ECA pressing is a specialised scientific and technological task. In alloys, subjected to severe plastic deformation, the final structure is determined not only by the processing route but also by the initial microstructure. In one-phase solid

(a)

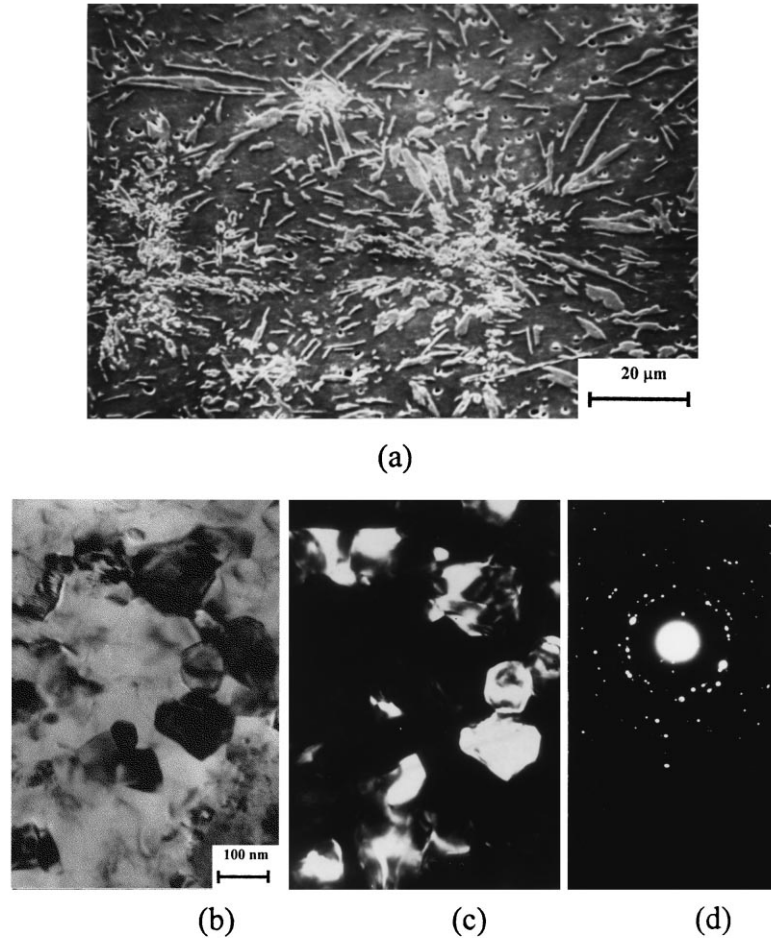(b)   (c)   (d)

Fig. 11. Microstructures of the A1-7.5% Fe alloy: (a) initial cast state (light microscopy) and after severe torsion straining at room temperature (TEM); (b) bright field image; (c) dark field image; (d) SAED pattern.

solutions the formation of the nanostructure occurs analogously to pure metals. The difference is only in grain size obtained which is significantly less in the case of alloys. For example, in quenched Al alloys subjected to SPTS the mean grain size was usually 70–80 nm [54,55]. In multiple phase alloys the nature and morphology of the second phases play a significant role. So, during severe deformation of the two-phase Zn-22%Al alloy a refinement of both phases was observed and after SPTS (five rotations) a nanodouplex structure with a mean grain size of both phases less than 100 nm can be formed at room temperature (Fig. 9) [56]. During severe deformation the second phase particles, which are present in the initial structure and are more stable than the matrix, are exposed to breaking and dissolution due to mechanical alloying resulting in the formation of a supersaturated solid solution.

Severe plastic deformation of high carbon (1.2 wt%) steel is also an interesting example of the formation of the metastable states [57]. The investigated steel was in a normalized state (Fig. 10(a)) and had a pearlite structure with an excess content of cementite. SPTS ($e = 7$, $P = 6$ GPa) resulting in the formation of an extremely disperse structure with a grain size of 20 nm (Fig. 10(b)) which was accompanied by complete dissolution of cementite. The obtained nanostructure presented the supersaturated solid solution of carbon in α-iron.

The formation of solid solutions was also revealed during SPD of a number of alloys belonging to some immiscible systems without mutual dissolution, namely Cu-50%Al [45], Al–Fe [58] and others. The Al-7.5%Fe alloy investigated in [58] was in a cast state and had a dendrite type structure containing fcc Al (matrix) and monoclinic type $Al_{13}Fe_4$ phase (Fig. 11(a)) with particle sizes more than 10 μm. After SPTS an ultra fine-grained structure with a grain size of about 100 nm was formed in the matrix (Fig. 11(b)). As the energy dispersive analysis showed, Al phase became an supersaturated solid solution, containing from 1.34 to 2.24 wt% (from 0.65 to 1.10 at%) iron. At the same time, $Al_{13}Fe_4$ phase dendrites transformed to spherical particles with a size of about 1 μm and partially dissolved forming the solid solution.

Such metastable states resulting from SPD are very interesting due to the fact that after heating there occurs dissociation leading to new unusual properties of the materials (Section 4.2).

One more interesting feature observed in alloys subjected to SPD is the development of twins. For example, alongside the strong refinement of the structure the appearance of a large number of twins was observed in Mg alloys after SPTS [59].

In intermetallic compounds, after severe plastic deformation one can observe not only the formation of a nanostructure but also atomic disordering. This question was investigated thoroughly in Ni_3Al [60,61] and TiAl [62] intermetallic compounds. As TEM investigations showed, a nanostructure with a grain size of about 50 nm is formed in Ni_3Al after SPTS ($e = 7$, $P = 8$ GPa). The structure has a large number of disperse microtwins with a thickness of only 1–2 nm. At the same time, the long range order parameter S was estimated by means of X-ray structural analysis using the ratio between the intensities of {100} or {110}
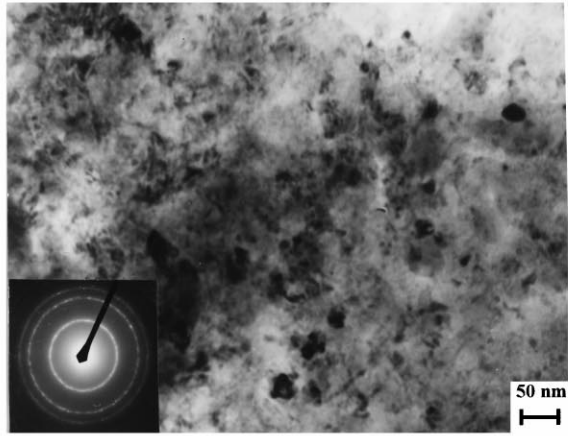
(a)
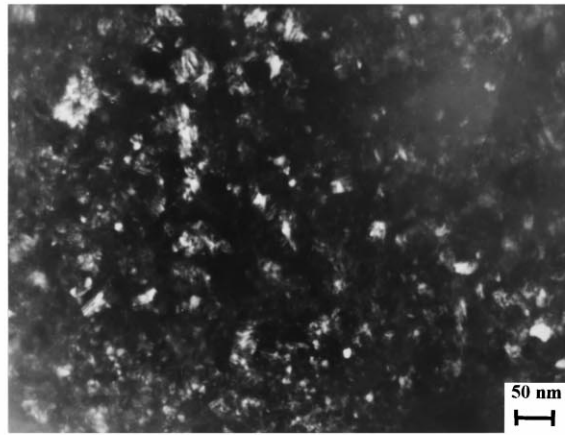
(b)
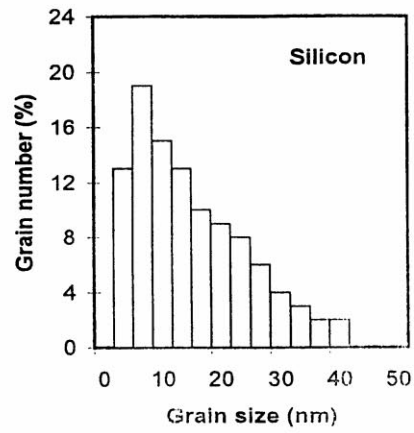
(c)

Fig. 12. Typical TEM microphotographs of nanostructed silicon after severe torsion straining: (a) bright field image and diffraction pattern; (b) dark field image; (c) histogram of grain size distribution.

superlattice peaks and {200} or {220} fundamental peaks, respectively. These estimations showed complete disordering of the atom structure in the Ni_3Al intermetallic compound after severe deformation. However, heating of the samples even at 350°C resulted in a partial restoration of ordering (Section 3.1). After severe deformation the long range order parameter $S = 0.1$ was attained in the TiAl intermetallic compound [62]. But in this case a higher pressure ($P = 10$ GPa) was applied.

In semiconductors, such as germanium and silicon, having a crystal lattice of a diamond type, the application of SPTS also provided the formation of a highly disperse structure (Fig. 12) [63,64]. The analysis of dark field images showed that nanostructures of germanium and silicon were characterized by logarithmic normal grain size distribution, the mean grain size being 24 and 17 nm, respectively. The examination of diffraction patterns from a sample area of 2 μm^2 revealed concentric rings consisting of a number of spots. At the same time, polymorphic transformations were revealed in nanostructured germanium and silicon processed by severe torsion straining under a pressure of 7 GPa. In particular, the appearance of a tetragonal phase with the $P4_32_12$ type crystal lattice [65] was observed in germanium and a cubic phase with the Ia3 type crystal lattice [65] was observed in silicon.

In metal-matrix composites the application of the SPD method also leads to the formation of nanostructures. In particular, one of the methods of processing of nanocomposites is consolidation of metallic and ceramic powders by torsion straining. Types of nanostructures obtained by SPTS consolidation of Cu and Al micropowders and SiO_2 nanopowders were investigated, in detail, recently in [23].
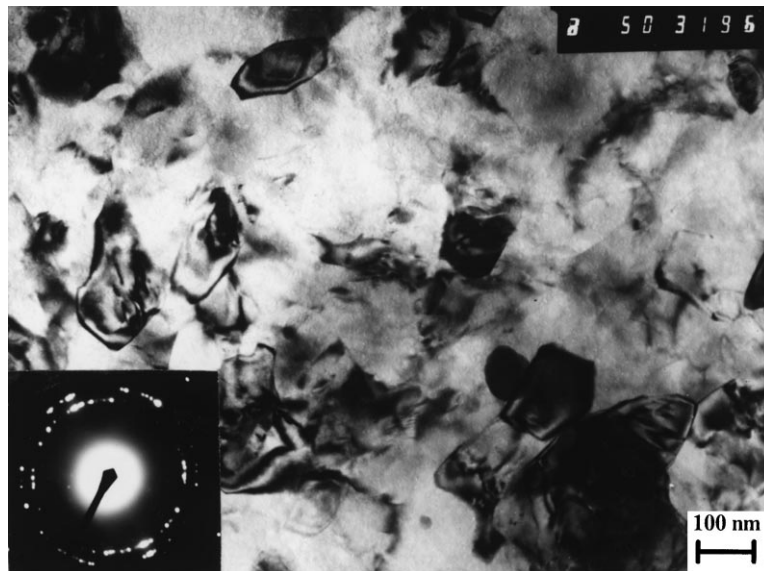

Fig. 13. A typical microstructure of the $A16061 + 10\%A1_2O_3$ composite after severe torsion straining.

Bulk samples of nanocomposites with a density above 98% were processed by this method. The mean grain size in Cu samples was 60 nm and in Al samples was 200 nm.

SPD methods were also used for the formation of nanostructures in metal-matrix composites where ceramic particles were distributed uniformly within a metallic matrix [66,67]. For example, due to severe torsion straining a homogeneous structure with a mean grain size of about 100 nm (Fig. 13) was formed in the $Al6061 + 10\%Al_2O_3$ [66] and $Al2009 + 15\%SiC$ [67] composites. However, during deformation the ceramic particles did not change their initial shapes and sizes. In the $Al6061 + 10\%Al_2O_3$ composite the ceramic particles were of a globular shape, from 0.2 to 5 μm in size, and in the $Al2009 + 15\%SiC$ composite the ceramic particles were of a lamellar shape, more than 10 μm in length and up to 0.5 μm in cross section.

Summing the results obtained, it should be noted once more that numerous investigations demonstrate the possibility of formation of nanostructures by means of methods of severe plastic deformation in various metallic materials, composites and semiconductors. The character of the structure forming is determined not only by the material itself (initial microstructure, phase composition and type of crystal lattice) but also by the severe deformation regime (strain rate, temperature and pressure, etc.). In general, decrease in temperature, increase in pressure and alloying all contribute to refinement of structure and obtaining a minimal grain size.

In conclusion of this section let us consider in brief mechanisms of nanostructure formation during SPD. Unfortunately, there are known only several works on evolution of structure during SPD which tried to reveal the regularities of nanostructure formation, and at present this problem still remains unclear. One of the first such works [17] dealt with investigation of evolution of microstructure in single crystals of Cu, Ni and a Ni–Cr based alloy during SPTS. The refinement of microstructures of up to a crystallite size of 100 nm was observed in the final stage of SPTS. On the basis of their analysis of microstructural evolution processes and measurements of microhardness the authors [17] made an attempt to determine a sequence of structural transformations during severe plastic deformation. It was revealed that in materials having high stacking fault energy (Cu and Ni) with increasing logarithmic strain value up to $e = 2$ dislocations are concentrated in cell walls and almost absent inside cells. Further increase in the strain up to $e = 5$ results in a decrease in a cell size and an increase in cell misorientations. As the authors assumed, this can lead to intensification of rotation modes of deformation within the whole sample volume at once. A decrease in stacking fault energy (Ni–Cr alloy) causes a change in the mechanism of severe plastic deformation when the refinement of the microstructure is realized via formation of shear bands which embrace gradually the whole sample volume.

The TEM studies conducted in [20] also showed that the process of nanostructure formation in Armco-Fe and one-phase steels during SPTS was of a distinct step character. A cellular structure with a mean cell size of 400 nm is typical (Fig. 14(a)) for the first stage, corresponding to torsion in the range from
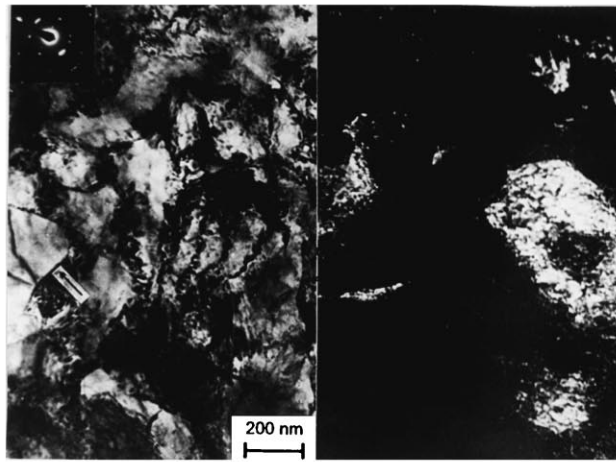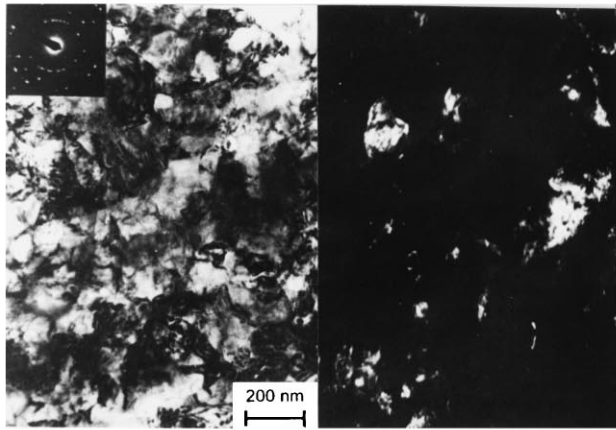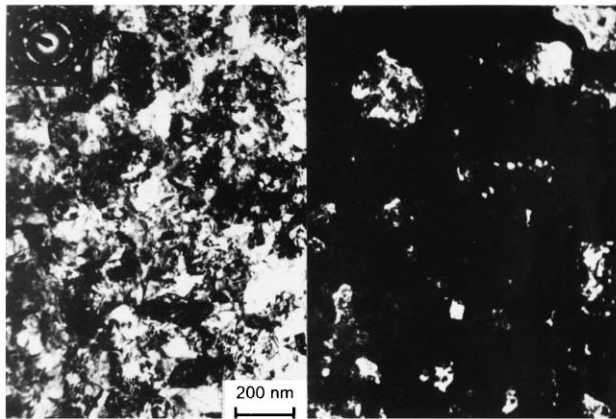
Fig. 14. Typical TEM micrographs of nanostructures in Armco-Fe subjected to severe torsion straining:
(a) $N = 1/4$, (b) $N = 1$, (c) $N = 5$. Bright field and dark field image and diffraction patterns presented
in different stages of deformation.

1/4 to 1 rotation. The angle of misorientation between cells is 2–3°. In the second stage, corresponding to the range 1–3 rotations, one can observe the formation of a transition structure having features of both cellular and nanostructures (Fig. 14(b)) with high angle misorientations. As the strain value increases, a decrease in cell size and an increase in cell wall misorientations occur. The third stage is characterized by the formation of a homogeneous nanostructure with a mean grain size of about 100 nm in Armco-Fe (Fig. 14(c)) and a smaller grain size in steels. The grains are elastically distorted which is especially prominently seen in dark field images. The cause of these elastic distortions are evidently attributed to long range stresses from non-equilibrium grain boundaries containing extrinsic grain boundary dislocations of high density (Section 3). On the basis of the experimental data obtained the authors [20] proposed the following model of evolution of the defect structure of materials during SPD (Fig. 15). The main idea is based on transformation of a cellular structure (Fig. 15(a)) to a granular one, when the dislocation density in the cell walls achieves some critical value [68], and a partial annihilation of dislocations of different signs occurs at the cell boundaries (Fig. 15(b)). As a result, excess dislocations of single sign remain (Fig. 15(c)). The excess dislocations play various roles: dislocations with Burgers vectors perpendicular to the boundary lead to an increase of misorientation and when their density rises they cause the transformation to a granular structure; at the same time long range stress fields are connected with glide dislocations which can also lead to sliding of grains along grain boundaries, i.e. reveal rotation deformation modes which is indicated earlier for large plastic straining [8].

3. Structural characterization and modeling of SPD materials

Nanostructured materials processed by SPD methods are characterized by a very high density of grain boundaries and are interface-controlled materials. Thus, it is quite natural that their grain boundaries are in the center of all structural investigations. As shown below, evidence for a non-equilibrium structure of grain
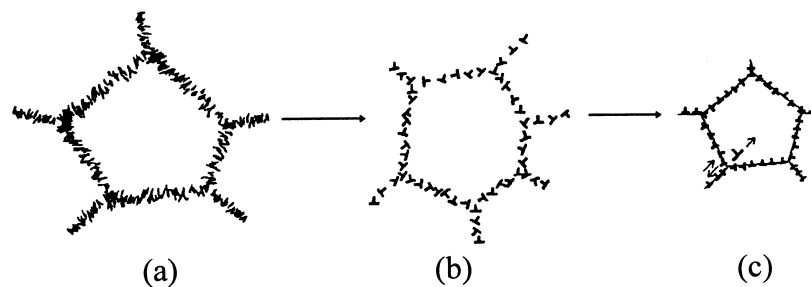

(a)   (b)   (c)

Fig. 15. Schematic model of dislocation structure evolution at different stages during severe plastic deformation.

boundaries in SPD materials is of special importance. The notions on non-equilibrium grain boundaries were first introduced in the scientific literature somewhere in the 70–80s [69,70] reasoning from investigations of interactions of lattice dislocations with grain boundaries. According to [70] the formation of a non-equilibrium grain boundary state is characterized by two main features, namely, excess grain boundary energy (at the specified crystallographic parameters of the boundary) and the presence of long range elastic stresses (Fig. 16). Assuming that grain boundaries have a crystallographic ordered structure, discontinuous distortions of such a structure, i.e. grain boundary dislocations and their assemblies, can be considered as sources of elastic stress fields.

Investigations of grain boundaries in nanostructured materials processed by SPD methods were carried out using various, often mutually complementary methods: transmission, including high resolution, electron microscopy, X-ray structural analysis, Mössbauer spectroscopy, differential scanning calorimetry and others. The present Section deals with the main results obtained by means of these investigations aimed to study the defect structure of both the grain boundaries and the grain body in nanostructured SPD materials. Using the experimental data structural models of NSM are considered.

3.1. Experimental investigations

To reveal the main features of the defect structure of SPD materials, let us consider first of all the results obtained via investigations of pure metals and/or one-phase alloys, where the complex influence of second-phases is absent.

The first TEM studies of nanostructured materials processed by severe plastic

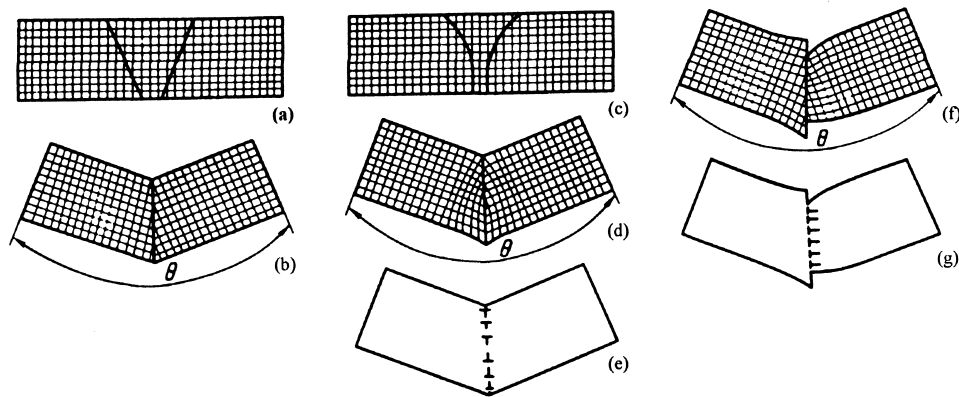Fig. 16. Engineering of grain boundaries via thought cuts: (a) → (b) — equilibrium grain boundary (bunches of deformation are connected without strain); (c) → (d), and (a) → (f) — non-equilibrium grain boundaries (deformation is required for crystal joint — bending and tension — compression, respectively); (e), (g) — schemes of GBD complexes initiating the same character of elastic distortions as in (d), (f) [70].

deformation revealed a specific image of grain boundaries in NSM as compared to ordinary annealed counterparts [13,71]. A typical example of such a diffraction contrast is the image of the microstructure of the Al-4%Cu-0.5Zr alloy [10,71] having a mean grain size of about 200 nm (Fig. 17(a)) after torsion straining. For comparison, a microstructure of the same sample subjected to additional annealing at 160°C for 1 h is also shown (Fig. 17(b)). A granular type structure with high angle grain boundaries is mainly observed in both cases. Nevertheless, the image of the grain boundaries in Fig. 17(a) is distinguished significantly from Fig. 17(b) by a strong spreading of thickness extinction contours being a feature of non-equilibrium grain boundaries [70].

According to the dynamic theory of diffraction contrast [72–74] the thickness extinction contours on inclined grain boundaries are contours of similar grain depth in a thin foil and they appear in TEM images when some family of planes of the given grain is in the Bragg reflection conditions. The works [75,76] analyze the physical nature of the spreading of thickness extinction contours in TEM images of grain boundaries in nanostructured materials and show that this spreading is connected with a high level of elastic stresses and crystal lattice distortions near the grain boundaries in NSM, processed by SPD. On the basis of this analysis a procedure for determination of values of elastic strains depending on a distance from a grain boundary is proposed. This approach was realized in [76] for investigation of elastic strains near grain boundaries in nanostructured copper processed by ECA pressing. It was revealed that the distribution of such elastic strains is not uniform. It has its maximum in the vicinity of the grain boundaries and an exponential slope at a distance of several nanometers from grain boundaries (Fig. 18). Moreover, the maximum value of elastic strains near
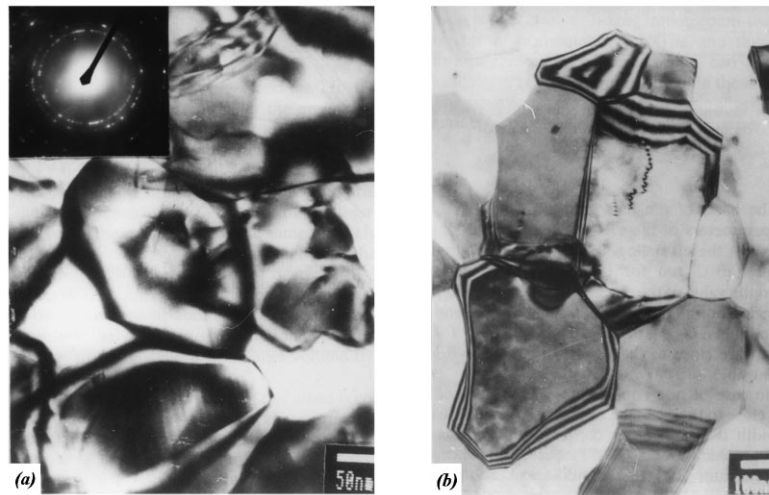

Fig. 17. TEM micriphotographs of the A1-4% Cu-0.5% Zr alloy: (a) after severe torsion straining, (b) after additional annealing at 106°C for 1 h.

the grain boundaries in the nanostructured copper were equal to 3.3×10^{-3}, higher than the average value determined by the X-ray structural analysis by a factor of 5 [77,78].

In turn, such a distribution of elastic strains near the grain boundaries can be described by the array of edge gliding grain boundary dislocations (Fig. 19) which, in terms of the theory of dislocations [79], can provide the following equation for the tensor component of elastic strains ε_{xx}

$$\varepsilon_{xx} = \frac{\pi b x}{(1 - v)D^2 \cosh^2(2\pi x/D)} \tag{7}$$

where x is the distance from a grain boundary, D is the average distance between grain boundary dislocations, b is the Burgers vector, v is the Poisson's ratio, cosh is a hyperbolic cosine.

The distribution of elastic strains near the grain boundary with such a dislocation array calculated according to Eq. (7) has features analogous to curve 1 in Fig. 18 plotted experimentally and shows a maximum of elastic strain near the boundary and an exponential slope from the boundary. Let us note that a rapid decrease of elastic strain with increasing distance from the non-equilibrium grain boundary was foreseen in other works [16,80]. From Fig. 18 it follows that a good fit of data calculated according to Eq. (7) with experimental data is achieved for the grain boundary dislocations density of 2.3×10^7 m^{-1} at the Burgers vector b = 2.56×10^{-10} m (curve 2). If we assume, however, the grain boundary Burgers vector $b_{GBD} = b/6$ [70], the value of density of grain boundary dislocations will be 1×10^8 m^{-1} (curve 3).

The results obtained allowed us to conclude [76] that widening of thickness extinction contours in TEM images of grain boundaries in nanostructured
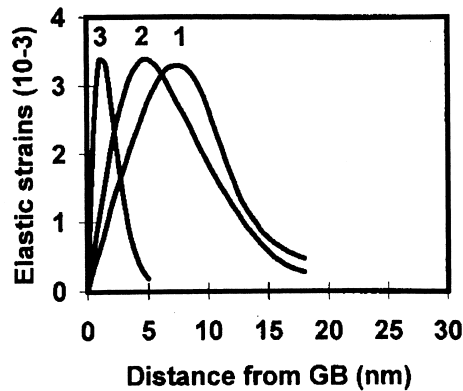
Fig. 18. Distribution of elastic strains depending on distance from grain boundary: (1) experimental curve; (2), (3) calculated curves for a density of grain boundary dislocations of 2.3×10^7 and 1×10^8 m^{-1}, respectively.
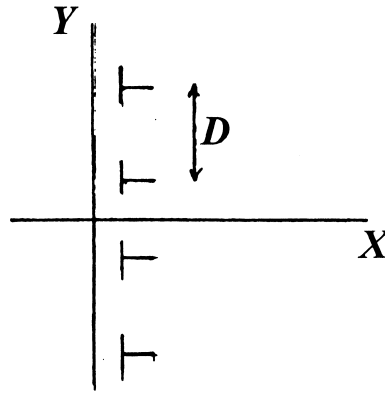
Fig. 19. The distribution of edge gliding grain boundary dislocations, which results elastic strain shown in Fig. 18. Here D is the average distance between dislocations.

materials is actually connected with large elastic strains. Moreover, the maximum values of elastic strains are observed near grain boundaries where their level is significantly higher than inside of the grain body.

Let us note that similar results were obtained recently in the work [81] dealing with TEM observations and measurements of crystal lattice curvature near grain boundaries. In this work, measurements of the curvature of crystal planes parallel to the wave vector were performed, since this curvature is not changed in the case of a possible bend of the thin foil in the process of its preparation. The results of TEM investigations have revealed high crystal lattice curvature of $10 \div 20$ grad/μm in nanostructured nickel processed by ECA pressing. In [81] a disclination approach was used to describe such non-equilibrium grain boundaires with a high curvature of the crystal lattice and variable misorientation. According to this approach the a non-equilibrium grain boundary can be modeled by a high density of continuously distributed partial disclinations of one sign (Fig. 20). Moreover, it
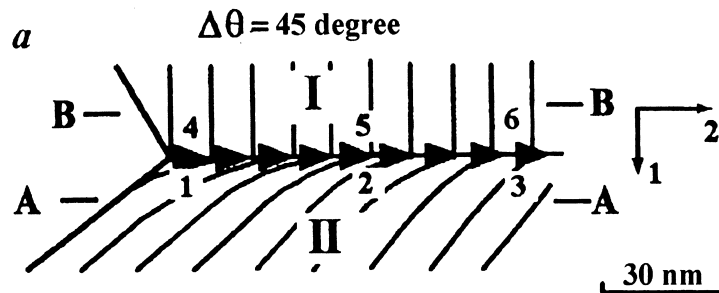
Fig. 20. Scheme of grain boundaries with high density of continuously distributed disclinations leading to high elastic strain.

was shown that such a grain boundary is a source of high elastic stresses achieving a value of $G/33$ near grain boundaries, where G is the shear modulus of a coarse-grained metal.

Let us now consider the results of detailed investigations of nanostructured SPD materials carried out by means of high resolution transmission electron microscopy. This method provides data on only a very local area of a structure. Nevertheless, its obvious advantage consists in conducting detailed investigations of grain boundaries on an atomic level. Similar investigations recently conducted in a number of works allowed one to reveal important feature of grain boundary structure of the materials under study.

It is known [72,82] that application of the Moiré picture reveals small distortions of a crystal lattice since even small changes in translation symmetry of the lattice leads to noticeable changes in Moiré pictures. Moiré pictures are often observed in such cases when images of crystal lattices of two neighboring grains superimpose on one another. Typical features of Moiré pictures are their bending in the presence of distortions of crystal planes and changes of distance between them. At the same time, artificial Moiré pictures can be obtained by superimposition of a special grid of parallel lines on HREM images of crystal planes of the nanostructured materials investigated [83].

Such investigations of nanostructured pure nickel with a grain size of 50 nm and Ni_3Al intermetallic compound with a grain size of 70 nm showed that Moiré
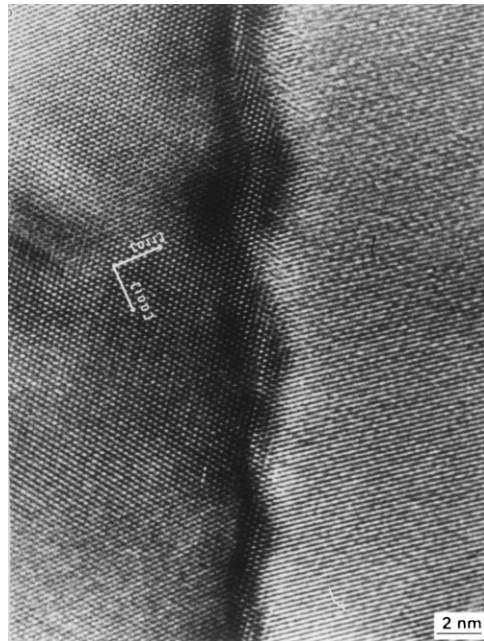
Fig. 21. HREM image of grain boundary in nanostructed A1-3% M_g alloy.

lines were bent near grain boundaries through an angle of $10°$–$15°$ that correspond to bending of lattice fringes through an angle of about $2°$ [83]. Such distortions of the crystal lattice were observed only near grain boundaries and they were absent inside of the grain body. Moreover, dilatations of the crystal lattice near grain boundaries achieved 1.5%.

HREM investigations were also conducted in the nanostructured Al-3%Mg alloy with an fcc lattice [84] where the formation of periodic facets of parallel (111) planes was revealed (Fig. 21). Each facet contains about ten atomic layers parallel to a (111) plane. The average density of facets was very high and achieved a value of about 5×10^8 m^{-1}. At the same time one can observe distortions of crystal lattice images near grain boundaries that indicates a non-equilibrium state. Analogous distortions of the crystal lattice near grain boundaries were revealed in HREM images of the structures of copper, nickel and Armco-iron subjected to SPTS [20,85].

As known, dislocations can be revealed using the HREM method via direct observation of the extra planes of a crystal lattice. For example, in the image of the crystal lattice of a nanostructured Al-3%Mg alloy (Fig. 22) some crystal planes in the near boundary area end in the points indicated by the symbol ⊥, which assumes the presence of dislocations in these areas.

In general, the structural features of grain boundaries revealed by HREM were similar in all materials investigated [20,83,84,85]. First of all, the width of the
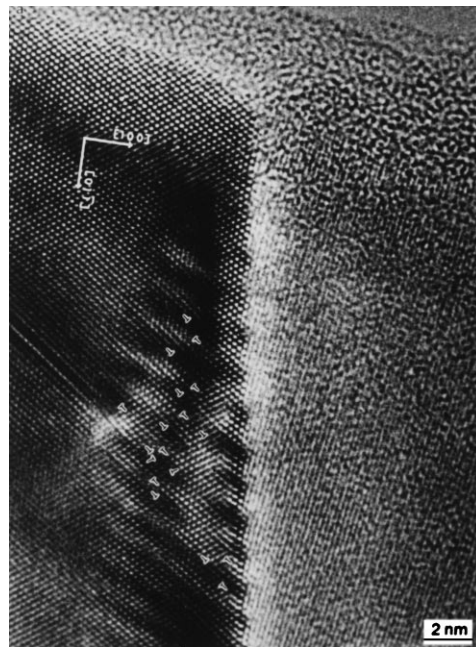
Fig. 22. HREM image of grain boundary in nanostructed A1-3%Mg alloy. Areas where extra planes are observed are marked by the symbol ⊥.

grain boundaries is 1–2 interatomic spaces, i.e. close to the width of the grain boundaries in conventional coarse-grained materials. However, grain boundaries in nanostructured metals and alloys are not perfect by their structure since they contain various defects: steps, facets, dislocations, and the high defect density leads to elastic distortions near the grain boundaries. At the same time, facets and steps observed at typical grain boundaries in a nanostructured Al-3%Mg alloy were more ordered and uniformly distributed in comparison with nanostructured Cu, Ni and Fe [20,85]. This assumes that a partial ordering of grain boundary defect structures takes place in the Al-3%Mg alloy already during SPD conducted at room temperature. A comparatively high homologous temperature for the SPD processing of the Al-3%Mg alloy as compared to other materials, can result in this phenomenon.

One more very interesting result which was obtained by HREM investigations [84] was migration of grain boundaries occurring due to radiation of a foil by high energy electrons. In particular, Fig. 23 demonstrates changes in the image of the grain boundary in the Al-3%Mg alloy resulting from electron radiation for
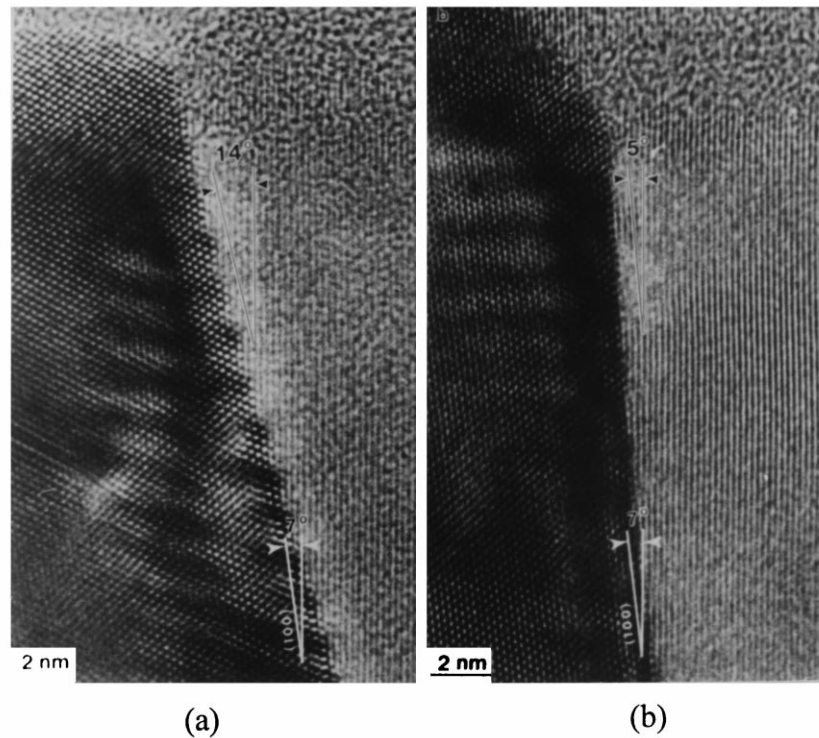
Fig. 23. HREM image of grain boundary in nanostructured Al-3% Mg alloy illustrating the influence of high power electron irradiation; (a) in the initial moment of irradiation; (b) after several minutes after irradiation (after Horita et al. [84]).

several minutes. So, the angle between the boundary and (220) lattice fringes of the right grain has decreased from 14° (Fig. 23(a)) to 5° (Fig. 23(b)), though the angle between the image of (200) planes in both grains remains constant. At the same time, the observed decrease in the number of facets and steps as well as the absence of extra planes in the near grain boundary area (Fig. 23(b)) indicates the relaxation of the non-equilibrium grain boundary state in the process of migration.

Thus, the results of TEM/HREM investigations allow us to conclude that grain boundaries in nanostructured materials processed by SPD methods, are characterized by significant distortions of the crystal lattice near the grain boundaries, a high density of dislocations and other grain boundary defects, as well as often by a curve and wavy configuration that testifies to their non-equilibrium state.

X-ray structural analysis is another method providing important data on the defect structure of NSM. X-ray patterns of nanostructured materials processed by SPD methods [47,48,77,78] differ significantly from X-ray patterns of corresponding coarse-grained materials. These differences are revealed, first of all, in changes of integral intensity of background, changes of width and intensity of X-ray peaks and appearance of crystallographic texture.

The background on X-ray patterns is a result of diffuse scattering of X-rays [86]. The reasons for background appearance in pure metals can be thermal diffuse scattering and absence of long and/or short range atomic order. In this connection, investigation of background on X-ray patterns acquires a special role
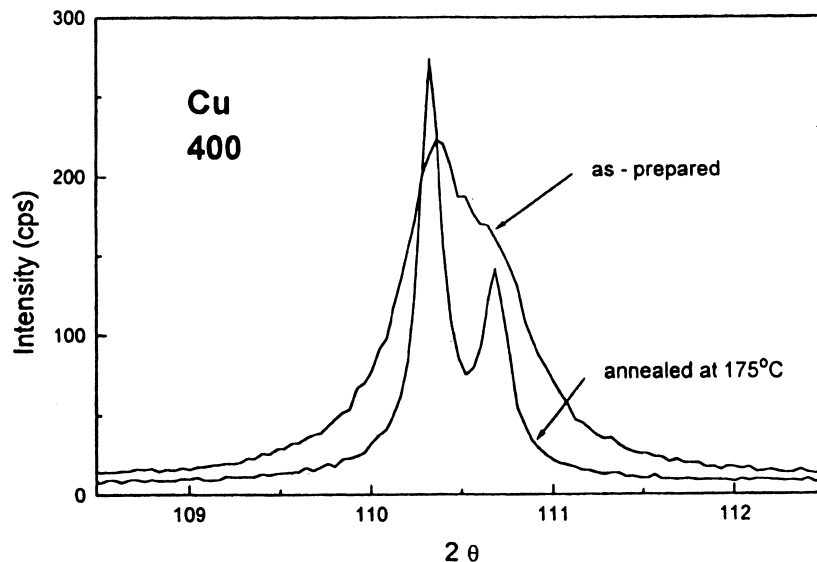
Fig. 24. Comparison of profiles of X-ray (400) peak in nanostructed copper subjected to severe torsion straining and after annealing at 175°C.

in nanostructured materials characterized by large volume fractions of grain boundaries, because a displacement of atoms in grain boundaries from equilibrium states in the crystal lattice should significantly influence the intensity of diffuse scattering of X-rays. The recent results of calculations show that the integral intensities of the background on the X-ray pattern of nanostructured copper processed by torsion straining and by ECA pressing exceed the corresponding value for coarse-grained copper by a value of $(6 \pm 3)\%$ and $(6.1 \pm 2.7)\%$ [77], respectively. The increase in the integral intensity of the background indicates an elevated density of crystal structure defects and a possible change in the vibrational spectrum of atoms in nanostructured copper.

Another feature of X-ray diffraction patterns in nanostructured SPD materials is a significant decrease in the intensity of X-ray peaks and their strong broadening. In particular, a comparison of X-ray peak profiles in nanostructured and coarse-grained copper and germanium testifies to this (see Figs. 24 and 25) [47,63].

It is known that the analysis of broadening of X-ray peaks can provide information on elastic strains and grain (domain) size in polycrystalline materials. Several approaches were developed to calculate this value. The methods of Warren–Averbach and Williamson–Hall are the most widely used ones [86–93].
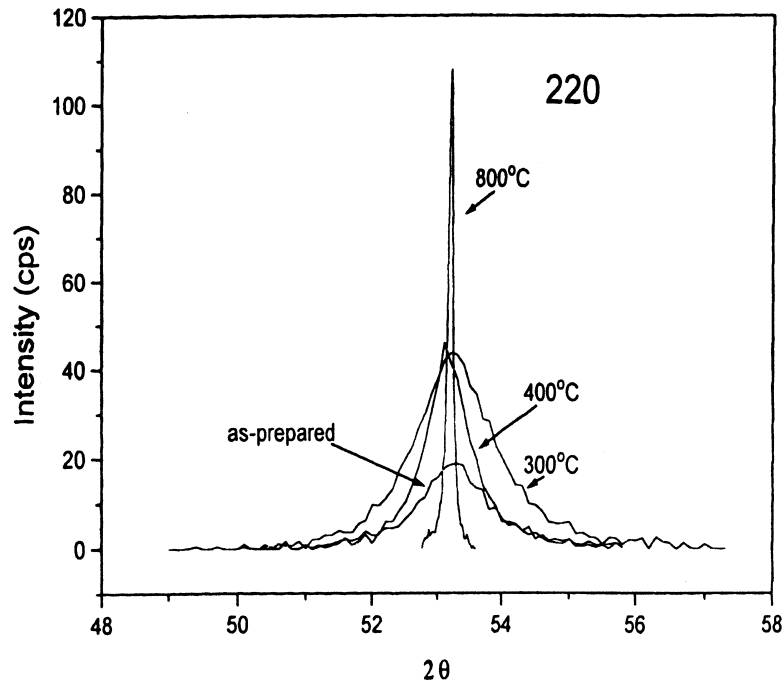
Fig. 25. Profiles of X-ray (200) peak in germanium after severe torsion straining and subsequent annealing at 300, 400 and 800°C.

The idea of the Warren–Averbach method consists in the separation of the contributions of grain size and elastic strain to broadening of X-ray peaks based on their different dependence on the order of reflection. In this case, an approximation of a physical profile by a Fourier series is used and coefficients of this distribution are determined. The Warren–Averbach method provides an area-weighted average grain size [87].

The method by Williamson–Hall is used in cases when X-ray peaks corresponding to reflections of different orders from one family of planes are not available or do not possess a shape favorable for representation by a Fourier series. The grain size is obtained by extrapolating the variation of the X-ray peak integral width with scattering vector to zero. In this case the result is a volume-weighted average grain size. The microdeformation is determined from the slope of the curve [47,89,90].

The questions relating the application of methods of X-ray structural analysis for determination of elastic strain and grain size in nanostructured materials processed by SPD methods were considered recently in [78]. The analysis of broadening of X-ray peak profiles showed that the grain size D in the nanostructured copper processed by severe torsion straining was equal to 53 nm (111)–(222) and 33 nm (200)–(400) in the case of the Warren–Averbach method [77] and 71 nm (111)–(222) and 50 nm (200)–(400) in the case of the Williamson–Hall method [47]. The distinction in the grain sizes obtained is evidently attributed to the specific features of the given X-ray methods mentioned above, as well as by differences in a grain structure belonging to different texture components.

Nevertheless, the grain sizes obtained by X-ray structural analysis methods are usually significantly less than the ones determined using histograms of grain size distribution plotted on the basis of dark field [47] or bright field [48] TEM images. The possible reason for this distinction can be physical difference in values to be determined. The X-ray structural method actually allows us to determine a size of coherently scattering domains connected with internal grain areas having a weakly distorted crystal lattice, whereas the TEM method measures a complete grain size which includes near boundary strongly distorted areas. Thus, in SPD materials characterized by strong distortions of the crystal lattice, the difference in TEM and X-ray structural data can be rather significant [78]. It should be also noted that the anisotropy of grain shape can significantly influence the results obtained by TEM and X-ray structural methods, since TEM measures grain size in the plane parallel to the sample surface, while the X-ray structural method measures the size in the direction perpendicular to this surface.

Values of root-mean square strain determined in nanostructured copper using both X-ray structural analysis methods are in reasonable agreement. Thus, the values of elastic strain determined in accordance with the Warren–Averbach method were $6.1 \times 10^{-2}\%$ and $11.8 \times 10^{-2}\%$ for (111) and (200) planes, respectively [78], whereas the values of elastic strain calculated by means of the Williamson–Hall method for the same planes were $4 \times 10^{-2}\%$ and $8 \times 10^{-2}\%$, respectively [47].

Release in intensity of X-rays due to thermal motion of atoms in a crystal

lattice is characterized by means of the thermal factor $\exp(-2M)$ [86] which is called the Debye–Waller factor. The value M is directly proportional to the square of the root-mean square displacement $\langle \mu_0^2 \rangle$ of atoms from the equilibrium state and depends on the temperature T. In the case of cubic crystals the Debye–Waller parameter is proportional to M and is given by

$$B = \frac{M}{(\sin\theta/\gamma)^2} = \frac{8\pi^2}{3\langle\mu^2\rangle} \tag{8}$$

where $\langle\mu^2\rangle$ is the value of a root-mean square displacement of atoms in the direction of the scattering vector.

Since the nanostructured metals processed by SPD are textured [95], a special approach [96] was used to determine the Debye–Waller parameter in [94]. According to this approach peaks of only one family of planes but with different orders of reflection were used, i.e. the influence of a crystallographic texture was excluded. The obtained X-ray results for nanostructured and coarse-grained nickel showed [94] that in both samples the values of the Debye–Waller parameter B and the root-mean square atomic displacements $\langle\mu^2\rangle$ reduced linearly with decreasing temperature (Fig. 26). In the case of nanostructured nickel the slope of the temperature dependence of the Debye–Waller parameter was sharper than in the coarse-grained sample. This shows that the Debye temperature has changed in the nanostructured nickel (Section 4.1).

The results of analogous investigations for nanostructured copper (Table 1)
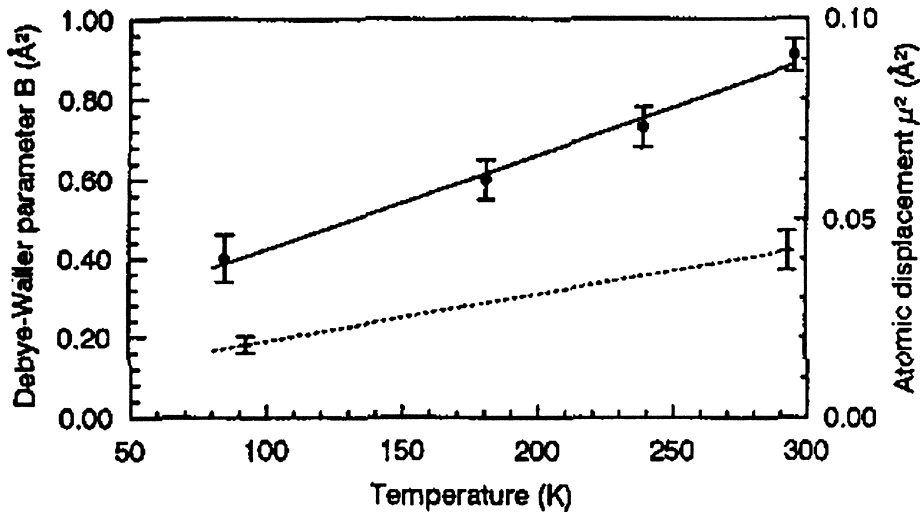

Fig. 26. Averaged value of the Debye–Waller parameter B and atomic displacements depending on temperature for nanostructured (continuos line) and coarse-grained Ni (dash line).

showed that the root-mean square displacement $\langle \mu^2 \rangle$ was equal to (0.120 ± 0.003) Å, i.e. 5.0% of the shortest distance between atoms for copper. Using the known approaches described in [97], the values of the temperature dependent thermal B_T and the temperature independent static B_S being components of the Debye–Waller parameter were calculated. As known, they are connected with dynamic and static atomic displacements, respectively. Values of both components of the Debye–Waller parameter for nanostructured copper and nickel exceeded significantly corresponding values for coarse-grained metals. This indicates changes occurring in the character of thermal vibrations of atoms which is also confirmed by calculations of Debye temperature (Section 4.1).

The study of crystallographic texture in nanostructured materials processed by SPD methods has special interest as well. The conducted investigations showed that crystallographic texture is a typical feature of nanostructured pure metals and it is observed in NSM processed both by torsion straining and ECA pressing [95]. An axial texture is formed in nanostructured copper exposed to severe torsion straining. As for ECA pressing, it results in formation of a complex texture which reflects a shear character of deformation.

The analysis of evolution of the crystallographic texture during plastic deformation usually helps to establish deformation mechanisms. Moreover, the crystallographic texture exerts significant influence on many physical and mechanical properties of SPD materials. In this connection, further extension of investigations of processes of texture formation during SPD is a very urgent task.

The results given above show that X-ray structural analysis in addition to TEM investigation provides quantitative data on nanostructures processed by SPD methods. In particular, by means of X-ray structural analysis one can estimate a higher level of elastic strain as compared to coarse-grained materials, significant atomic displacements from the equilibrium state in crystal lattice units, as well as a vibrational spectrum of atoms which are increased in nanostructured materials.

The results of Mössbauer investigations of nanostructured iron (purity 99.97%) are also very interesting. These results provide information not only on grain boundaries but also on near boundary areas [98,99]. It was established that Mössbauer spectra of nanostructured iron (Fig. 27) can be divided into two subspectra significantly distinguished in parameters of electric and magnetic superfine structure (Table 2). This shows that atoms of nanostructured iron are characterized by two different states. Parameters of the first, more intensive subspectrum almost coincide with ones of the coarse-grained iron spectrum. The

Table 1

Data on structure and thermal characteristics of nanostructured copper and nickel

Sample	Nanostructured copper	Nanostructured nickel
Average grain size, nm	50 ± 2	152 ± 2
r.m.s. strain $\langle e^2 \rangle^{1/2}$, 10^{-3}	6.60 ± 0.15	1.3 ± 0.4
Debye–Waller parameter B, (295 K), Å^2	1.26 ± 0.05	0.91 ± 0.04
Debye temperature Θ, K	233 ± 6	293 ± 7
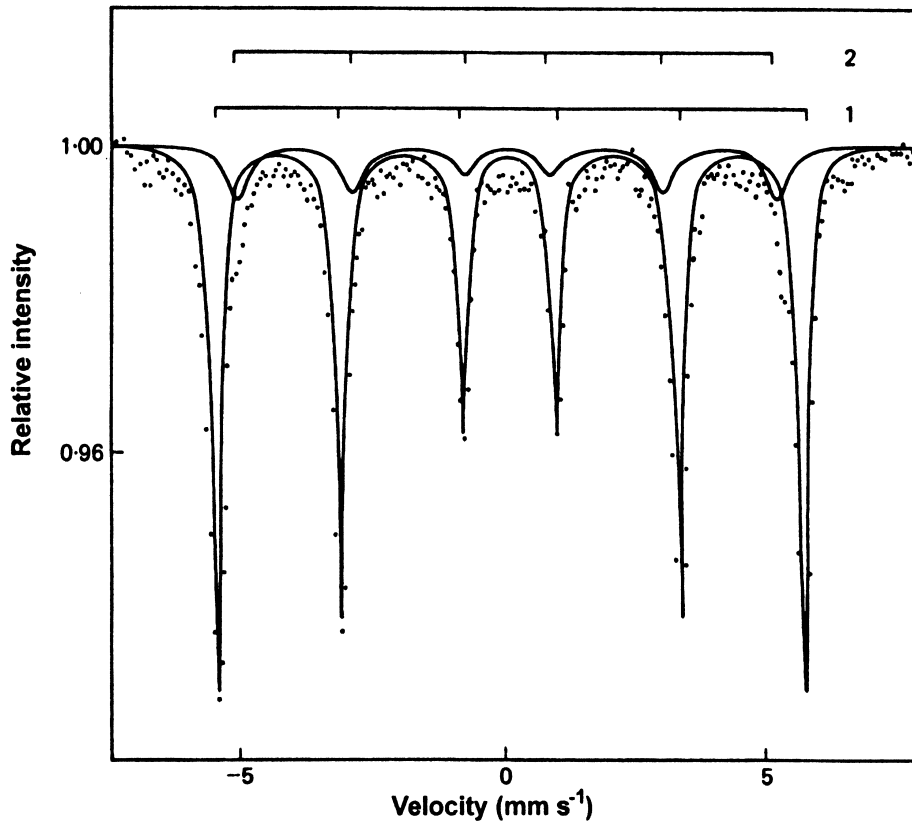
Fig. 27. Mössbauer spectrum of the nanostructured Armco-Fe.

presence of the second subspectrum is connected with a special state of iron atoms near grain boundaries [98]. Reasoning from the relationships of integral intensities of subspectra 2 and 1 for the grain size 0.23 μm (Table 2), the volume fraction of such atoms is $(11 \pm 1)\%$. Therefore, the thickness of a near boundary atom layer is (8.4 ± 1.5) nm. The presence of distinctly fixed parameters of the superfine structure for the part of atoms under study [98,99] allows us to assume the existence of a special grain boundary state of iron atoms or a grain boundary phase alongside the granular phase, though no difference was revealed in the crystallographic structure of these phases. It is evident that the difference observed in superfine parameters of subspectra 1 and 2 is connected, first of all, with higher dynamic activity of atoms of the grain boundary phase as compared to the granular phase which results from some difference in their electron structures and background spectra.

Summarizing the results of the investigations conducted on pure metals copper,

Table 2
Parameters of superfine structure of subspectra 1 and 2 for iron with different grain sizes

Mean grain size, μm	Sub-spectrum	Relative integral intensity (subspectrum area)	Efficient magnetic field, KOe	Isomer shift in respect to a standard one α-iron, mm/s^{-1}
0.12	1	0.78 ± 0.02	331 ± 5	0.00 ± 0.06
	2	0.22 ± 0.02	301 ± 5	-0.36 ± 0.06
0.23	1	0.91 ± 0.02	331 ± 5	0.00 ± 0.06
	2	0.09 ± 0.02	301 ± 5	-0.35 ± 0.06
0.65	1	0.95 ± 0.02	330 ± 5	0.00 ± 0.06
	2	0.05 ± 0.02	302 ± 5	-0.33 ± 0.06

nickel, iron and single-phase Al alloys reveals a number of typical features of the defect structure of nanostructured materials processed by SPD. It should be also noted that TEM/HREM, X-ray and Mössbauer spectroscopy are mutually complementary methods of investigations. The first methods, namely TEM and HREM, provide local information, in particular, about individual grain boundaries while X-ray and Mössbauer spectroscopy provide average information about the material structure. It is very important that the results of all these investigations do not contradict but even complement one another.

The common feature typical for all nanostructured materials processed by SPD is high internal stresses and distortions of the crystal lattice. According to X-ray data the root mean square strain $\langle e^2 \rangle^{1/2}$ is equal to 10^{-3}–10^{-4} while according to the TEM/HREM investigations of the same materials local elastic strains, especially near grain boundaries, are higher by an order of magnitude and even more. The fact that the level of internal stresses is high, while the density of lattice dislocations inside grains is often insignificant confirms that non-equilibrium grain boundaries are sources of these stresses. The HREM observations of grain boundaries provide evidence for their specific defect structure in nanostructured materials due to the presence of atomic steps and facets and grain boundary dislocations (GBD). In turn, high stresses and distortions of the crystal lattice lead to the dilatation of the lattice with changes of interatomic spacing, and significant
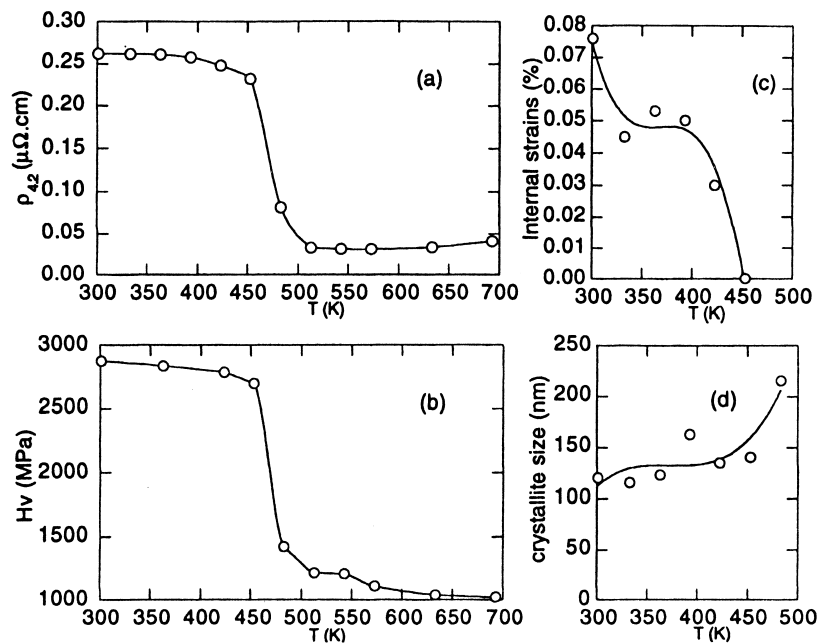

Fig. 28. Evolution of residual resistivity (a), microhardness (b), internal strains (c) and crystallite size (d) deduced from the broadening of the (220) X-ray line, as a function of annealing temperature in nanostructured nickel.

static and dynamic atomic displacements which were experimentally observed by X-ray and Mössbauer investigations.

At the same time, the high density of crystal lattice defects in nanostructured SPD materials is attributed to their excessive energy and metastable state, which transfers to a more equilibrium state at elevated temperatures. The recent investigation of evolution of nanostructures during heating of materials processed by SPD was a subject of special interest in a number of works where alongside with TEM and X-ray methods the investigations of electric resistance [61], dilatometry [71] and differential scanning calorimetry [47] were used. Such investigations have a number of interesting aspects. Firstly, they provide information about the thermal stability of nanostructured materials. It is known that nanomaterials are often rather non-stable and their grain growth occurs at temperatures 0.4T and even lower [2,100]. That is why, the knowledge of the origin of their low temperature stability is important for development of ways of its improvement. Secondly, the investigation of the evolution of nanostructures during heating contributes to better understanding of their complex defect structure, in particular, due to application of additional experimental methods, namely, DSC, dilatometry and others.

Not describing the results obtained in detail (they were sufficiently described recently in [62]) we should mention a non-monotonous character of changes occurring in different parameters during heating. For example, in Fig. 28 there are given data on changes in residual electric resistance, microhardness, internal stresses and crystallite size (according to X-ray data) depending on temperature of annealing of the nanostructured nickel processed by SPTS at room temperature [62]. It is seen that during annealing up to temperature 450 K the changes occurring in microhardness H_v and electric resistivity ρ values are rather insignificant. However, after annealing at higher temperatures the values change sharply. This takes place in a rather narrow temperature interval of 450–500 K and after that the changes become insignificant again. These effects are correlated with changes in grain size, since grain growth also begins at annealing above 450 K. At the same time, a decrease in internal stresses occurs at lower temperatures. In accordance with [47,62,101] a similar three-step change of various parameters occurs in different pure metals subjected to SPD depending on temperature of annealing. Moreover, the authors [101] made estimates of the activation energies of the processes controlling the structural changes in the different stages of recovery in copper subjected to SPD. Their values were 55 and 98 kJ/mol for
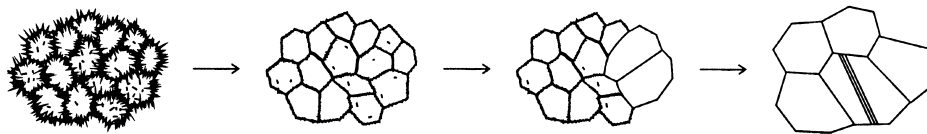

Fig. 29. Scheme of structure evolution during heating of nanostructured copper.

stages 2 and 3, respectively. These results as well as data from dilatometry [71] and DSC measurements [102] allow us to distinguish the main processes responsible for structural changes in the different stages of annealing of nanostructured metals (Fig. 29). In the first stage the main process is recovery from the non-equilibrium structure of the grain boundaries. This process is connected with partial annihilation of defects at grain boundaries and inside grains and it is accompanied by relaxation of internal elastic stresses. The second stage is characterized by the onset of migration of non-equilibrium grain boundaries which results partially in an abnormal grain growth. Finally the third stage is connected with subsequent normal grain growth. Of course, the model proposed reflects the evolution of nanostructures during heating of SPD materials rather approximately because depending on the rate of heating and time of annealing different stages are often overlapped. Moreover, the picture is more complex in the case of SPD alloys due to the formation and decomposition of supersaturated solid solutions, disordering and reordering during heating.

3.2. A structural model of NSM

The results of the investigations conducted are the basis for development of a structural model of NSM processed by severe plastic deformation [16]. The subject of this model is a description of the defect structure (types of defects, their density, distribution) and atomic crystal structure of NSM and its task is to explain unusual structural features observed experimentally, namely high internal stresses, distortions and dilatations of the crystal lattice, disordering of nanostructured intermetallics, formation of supersaturated solid solutions in alloys, large accumulated energy and others. All these data can be used as a basis for explanation and foreseeing of the unique properties of NSM (Section 4). At the same time, as noted above, typical nanostructures in alloys exposed to SPD are very complex. A more simple example is pure metals in which non-equilibrium grain boundaries are considered to be the main element of the nanostructure resulted from SPD. The structural model of SPD metals can be presented in the following way.

Non-equilibrium grain boundaries in NSM, due to the presence of a high density of extrinsic defects in their structure, are characterized by excess energy and long range elastic stresses. These stresses result in significant distortions and dilatations of the crystal lattice near grain boundaries which are revealed experimentally by TEM and X-ray methods. In turn, atomic displacements in near boundary regions change the dynamics of lattice vibrations and, as a result, changes such fundamental properties as elastic moduli, Debye and Curie temperatures and others (Section 4.1).

Assuming that several types of extrinsic defects are present in non-equilibrium grain boundaries [16,80], namely, stationary GBD with Burgers vectors normal to a boundary plane, gliding or tangential GBDs with Burgers vectors tangential to the boundary plane, and disclinations in triple junctions, the structural model of NSM with a grain size of about 100 nm can be described by a scheme shown in

Fig. 30(a). In this case one can speak about elastically distorted zones-regions of the crystal near the grain boundaries, several nanometers in width, and central portions of grains with a perfect crystal lattice. If the grain size is reduced to 10–20 nm, then the distortions and dilatation of the crystal lattice embrace the whole grain (Fig. 30(b)). In this case, the lattice loses its strict periodicity and a pseudoamorphous structure is formed in NSM. The latter was confirmed experimentally by X-ray structural analysis and TEM studies of nanostructured metals processed by SPD consolidation of ball milled powders with an extremely small grain size of less than 15–20 nm [21,22,44,45].

Nazarov et al. [103–105] proposed the theoretical description of these model concepts. Three non-equilibrium assemblies of dislocations are assumed to exist in
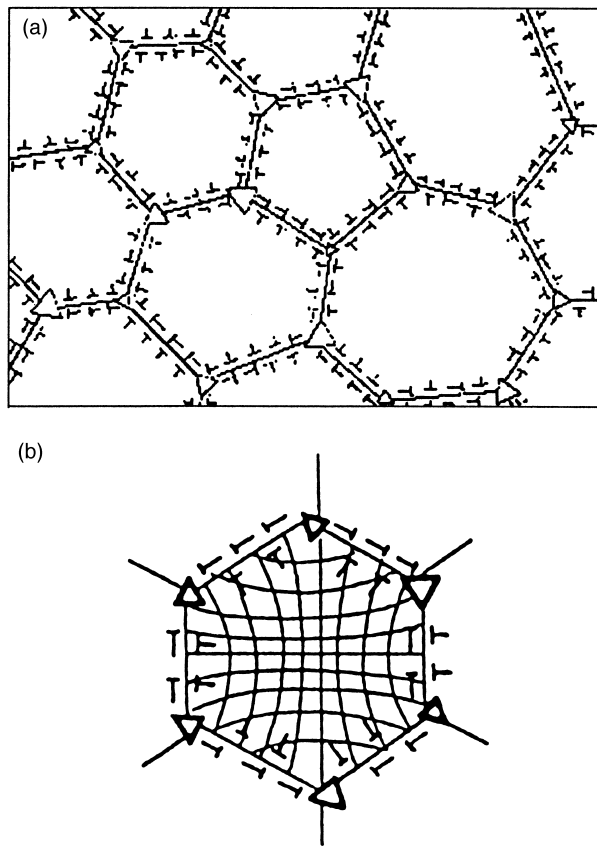
Fig. 30. (a) Schematic representation of a ultrafine grained structure having a mean grain size of about 100 nm. Triangles of different sizes and orientations designate disclinations of different powers and signs. Disclinations and grain boundary dislocations form elastically distorted layers (zones) near grain boundaries. (b) Nanostructured pseudoamorphous solid, i.e. a nanocrystal with dislocations disturbed grain boundaries and highly distorted crystal lattice.

the grain boundaries of NSM. These assemblies are the following: (1) dipoles of junction disclinations resulting from accumulation of sessile GBDs; (2) assemblies of gliding GBDs and (3) disordered arrays of GBDs being a result of non-homogeneous distribution of lattice dislocations in the grain boundaries. All these systems of defects initiate long range stress fields, whose radius of screening exceeds significantly a grain boundary width. Each non-equilibrium assembly of dislocations in the grain boundaries provides an independent contribution to the elastic strain, excess energy and expansion in a volume of NSM.

In the frame of the given approach the following equations were obtained in the works mentioned above. They can be used for determination of the root-mean square elastic strains ε_i caused by assemblies of dislocations at non-equilibrium grain boundaries, the excess energy of grain boundary γ, and the changes in volume of nanostructured materials. In the case of disordered arrays of GBDs these equations have the following form [103,105]:

$$\varepsilon_{\text{disl}} = 0.13\sqrt{\rho_v}\ln(d/b) \tag{9}$$

$$\gamma = \frac{Gb^2\,\rho_v d}{12\pi(1-v)}\ln(d/b) \tag{10}$$

$$\frac{\Delta V}{V} = 0.14b^2\rho_v\ln\left(\frac{d}{b}\right) \tag{11}$$

where ρ is the volume density of dislocations in the material, d is the grain size, b is the Burgers vector, G is the shear modulus, v is the Poisson's coefficient.

Eq. (11) describes the excess volume of NSM attributed to the presence of disordered arrays of GBDs. As known [106], due to non-linear effects, the presence of dislocations can result in an expansion of the crystal whose value is proportional to the elastic energy. This behavior becomes significantly important in the case of high densities of dislocations typical of SPD metals.

In [105] the following equations for assemblies of disclinations were obtained. They were used to estimate their contributions to values of the internal elastic strain ε and the excess energy of grain boundaries γ_{ex}:

$$\varepsilon_{\text{discl}} = 0{,}1\langle\Omega^2\rangle^{1/2} \tag{12}$$

$$\gamma_{\text{ex}} = \frac{G\langle\Omega\rangle d\ln 2}{16\pi(1-v)} \tag{13}$$

where Ω is the power of the disclinations.

Following the works [104,105] let us calculate the contributions of dislocations and disclinations, as well as all defects, to the root-mean square elastic strain, the excess energy of the grain boundaries and the increase in the volume of nanostructured SPD materials.

It is assumed that a typical value of the density of dislocations in severely deformed metals has the order of magnitude $\rho = 6 \times 10^{15}$ m^{-2}. The power of disclinations at junctions cannot exceed values 4–6°, since these values are sufficient for initiation of microcracks. Even at less values of Ω disclinations can be relaxed initiating a process of grain boundary fracture [105]. Thus, one can assume that $\langle\Omega^2\rangle^{1/2} \approx 0.03$. Further, taking $b = 0.25$ nm and $d = 50$ nm from Eqs. (9) and (12) we obtain $\varepsilon_i^{\text{disl}} \approx 5.8 \times 10^{-3}$ and $\varepsilon_i^{\text{discl}} \approx 3 \times 10^{-3}$. Taking into account an additive character of these values, the root-mean square strains and elastic stresses of two assemblies can be summed to attain the total results of these defects. Thus, $\varepsilon_i = [(\varepsilon_i^{\text{disl}})^2 + (\varepsilon_i^{\text{discl}})^2]^{1/2} \approx 6.5 \times 10^{-3}$. Similar values of the root-mean square strain were observed in nanocrystalline Ni_3Al with a grain size of about 50 nm [59].

To estimate the excess energy of grain boundaries in SPD Al alloy one can accept $G = 2.65 \times 10^{-4}$ MPa, $b = 0.29$ nm and $d = 100$ nm. From Eqs. (10) and (13) we obtain $\gamma_{\text{ex}}^{\text{disl}} = 0.30$ J/m^2 and $\gamma_{\text{ex}}^{\text{discl}} = 0.05$ J/m^2 for the case under consideration. Thus, the total excess energy of defects is equal to $\gamma_{\text{ex}} = 0.35$ J/m^2.

The change in the volume of the material caused by internal stresses is proportional to the elastic energy with a coefficient of proportionality depending on the material. To a first approximation this coefficient can be considered similar both for dislocations and disclinations. Consequently, in Al the increase in the volume due to disclinations is less than due to dislocations by approximately a factor of 6. From Eq. (11) it follows that $(\Delta V/V)_{\text{disl}} \approx 4 \times 10^{-4}$ and $(\Delta V/V)_{\text{discl}} \approx 0.7 \times 10^{-4}$, hence the total dilation caused by defects is equal to $\Delta V/V \approx 4.7 \times 10^{-4}$. The experimental values of the increase in the volume measured during dilatometric studies of the SPD Al alloy with a similar grain size have the order of magnitude 10^{-3} [83], i.e. rather close to the calculated value.

Analogously, in the case of Cu with a grain size of 200 nm, the following value of the excess energy of grain boundaries can be obtained from Eqs. (10) and (13): $\gamma_{\text{ex}} \approx 1.2$ J/m^2. This corresponds to the accumulated energy 1.35 J/g. At the same time the measurements by means of the method of differential scanning calorimetry show that during heating of Cu processed by SPTS a value of heat release is equal to 4.58 J/g [107], i.e. it is also close to the calculated value.

In works [100,103,105] were shown the possibilities of applying the concept of non-equilibrium grain boundaries to numerical description of kinetic processes occurring during heating of nanostructured materials, namely low temperature grain growth [100] and the results of dilatometric measurements [71].

Of course, the developing model concepts of non-equilibrium grain boundary defects are still rather simple in character since they consider two and not three-dimensional dislocation assemblies. Moreover, the substituting parameters describing the defect structure of NSM, namely, density of GBDs, their Burgers vectors and others, have only approximate values. At the same time, the new concepts have possibilities for numerical estimates as well as the potential for providing qualitative explanation of basic physical properties of NSM (Section 4) demonstrating their physical reality and usefulness.

4. Properties of nanostructured SPD materials

As already mentioned, the increased interest in nanostructured materials is associated with foreseeing new advanced physical and mechanical properties attributed to their unusual structure. At present it has already been established that many fundamental properties undergo significant changes both in nanostructured materials processed by SPD methods and in nanocrystals processed by other methods, for example by gas condensation [2]. Among these properties the most interesting are changes in Curie and Debye temperatures and saturation magnetization, being commonly structure insensitive, and usually reflecting changes occurring in the atomic crystal structure of solids. Another example is the change in elastic properties which are determined by interatomic interactions as well.

One more important direction, which has been developed intensively in recent years, is investigation of mechanical properties of nanostructured materials. In terms of mechanical properties the formation of nanostructures in various metals and alloys should lead to a high strength of these materials according to the well-known Hall–Petch relationship [108,109] and occurrence of low temperature and/or high strain rate superplasticity [110,111]. Such great interest to physics of strength and plasticity of ultra fine-grained materials is caused by a possible change in mechanisms of plastic deformation since, according to theoretical estimates, initiation and movement of dislocations may be prohibited in grains of a nanometric size [108,112]. In terms of practical application one can expect engineering of new advanced high strength materials and achievement of enhanced superplastic properties.

Until now the majority of investigations relating to mechanical properties of nanocrystals dealt with measurements of microhardness in small samples. However, the data obtained were rather contradictory. For example, in some works [113,114] a negative deviation from the Hall–Petch relationship was observed in the case of small grains while in other works [115,116] an opposite tendency was revealed. One of the reasons responsible for such contradiction can be residual porosity or contaminations in samples, processed via consolidation of different powders. In this connection, great interest in the processing of bulk fully dense samples of nanostructured metals and alloys is quite natural. The fabrication of such materials by means of SPD methods provided an opportunity to start systematic studies of their mechanical properties.

Below we consider the main results of investigations relating to the fundamental parameters of nanostructured materials processed by SPD methods as well as their mechanical properties at room and elevated temperatures.

4.1. Fundamental parameters

Values of some fundamental parameters of nanostructured SPD materials in comparison with coarse-grained analogous are given in Table 3. It is seen that the formation of nanostructures leads to changes in fundamental magnetic

characteristics such as the Curie temperature and saturation magnetization. Though these properties are characteristics of ferromagnetic materials, nevertheless, they reflect features of a nanostructured state.

Significant changes were revealed also in the value of the Debye temperature which was measured by means of X-ray methods and Mössbauer spectroscopy. As shown below, the Debye temperature in the near boundary region can be estimated on the basis of a structural model. The decrease revealed in the Debye temperature manifests an increase in the dynamic properties of atoms which are attributed to changes in the diffusion coefficient as well. As an example, the data for diffusion coefficient of copper in the nanostructured nickel processed by ECA pressing are presented in Table 3.

Among other parameters, changes which are attributed to a nanostructured state, are elastic moduli and ultimate solubility of carbon in α-Fe (Table 3). Let us consider possible reasons for the changes occurred.

4.1.1. Curie temperature and saturation magnetization

The first studies of nanostructured nickel processed by SPTS of monolithic samples demonstrated that a value of saturation magnetization at room temperature was less than in coarse-grained nickel by 3–5% [117,118]. Moreover, investigations of nanostructured nickel with a mean grain size of less than 20 nm which was processed by SPD consolidation of ball-milled powder [119] revealed even more significant changes in magnetic characteristics.

The curves of the temperature dependence of saturation magnetization for nanostructured nickel showed that each cycle consisting of heating up to different temperatures, holding and cooling, results in a change of a curve shape (Fig. 31). In particular, saturation magnetization of the nanostructured nickel after SPD consolidation was less than in the coarse-grained one by 31%. In the nanostructured nickel subjected to annealing at intermediate temperatures from 473 to 873 K one can observe a gradual recovery to a value of saturation magnetization typical of a coarse-grained state. Moreover, in the sample subjected to annealing one can observe some changes in the shape of the $\sigma_s(T)$ curves. In

Table 3
Some fundamental properties of metals in nanostructured (NS) and coarse-grained (CG) states

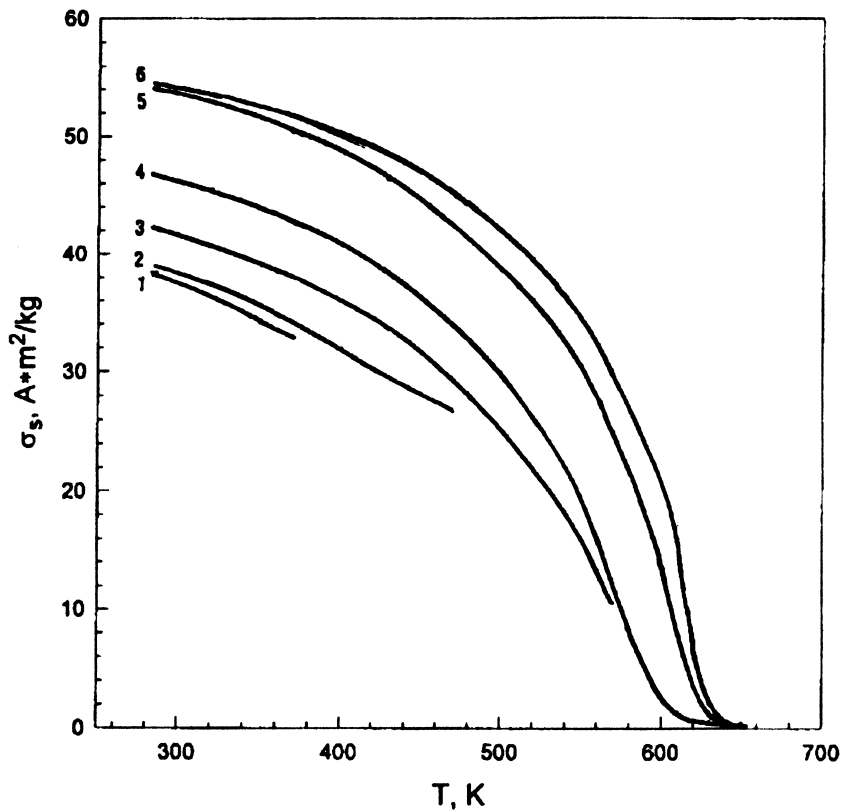| Properties	Materials	Value		Reference
		NS	CG	
Curie temperature, K	Ni	595	631	[119]
Saturation magnetization, Am^2/kg	Ni	38.1	56.2	[119]
Debye temperature, K	Fe	240[a]	467	[98]
Diffusion coefficient, m^2/s	Cu in Ni	1×10^{-14}	1×10^{-20}	[126]
Ultimate solubility at 293 K, %	C in α-Fe	1.2	0.06	[57]
Young's modulus, GPa	Cu	115	128	[130]

[a] For near boundary regions.

Fig. 31. Temperature dependences of saturation magnetization $\sigma_s(T)$ for one and the same nickel sample processed by SPD consolidation of powder after ball milling (curve 1), heating to temperature 373 K (curve 2), 473 K (curve 3), 723 K (curve 4), 873 K (curve 5) and 1073 K (curve 6) holding and cooling at different temperatures.

particular, after annealing at 373 K one can see a small bend which testifies to the existence of another magnetic phase with lower Curie temperature [119]. Annealing of the sample at a higher temperature resulted in disappearance of such a bend and the $\sigma_s(T)$ curves acquired a more usual convex shape.

The character of changes occurring in the Curie temperature seem rather interesting as well. For example, after annealing at 573 K the Curie temperature was 607 K which is significantly lower then the standard T_c for pure nickel equal to 631 K. The complete recovery of T_c to its usual value 631 K was observed only after annealing at 873 K.

To reveal the influence of the process of consolidation on changes in magnetic properties of nanostructured nickel, the $\sigma_s(T)$ dependence of the powder subjected to ball milling was investigated as well. From Figs. 31 and 32 it is seen that the shape of the $\sigma_s(T)$ dependence for this powder was similar to the one for the compacted sample. However, in the case of the powder the maximum difference

between σ_s in starting and annealed states was only 16%, while its Curie temperature after annealing at 573 was 618 K.

The decrease in σ_s and T_c observed in the powder and the sample subjected to SPD consolidation cannot be connected only with a small grain size in the structure of the nickel, since the grain size was similar in both cases. At the same time their magnetic characteristics differed significantly. On the other hand, as noted above, significant distortion of the crystal lattice was typical to the nickel under study, and after SPD these distortions were more significant. As a result, the structure of the nanostructured SPD nickel approaches the structure where the distribution of atoms inside a grain interior becomes not fully periodic (Section 3.2). Similar to the amorphous state [120], a non-periodic character can lead to a sharp decrease in σ_s and T_c values. The presence of a wide spectrum of interatomic distances in some crystal area is responsible for significant changes in exchange energy due to its special sensitivity to atom–crystal structure [121]. This,
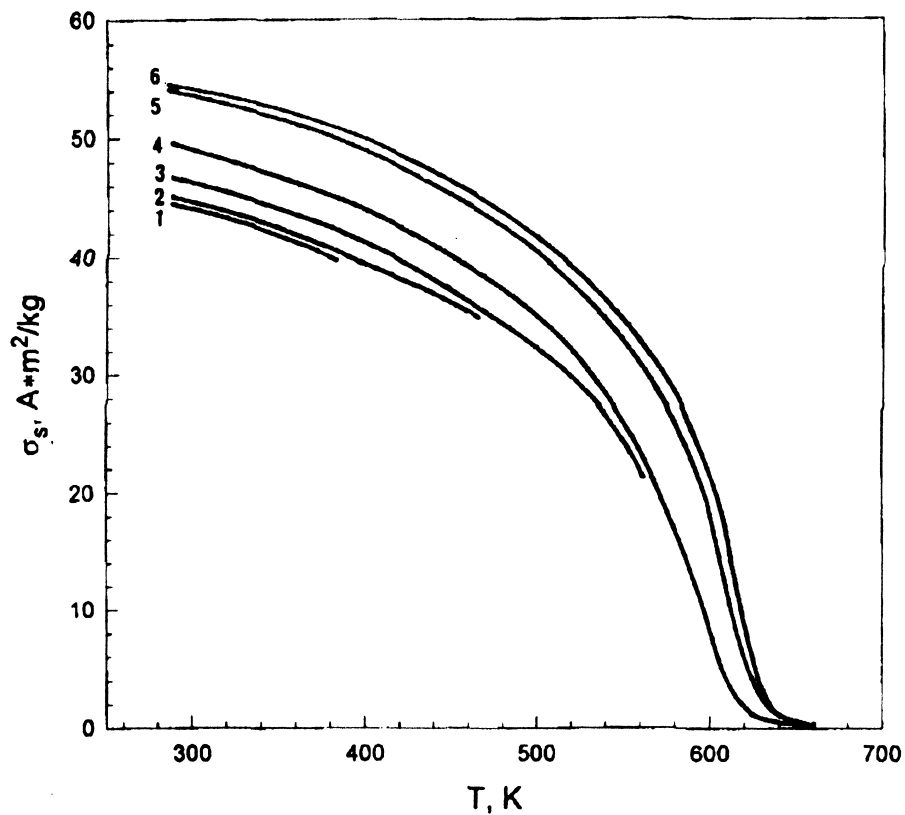

Fig. 32. Temperature dependence of saturation magnetization $\sigma_s(T)$ for ball milled nickel powder in the initial state (curve 1), after heating to temperature 373 K (curve 2), 473 K (curve 3), 723 K (curve 4), 873 K (curve 5) and 1073 K (curve 6) holding and cooling at different temperatures.

in turn, decreases spontaneous magnetization within the whole volume of the ferromagnetic phase and lowers the value of the Curie temperature. The decrease in crystal lattice distortion starts during heating even prior to the onset of intensive grain growth and this results in recovery of the values of magnetization and the Curie temperature [119].

4.1.2. Debye temperature

In SPD metals the Debye temperature has been determined on the basis of the dependence of the Debye–Waller parameter on temperature [94]. The results of calculations showed that for nanostructured nickel the Debye temperature was 293 K, being significantly less than the usual value for nickel equal to 375 K. At the same time, the Debye temperature in nanostructured copper was equal to 233 K which is less than the usual value by 23%.

Changes in the Debye temperature were first revealed in nanostructured metals fabricated by gas condensation [2,122]. It was assumed that such changes in the Debye temperature are attributed to an increased amplitude of thermal vibrations of atoms in grain boundaries and an elevated concentration of point defects in near grain boundary regions.

The grain size in nanostructured copper and nickel processed by SPD is usually significantly larger than the grain size in typical nanocrystals processed by gas condensation. Due to that, the changes in the Debye temperature observed in these materials cannot be connected only with atoms in grain boundaries since their amount is not sufficient for that. However, due to non-equilibrium grain boundaries and long range elastic stress fields, nanostructured SPD materials display elevated static and dynamic atomic displacements in some zone — near boundary regions (Section 3.2). Taking into account this fact one can assume that the main reason for decreasing the Debye temperature in nanostructured SPD copper and nickel is its reduced value in elastically distorted near boundary regions, whereas inside the grain interiors the Debye temperature is similar to that in coarse-grained samples.

The results of calculation [94] of the Debye temperature in near boundary regions gave a value of 127 K for nanostructured nickel which is significantly lower (almost by 200 K) than the corresponding normal value for nickel.

An analogous conclusion has been made recently on the basis of the results of Mössbauer studies of nanostructured iron processed by SPTS [98] (Section 3.1). In this case the relative intensity of subspectra of grain boundary and granular phases was studied at different temperatures and it was established that the Debye temperature of the grain boundary phase in the nanostructured iron is also lower than in coarse-grained iron by 200°C.

The lower Debye temperature in near boundary regions of nanostructured SPD materials shows the increased dynamic activity of their atoms. As a result one can expect enhanced diffusion rates.

4.1.3. Diffusivity

Diffusion processes occurring in nanostructured materials were an object of

intense studies [123–125]. However, the obtained experimental results are ambiguous due to structural varieties during the process of diffusive experiments. However, the sharp acceleration of diffusion in these materials is not in any doubt.

The kinetics of diffusion processes in nanostructured SPD materials were investigated in several works [126–128]. In particular, the investigations of copper diffusivity in nanostructured nickel having a copper coating were conducted in [126]. Experiments on determination of the depth of copper penetration into nickel were conducted by means of secondary ion mass-spectroscopy. Comparative diffusion experiments were conducted at temperatures of 423 and 523 K for 3 h using ECA-pressed nanostructured and coarse-grained nickel.

Under the given conditions copper atoms were not detected in the coarse-grained nickel even at a depth of 2 μm. At the same time, the diffusive copper fluxes in nanostructured nickel penetrated to a depth greater than 25 and 35 μm at 423 and 573 K, respectively (Fig. 33). The calculations of the grain-boundary diffusion coefficients of copper in nanostructured nickel were based on these data. The volume diffusion was assumed to be practically absent.
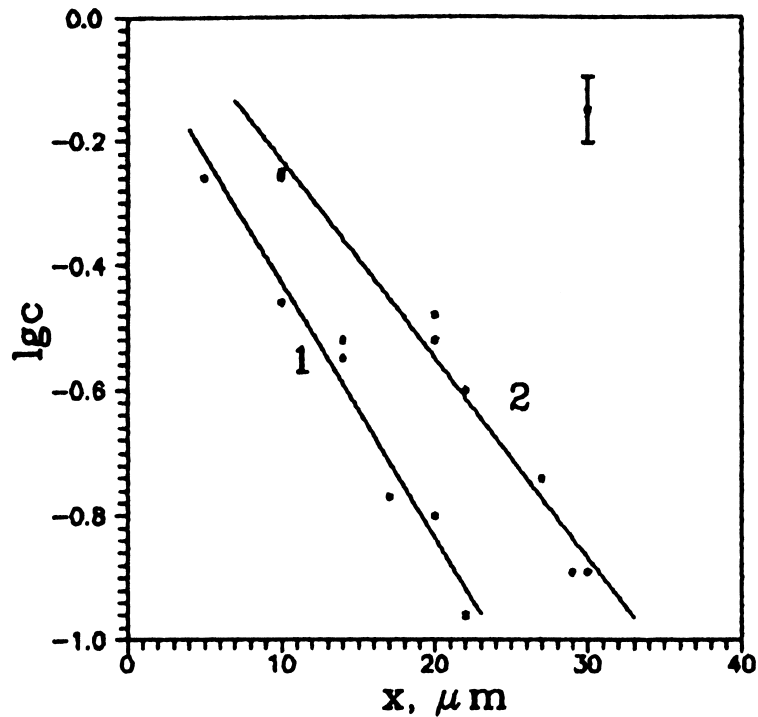

Fig. 33. Concentration profiles of copper penetration into nanostructured nickel: $1 - T = 423$ K; $2 - T = 573$ K.

At 423 K grain boundaries were found not to migrate in nanostructured Ni. Accordingly, the diffusion coefficient could be determined using the equation describing the change of the grain-boundary impurity concentration vs time in the C regime [129]:

$$c = c_0 \text{erfc} \frac{x}{2\sqrt{D_b t}} \qquad (14)$$

where c_0 and c are the concentrations of copper on the source's surface, x is the depth, respectively and t is the time of the diffusion anneal. The value x is the distance from the surface at which $\log c = -1$ ($c = 0.1\%$, which corresponds to the resolution limit of the SIMS unit). The value of c_0 was obtained by extrapolation of the experimental concentration curve at $x \rightarrow 0$. In this case $D_b = 1 \times 10^{-14}$ m^2/s ($t = 3$ h).

During annealing at 573 K grain growth occurs in nanostructured nickel. Reasoning from kinetics, it was estimated the nickel grain boundaries migrate with a velocity of $V \approx 7 \times 10^{-11}$ m^2/s. In this case D_b could be calculated from the equation [129]:

$$c = c_0 \exp\left(-x\sqrt{V/D_b \beta}\right) \qquad (15)$$

Considering the diffusion width of the boundary $\beta = 10^{-8}$ m one can obtain that $D_b = 1.4 \times 10^{-12}$ m^2/s.

These experimental data demonstrate the increase in the grain boundary diffusion coefficient of copper in nanostructured nickel in comparison with the coarse-grained nickel. According to the data presented in [126] this difference is of 4–6 orders.

The enhanced diffusivity and permeability of grain boundaries which was revealed in other nanostructured SPD materials [127,128] is important evidence for a specific structure of their boundaries. Further investigation aimed at developing numerical models of diffusivity in nanostructured materials are very urgent. At the same time one can assume that the concept of non-equilibrium grain boundaries suggesting their enhanced free volume, excess energy and long range stresses should be important for these investigations (see Section 3.2).

4.1.4. Elasticity

The detailed studies of the elastic properties of nanostructured copper samples processed by ECA pressing were conducted in [130], where elastic moduli were determined by means of an ultra sound method. To estimate the possible anisotropy of elastic properties attributed to texture which occurs during deformation the measurements of the velocity of longitudinal waves were made in three space directions. The measurements of transverse waves were made in two opposite polarizations in the plane of vibrations.

The conducted investigations showed that three specific regions can be distinguished on curves of the dependence of velocities of longitudinal and

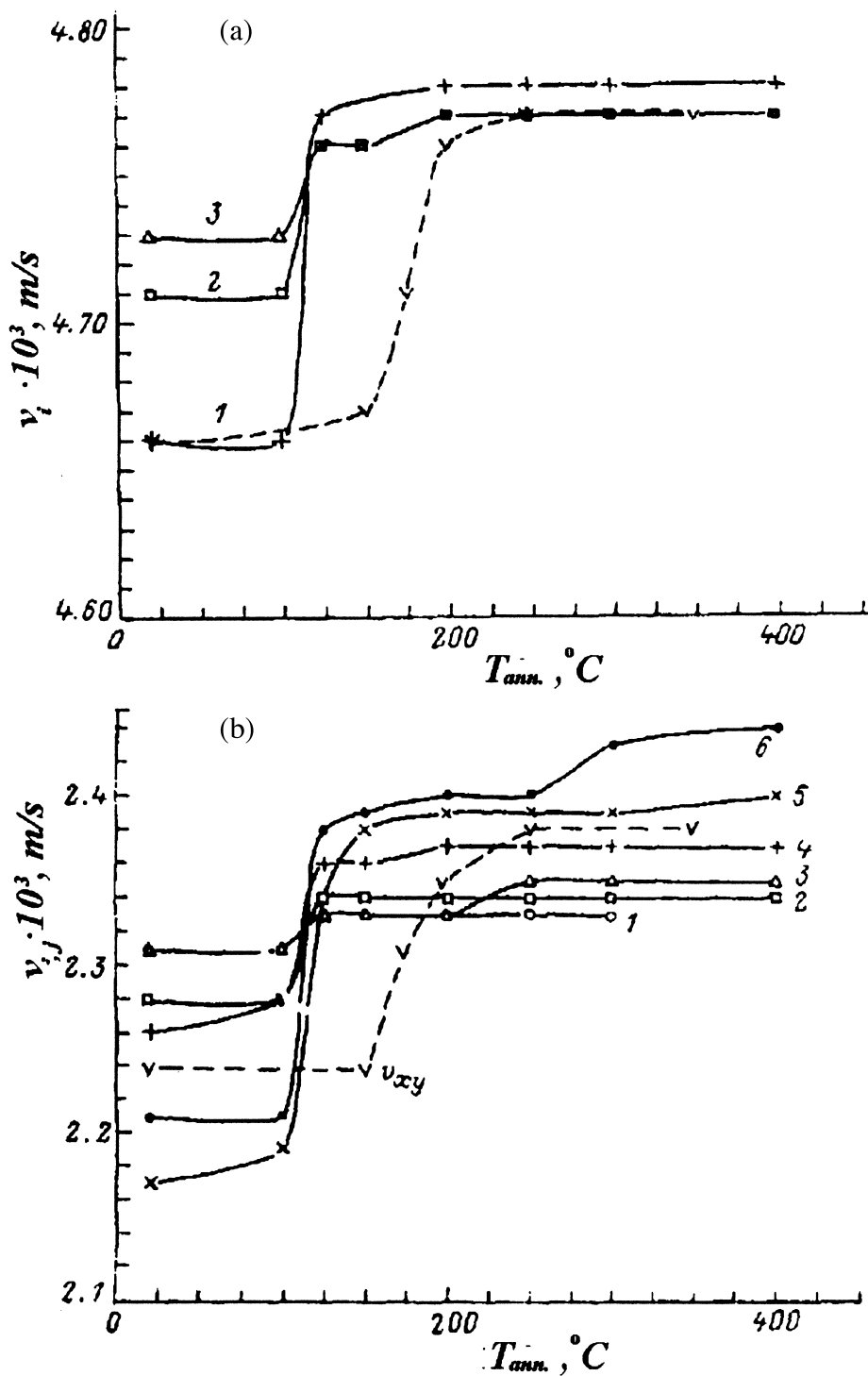Fig. 34. Velocities of longitudinal (a) and transverse (b) ultra sound waves in three mutually perpendicular directions (the x axis is along the axis of deformation) depending on temperature of annealing for copper samples (purity 99.997%). Analogous dependencies for copper (purity 99.98%) are marked by dash lines a:1 $- v_x$, 2 $- v_y$, 3 $- v_2$; b:1 $-_{yo}$ 2 $- v_{y2}$, 3 $- v_{2x}$, 4 $- v_{2y}$, 5 $- v_{x2}$, 6 $- v_{xy}$

transverse ultra sound waves on temperature of annealing for nanostructured copper (purity 99.997%) (Fig. 34). In the first region (up to $T = 100°C$) no significant changes in the velocity of longitudinal waves are observed, while the velocity of transverse waves in two directions, one in the direction of polarization, are slightly increased. At the same time a small distinction between the absolute values of the velocity along different directions of penetration is observed. This distinction is evidently connected with the texture of deformation.

Annealing at temperatures about 125°C leads to a sharp increase in sound velocity along all directions. The velocity of longitudinal waves is increased by 3% and that of transverse ones by 8%. With increasing temperature of annealing up to 150°C and higher (up to 500°C) changes in the values of velocity are insignificant. The character of changes of sound velocities with increasing temperature of annealing for copper with a purity of 99.98% is similar to the one of copper with a purity of 99.997% (Fig. 34), though the decrease in the material purity results in an increase of the temperature at which a sharp rise in sound velocities is observed, up to 175°C.

The measurements of ultra sound velocities obtained were used to calculate elastic moduli. As compared to coarse-grained copper, values of these moduli in nanostructured copper were lower by 10–15% [130]. The comparison of the elastic moduli behavior after annealing with TEM data allowed the conclusion that the transformation of non-equilibrium grain boundaries to an equilibrium state is responsible for the main recovery of elastic moduli in nanostructured copper, whereas with increasing grain size to more than 1 μm elastic moduli show almost no change.

Following [130] let us consider the possible reasons for such large changes in the elastic moduli of nanostructured copper after annealing. The analysis of various mechanisms showed that neither internal stresses nor lattice dislocations can cause such changes in elastic moduli. At the same time, if it is assumed that the elastic moduli of near boundary regions differ from the elastic moduli of an ideal crystal, then the overall moduli of nanostructured material could be combinations of the elastic moduli of the matrix and of the near grain boundary region. In this case, since near boundary regions constitute a significant volume of nanostructured materials, a noticeable change of moduli is observed in these materials. The estimates showed that the change in elastic moduli observed in nanostructured copper can be explained if we accept that the value of the elastic modulus of the near boundary regions is 15–17% of the value of the elastic modulus in coarse-grained metal.

Lower values of elastic moduli in copper and copper composites exposed to ECA pressing were also revealed in other works [131–133] where the ultra sound method and measurements of internal friction were used.

4.1.5. Internal friction

The study of internal friction in nanostructured copper processed by ECA pressing was considered in works [133,134] dealing with investigations of its

amplitude and temperature dependence by means of a method of a torsion pendulum.

It was revealed that a high level of the background internal friction is observed in nanostructured copper. The level of background in nanostructured copper is higher than in coarse-grained copper processed by annealing at high temperatures, by a factor of 4–5. Simultaneously it is higher by a factor of 2–3 as compared to the level of damping for gray cast iron (50×10^{-4}) being a criteria for damping [135,136].

For determination of the temperature dependence of internal friction [133] ECA-pressed Cu was first heated from 4 to 400 K. Then the sample was cooled to 4 K and the measurements were conducted again during heating to a higher temperature of 500 K. Such experimental procedure was performed several times with an upper temperature increased subsequently up to 500, 600 and 650 K, i.e. measurements were made over several cycles.

The results showed (Fig. 35) that the internal friction behavior of nanostructured copper (curves 1 and 2) differed significantly from coarse-grained copper (curve 4). In particular, in nanostructured copper the onset of the intense growth of the internal friction is significantly lower (by 120 K) and the curve has a strong maximum at 475 K. The presence of this peak which is called a grain boundary peak, is conditioned by intensification of grain boundary sliding in the material. According to [133,134] the significant difference in temperature dependence of internal friction revealed between nanostructured and coarse-grained copper can be attributed not only to different grain size but also to transformation of non-equilibrium grain boundaries to an equilibrium state during annealing above 500 K.

In conclusion we can summarize that the recent investigations demonstrate a number of anomalies of fundamental characteristics in nanostructured SPD materials. These changes are associated not only with small grain sizes but also
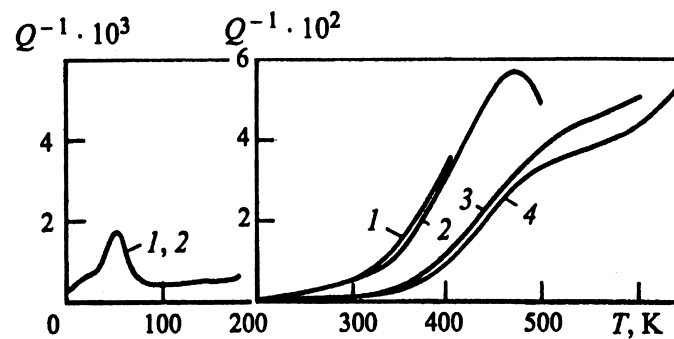

Fig. 35. Temperature dependencies of internal friction of nanostructured copper measured at consequent cycles of heating (the low temperature region is given with $10 \times$ magnification of an internal friction scale): 1,2,3,4 — internal friction during heating from 4 to 400, 500, 600, 650 K, respectively.

with specific defect structure connected with non-equilibrium grain boundaries. Therefore, the modeling of nanostructured materials (Section 3.2) can be useful for explanation of such anomalies.

4.2. Mechanical properties and behavior

Mechanical properties of nanostructured materials have a special interest among researchers in the material science due to their expected enhanced strength and superplastic properties. However, nanocrystalline materials with a grain size of 20–40 nm fabricated using methods of gas condensation or ball milling with subsequent consolidation usually exhibit low tensile ductility and are apt to strong localization of strain [3,5]. It is still difficult to say unambiguously whether this is caused by poor consolidation or whether some intrinsic physical reason is responsible. In this connection, the results of investigations concerning mechanical behavior of nanostructured metals and alloys processed by SPD methods seem very interesting and useful. These results are given in the present section. Special attention is focused on investigations of the influence of specific defects in the nanostructure on the high strength and fatigue behavior which are investigated at room temperature, as well as superplastic properties revealed at elevated temperatures.
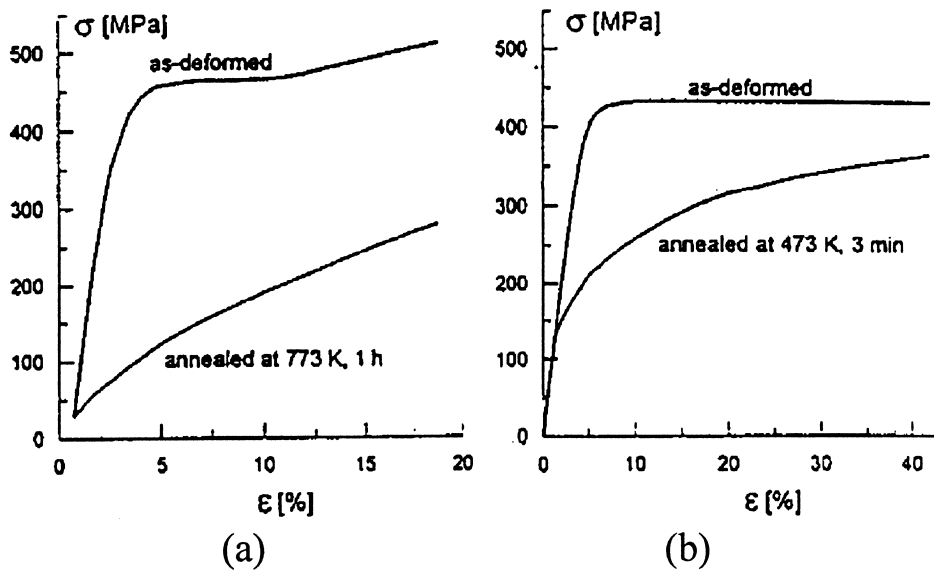

Fig. 36. True stress–strain curves in nanostructed copper at room temperature: (a) tension, (b) compression.

4.2.1. Strength behavior

Let us first consider the results of mechanical tests of nanostructured copper which was used as a model material in a number of recent investigations [48,52,109,137]. As shown in Section 2, ECA pressing of copper conducted using optimal regimes can lead to the formation of a uniform nanostructure with a mean grain size of 200–300 nm and mainly high angle grain boundaries. However, these boundaries are essentially non-equilibrium. Fig. 36 shows true stress–strain curves of ECA pressed copper in tension and compression in comparison with curves from fully annealed Cu after 1 h at 773 K [109,137]. As compared to the well annealed coarse-grained state (Fig. 36(a)), the behavior of nanostructured copper, is characterized by two significant distinctions: firstly, there is a very high value of yield strength close to 400 MPa, and, secondly, there is significantly less strain hardening, though ductility is still high. Fig. 36(b) shows the stress–strain curve for the ECA pressed Cu sample before and after short annealing at 473 K for 3 min. Such short annealing does not lead to a noticeable growth of grains, but results in recovery of the defect structure of the grain boundaries and a sharp decrease of internal stresses [137]. In spite of the similar grain size, there is a significant difference in the deformation behavior of these two states. After short time annealing the stress–strain curve becomes similar to that of the coarse-grained copper. This result is very important and shows that not only the mean grain size but also the high density of defects in the grain boundaries can influence the strength properties of nanostructured materials.

Analysis of the origin of these effects [52,109] shows that it can be connected with enhanced processes of recovery at grain boundaries and a change in deformation mechanisms in nanostructured metals. The density ρ of dislocations during deformation is expressed by the equation [52]:

$$\rho = \frac{\alpha \cdot \dot{\varepsilon} \cdot \tau}{b \cdot d} \tag{16}$$

where b is the Burgers vector, d is the grain size, $\dot{\varepsilon}$ is the strain rate, a is a geometric factor and τ is the time of absorption of dislocations by grain boundaries.

Taking $\rho \approx 10^{15}$ m^{-2}, $b = 2.5 \times 10^{-10}$ m, $d = 2.1 \times 10^{-7}$ m, $\dot{\varepsilon} = 1.4 \times 10^{-3}$ s^{-1} and $\alpha = 2.4$, in Eq. (16), we obtain $\tau = 15$ s.

In accordance with models of recovery at grain boundaries [138,139] the τ value is described by the equation:

$$\tau = \frac{0.03 \cdot K \cdot T \cdot H}{G \cdot \Omega \cdot D_b \cdot \delta} \tag{17}$$

where K is Boltzmann's constant, T is the absolute temperature, G is the shear modulus, $\delta = 10^{-9}$ m is the grain boundary thickness, Ω is the atomic volume, H = 30 nm is the distance of spreading of a dislocation image at grain boundaries in TEM before disappearing [70,138]. Assuming $D_b = D_0 \exp(-Q/RT)$, where $D_0 = 2.35 \times 10^{-5}$ m^2/s, the value of activation energy of grain boundary diffusion

in the ultra fine-grained copper is $Q = 78$ kJ/mol [52]. This value is lower than the activation energy for grain boundary diffusion in conventional coarse-grained copper which is $Q = 107$ kJ/mol. These data as well as the results of other investigations (Section 3.1) testify to the enhanced diffusivity in grain boundaries in nanostructured materials. In turn, the accelerated diffusion leads to intensification of processes of recovery at grain boundaries and the development of grain boundary sliding which can be responsible for the observed absence of noticeable strain hardening during deformation of ultra fine-grained metals. On the other hand, a high value of yield strength is probably connected with difficulties of dislocation generation from non-equilibrium grain boundaries in nanostructured metals [100]. From this point of view the influence of short time annealing at 473 K on a sharp decrease in the yield strength and appearance of strain hardening in the ultrafine-grained copper (Fig. 35(b)) can be explained by the fact that at grain boundaries with more equilibrium structure the dislocation generation is facilitated and the rate of recovery at these grain boundaries is decreased.

Another interesting example of the deformation behavior of nanostructured materials is the mechanical properties of titanium subjected to severe torsion straining [50]. The samples fabricated had a disc shape, about 10 mm in diameter. That is why bending tests were used for their investigation. The tests conducted resulted in obtaining interesting data on the yield strength (σ_y), the ultimate strength (σ_u) and the maximum value of deflection (Δ).

By TEM studies of titanium subjected to severe torsion straining (Fig. 37) it was revealed that their mean grain size is about 100 nm. The TEM studies also revealed high angle misorientations of neighboring grains. A complex non-uniform contrast inside the grains was observed on dark field images. This shows the

Fig. 37. TEM micrograph of titanium subjected to severe torsion straining.

presence of significant elastic strains and strong distortions of the crystal lattice. As TEM shows, noticeable structural changes start in the SPTS Ti during annealing at a temperature of 250°C and above. These changes concern, first of all, decrease of distortions of the crystal lattice which are observed distinctly on the dark field image. In this case, the mean grain size appears to become a bit larger, though migration of the grain boundaries has not started yet. The growth of grains in titanium subjected to SPD starts after annealing at $T = 350$°C. Grain boundaries become straighter and a banded contrast, typical of equilibrium annealed boundaries, is often observed.

The results of measurements of microhardness and bending tests (Fig. 38) showed that after SPD the microhardness and strength of titanium achieved their maximum values which were higher than in the annealed coarse-grained state by a factor of 3. After subsequent annealing H_v remains almost constant up to 300–350°C, but then, above 350°C decreases sharply. At the same time, the yield strength decreases significantly after annealing at 250°C. The ductility of nanostructured titanium measured on the basis of the maximum deflection in bending is small in the initial state but increases significantly after annealing and is equal to 0.33 mm at 250°C. The maximum values of H_v and the ultimate strength are observed at this temperature too. Such a combination of very high strength and significant ductility of the material is very attractive for its practical application.

On the basis of the results obtained one can make two conclusions. First, it becomes evident that the known empirical relationship $H_v = 3\sigma_y$ is not fulfilled in nanostructured materials if initial and annealed states are investigated. This can be explained as follows. The yield strength corresponds to the onset of plastic deformation i.e. a mean strain of < 1%, but microhardness corresponds to a mean strain of 9–10% [140]. Consequently, one can expect that in the case of strong variations in strain hardening there will be significant differences in the $H_v - \sigma_y$
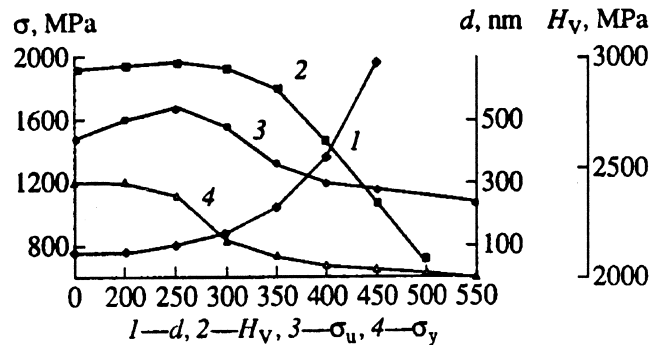

Fig. 38. Dependence of a mean grain size and mechanical properties of nanostructed titanium on the annealing temperature.

dependence between annealed samples, where deformation strengthening is significant and initial nanostructured ones, where deformation strengthening is insignificant. These results indicate that the $H_v = 3\sigma_y$ relationship should be used rather cautiously for investigations of mechanical properties of NSMs.

Second, the yield strength in nanostructured materials varies substantially depending on the defect structure of the grain boundaries (see, for example, Figs. 36 and 38), while the grain size remains the same, indicating the necessity to consider the role of the defect structure in investigation of the Hall–Petch relationship. Evidently, it is lack of attention to the structure of the grain boundaries that can explain the existence of contradictions in the data available on this matter [108].

The application of severe plastic deformation in alloys can provide even higher strength properties due to concurrent formation of nanostructure and metastable states and subsequent aging.

For example, to attain high strength in the 1420 aluminum alloy (Al-5.5%Mg-2.2%Li-0.12%Zr) [141], the alloy was exposed sequentially to quenching, severe torsion straining, and aging at 120°C. The temperature of aging was chosen with concurrent aims of preserving small grain size and providing precipitation of fine dispersed particles of second phases. Structural investigations of the alloy after quenching showed the absence of second phase particles. At the same time it was revealed that the mean grain size of the aluminum base matrix alloy is equal to 10 μm. The microhardness of the samples after quenching was 540 MPa in this case (Table 4).

SPTS of the 1420 alloy led to the formation of a nanostructure with a mean grain size of 70 nm (Fig. 39) [141] having a high level of internal elastic stresses and strong distortions of the crystal lattice. After SPD there was a significant increase in the microhardness of the alloy up to 1750 MPa. This level of microhardness was preserved even after of annealing for 30 min at 150°C. As the temperature of annealing was increased a significant decrease in the microhardness of the alloy was observed. This decrease is connected with relaxation of the structure and the onset of grain growth. Aging of samples at 120°C for 24 h did not change the mean grain size of the matrix alloy but resulted in precipitation of second phase particles having a size of about 20 nm. The microhardness of the nanostructuctured 1420 alloy after aging was increased to 2300 MPa in this case.

The processes of aging occurring in Al–Fe based alloys are also rather interesting. The components of these alloys are immiscible in the cast state but can form a supersaturated solid solution after severe plastic deformation (Section

Table 4
Microhardness of aluminum alloys (MPa) before and after SPTS

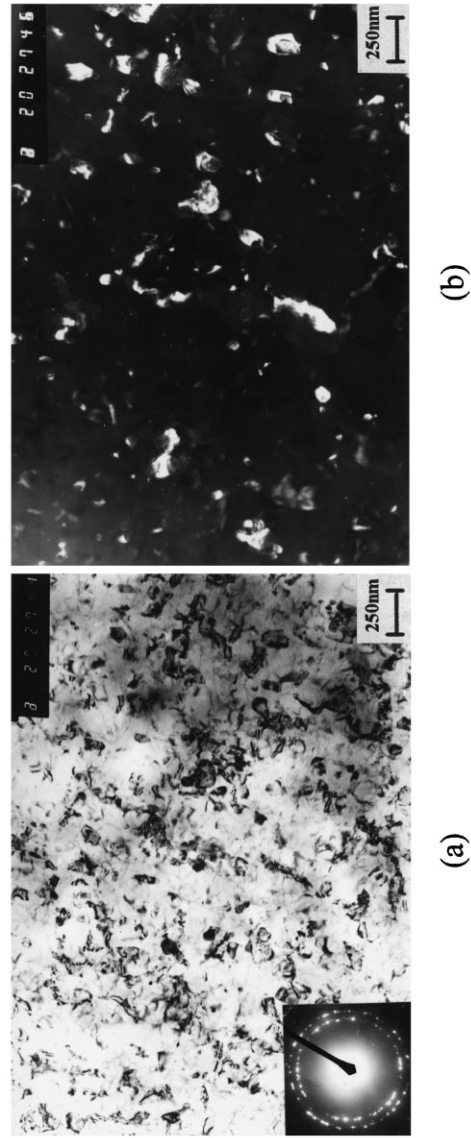| Alloy	1420	Al-11wt%Fe
As-quenched	540	–
After severe straining	1750	1650
After aging	2300	3020

Fig. 39. TEM micrographs of Al 1420 alloy after quenching and severe torsion straining: (a) bright field image and diffraction pattern, (b) dark field image.

2.2) [142]. For example, the Al-11%Fe alloy in the initial cast state had a dendrite type structure containing the aluminum matrix phase with a mean grain size of about 15 μm and the $Al_{13}Fe_{14}$ dendrite phase with a monocline type structure. SPD resulted in a homogeneous ultra fine-grained structure in which the aluminium matrix had a mean grain size of about 100 nm and the $Al_{13}Fe_{14}$ was homogeneously distributed in the form of separate particles, 0.3–1 μm in size. The EDS analysis of the Al matrix showed that it contained additionally 2.2 wt%Fe in the solid solution (Fig. 40), whereas the amount of Fe in particles of the $Al_{13}Fe_{14}$ phase was 22.6 at%.

The microhardness of the alloy in the initial state was 750 MPa, but after SPD it was 1650 MPa, and increased significantly after annealing at 100°C for 5 h (Table 4). The latter shows the effect of intensive aging of the alloy. After aging the microhardness in the Al-11%Fe alloy exceeded 3000 MPa.

4.2.2. Fatigue

Fatigue is the cyclic mechanical behavior of materials, and an increase in strength of metals and alloys in the nanostructured state allows one to expect an increase in fatigue strength as well. However, our present knowledge of the fatigue behavior of nanostructured materials is rather poor and requires further expansion [143–145]. It has been shown that the formation of nanostructures from SPD results in a significant increase in fatigue strength and durability (Section 4.4), but some data obtained on low cyclic fatigue of copper [144,145] subjected to ECA pressing seem contradictory. The fatigue behavior of copper processed by ECA pressing over the strain value range $\Delta\varepsilon_{pl} = 4 \times 10^{-4} - 1 \times 10^{-3}$ was studied in the work [145]. In Fig. 41 one can see curves of cyclic behavior of four copper samples: two samples after ECA pressing, the third sample after additional short time annealing at 473 K for 3 min, its grain size remaining the same, and finally, the fourth sample after annealing at 773 K which results in significant grain
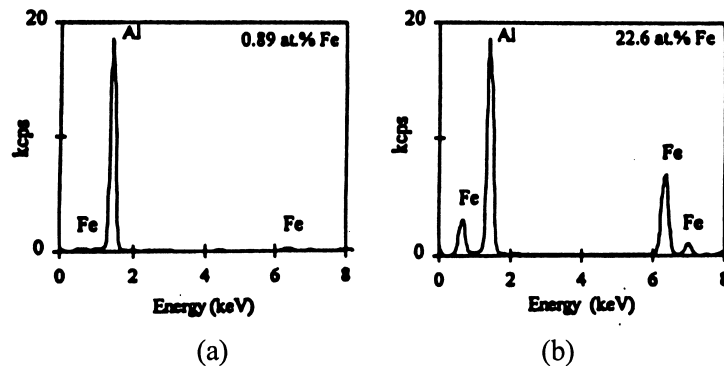

Fig. 40. EDS spectrum of the Al-11%Fe alloy subjected to severe torison straining: (a) spectrum from the matrix, (b) spectrum from the $Al_{13}Fe_4$
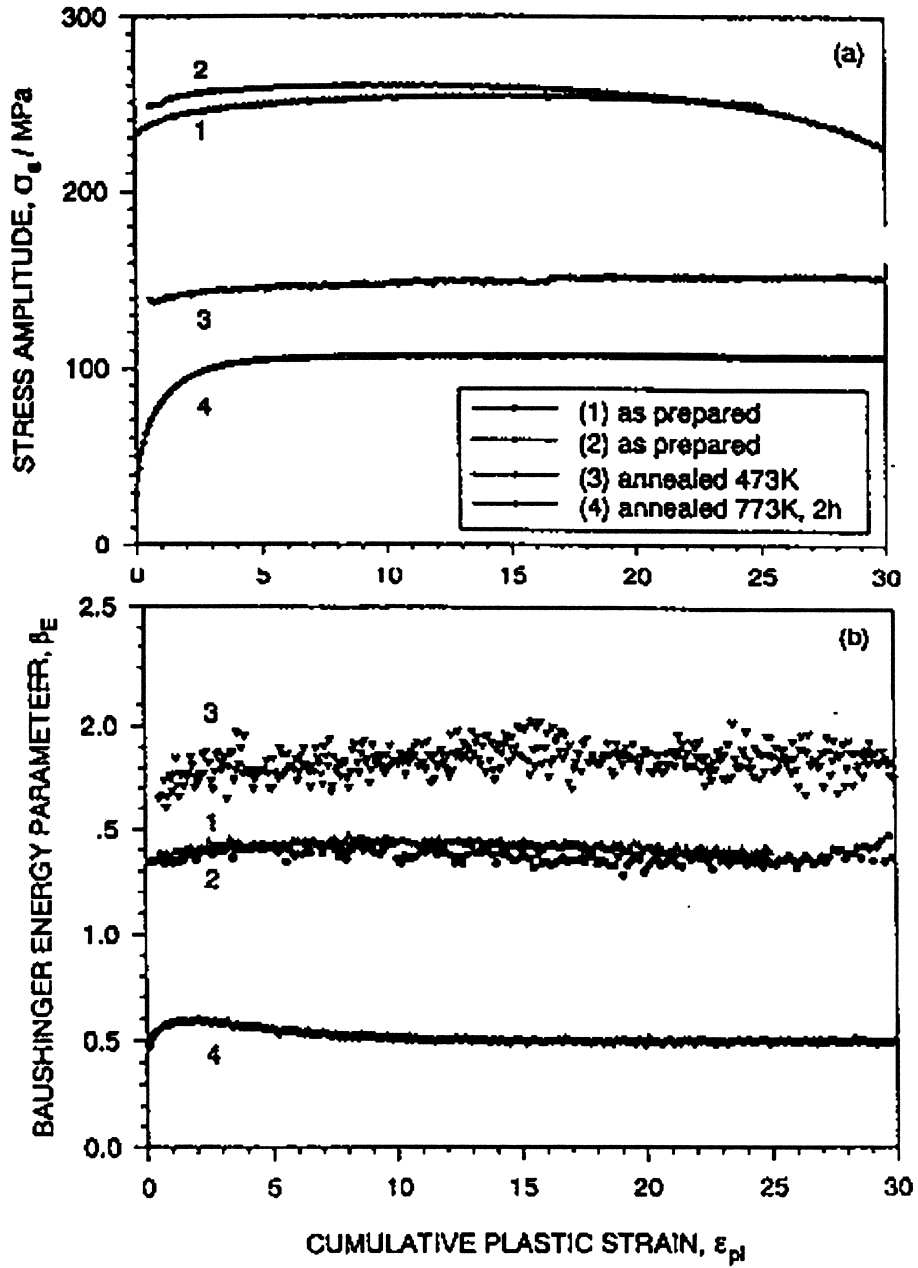
Fig. 41. Fatigue behavior of nanostructured copper: (a) curve of cyclic strengthening, (b) changes in the parameter of Bauschinger energy depending on accumulated plastic deformation.

growth, up to 50 μm. It is seen that after several cycles saturation is observed in all samples, but the saturation stresses, $\langle\sigma\rangle$, differ substantially.

Significant differences in fatigue behavior of ultra fine-grained and coarse-grained copper are seen in Fig. 41. Changes in the Bauschinger energy β_E which depends on accumulated plastic deformation are shown in this figure. The value β_E was calculated from the shape of the hysteresis loop by means of the equation [145]

$$\beta_E = \frac{2\sigma_p \cdot \Delta\varepsilon_{pl} - \oint_{loop} \sigma \cdot d\varepsilon}{\oint_{loop} \sigma \cdot d\varepsilon} \tag{18}$$

where σ_p is the maximum stress attained at tension and compression, $\Delta\varepsilon_{pl}$ is the amplitude of cyclic deformation.

The larger the value of β_E, the greater is the Bauschinger effect. From Fig. 41 it is seen that in all states β_E weakly depends on accumulated deformation but its maximum value is observed in the ECA-pressed Cu subjected to additional short time annealing. This attests to a noticeable influence of recovery of the non-equilibrium state of the grain boundaries on the fatigue behavior of the ultra fine-grained copper.

In contrast, cyclic softening similar to conventional cold deformed copper was manifested by ECA-pressed copper in [144]. Special investigations were conducted recently in [146] to reveal the reasons responsible for these differences in fatigue behavior of Cu after ECA-pressing. As noted in Section 2.2, different types of nanostructure can be formed depending on the regimes of ECA pressing. These nanostructure types differ significantly in their homogeneity within the sample volume and in the misorientations of the grains. This approach was used in [146] where the comparative behavior of two types of ECA-pressed copper samples was studied. One sample had a rather homogeneous ultra fine-grained structure, while in the other there were banded structures with elongated grains and fragments of low angle grain boundaries. The fatigue tests showed that under conditions of a constant amplitude of deformation a stage of cyclic saturation (strengthening) is observed in the first sample, while in the second sample a stage of cyclic dishardening (softening) is observed. Moreover, significant differences in the Bauschinger energy as well as in strain localization and surface morphology were also observed in these samples. The results obtained demonstrate the significant influence of the nanostructure type resulting from SPD on fatigue behavior and this question requires further investigations.

4.2.3. Superplasticity

Superplasticity of materials is a phenomenon of very high ductility providing hundreds and thousands elongation during tension (the most rigid mode of mechanical tests) which is observed in microcrystalline materials with a grain size being usually less than 10 μm and deformed in a definite temperature–strain rate

interval, as a rule, $T = 0.5$–$0.6T_m$ (T_m is the melting temperature) at the strain rates 10^{-3}–10^{-4} s^{-1} [147,148].

It is also well-known that superplastic flow of such microcrystalline materials is often described by a constitutive equation of the form:
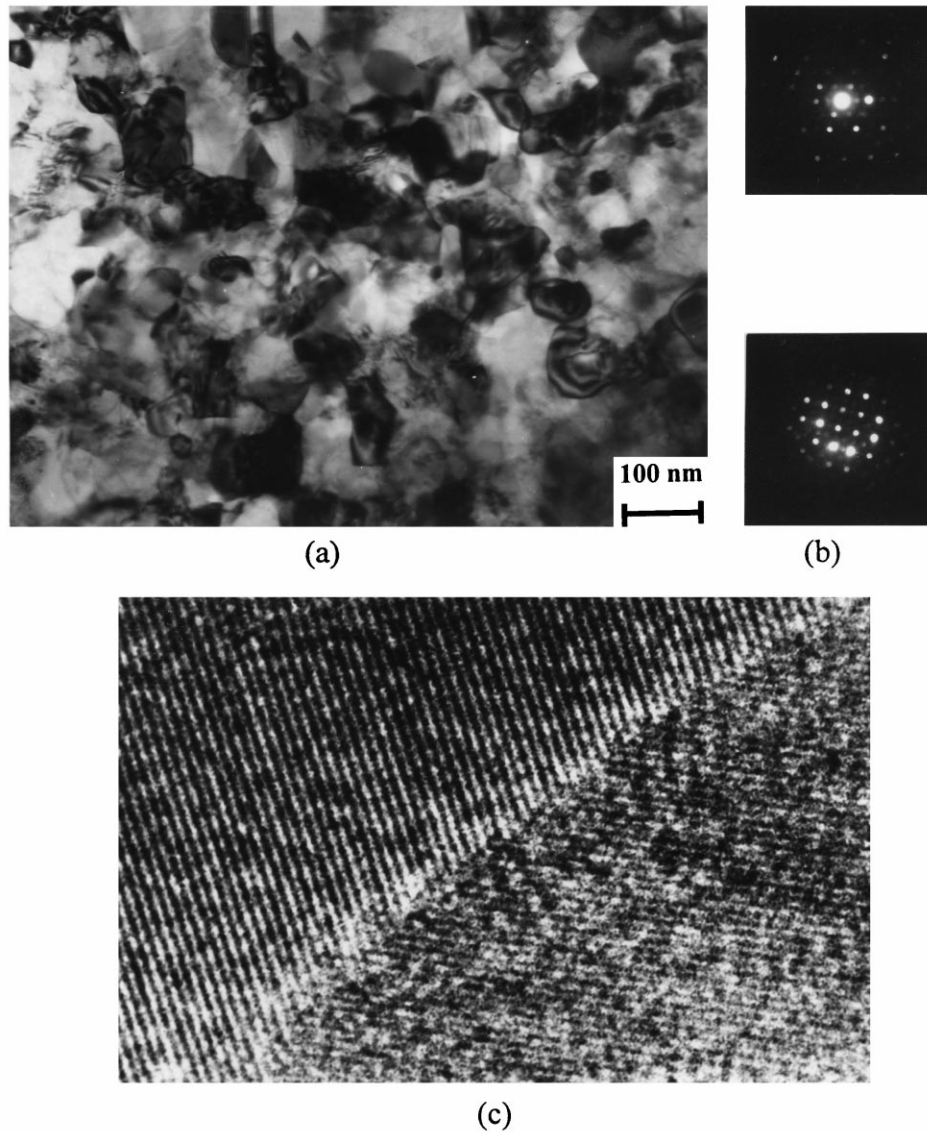

Fig. 42. TEM micrograph of Ni$_3$Al alloy after severe torsion straining and annealing at 650°C: (a) bright field image; (b) microdiffraction pattern of two neighboring grains, indicated by arrows; (c) HREM micrograph of typical grain boundary.

$$\dot{\varepsilon} = A \frac{D \cdot G \cdot b}{K \cdot T} \left(\frac{b}{d}\right)^{p} \left(\frac{\sigma}{E}\right)^{n} \qquad (19)$$

where $\dot{\varepsilon}$ is the strain rate, D is the coefficient of grain boundary diffusion, G is the shear modulus, b is the Burgers vector, K is the Boltzmann constant, T is the temperature of testing, d is the grain size, p is the grain size exponent (usually equal to 2), σ is the flow stress and n is the stress exponent.

Based on this constitutive law of superplastic flow one can expect [149,150] that a decrease in grain size should provide a sharp increase in superplasticity at relatively low temperatures and/or high strain rates. Therefore the development of SPD methods for processing of nanostructured materials has provided new opportunities in investigations of superplasticity in metallic materials and gave a possibility to begin systematic experimental studies in this field [111]. These investigations were started in two directions: first, processing of bulk large billets with homogeneous structure with a grain size of less than a micrometer (submicrocrystalline level) by means of ECA pressing or multiple forging; secondly, processing of nanocrystalline structures in small discs by means of severe plastic torsion straining.

We shall consider below some achievements in this area and comparative features of superplastic behavior of several ultra fine-grained alloys processed by two techniques — ECA pressing and severe torsion straining.

4.2.3.1. Nanocrystalline alloys. Superplastic behavior was studied in alloys, because nanostructures are characterized usually by low stability at elevated temperatures and, in fact, nanocrystalline pure metals are unstable often even at room temperature. However, nanostructures in alloys and intermetallics are more stable. Such structures were processed in the boron doped intermetallic Ni_3Al (Ni-3.5%Al-7.8%Cr-0.6%Zr-0.02%B) [151] and the light weight aluminium alloy 1420 (Al-5.5%Mg-2.2Li-0.12%Zr) [152,153] by means of torsion straining. This technique (see Section 2.1) has the advantage of producing small discs (12 mm in diameter and 0.5 mm in thickness) having uniform nanoscale microstructures. Tensile specimens of 1 mm gauge length were electro discharge machined from torsion straining processed discs. The tensile tests were performed on a custom-built computer-controlled constant strain rate testing machine [151,153].

After torsion straining a strong refinement of structure was revealed in intermetallic Ni_3Al. The mean grain size was about 50 nm. This value remained almost unchanged after annealing at $T = 650°C$ (Fig. 42(a)), and even after heating to 750°C the grain size did not exceed 100 nm. Microdiffraction patterns taken from two neighbouring grains show that they are characterized by high angle misorientations (Fig. 42(b)). Moreover, the appearance of some extra spots on the diffraction patterns indicates a reordering in the alloy subjected to annealing at 650°C. TEM/HREM observations indicated that the grains are almost free from lattice dislocations, but the grain boundaries still retained their non-equilibrium character because they are usually wavy and contained many

defects, such as facets, steps and grain boundary dislocations (Fig. 42(c)). This behavior as shown in Section 2.2, is typical for other metals processed by SPTS.

At 650°C nanostructured Ni_3Al revealed superplastic behavior and the appearance of an Ni_3Al specimen after testing is shown in Fig. 43 in which the upper specimen is the untested one. It is apparent from Fig. 43 that the specimens exhibit very high tensile ductilities (several hundred percent elongation to failure) without visible macroscopic necking. This confirms the manifestation of superplastic behavior. However, such superplastic behavior has several unusual features.

In particular, the stress–strain curves for Ni_3Al at a strain rate of 10^{-3} s^{-1} and 650°C and 725°C show an extensive region of strain hardening at both temperatures with the peak flow stress ranging from 0.9–1.5 GPa (Fig. 44(a)) [151], which is the highest flow stress reported in the literature for the Ni_3Al intermetallic. There was also found an unusual influence of heat treatment on the tensile behavior. When one sample was heat treated for 1 min at 750°C in argon before tensile testing, the sample did not show superplastic behavior (Fig. 44(b)) even though there was no grain growth. It should be noted that superplasticity in nanostructured Ni_3Al has been observed at temperatures which are more than 400°C lower when compared with the corresponding microcrystalline Ni_3Al [154].

In order to understand the mechanisms of unusual superplasticity in this nanostructured alloy, special TEM/HREM investigations have been performed where a thin foil was prepared from a gauge section of Ni_3Al sample strained about 300% (see Fig. 43). Although there is some grain growth during superplastic deformation, the grain size remained less than 100 nm (Fig. 45(a)). Grains were not elongated and we could not find any evidence of large dislocation activity inside the grains even though careful HREM investigations were
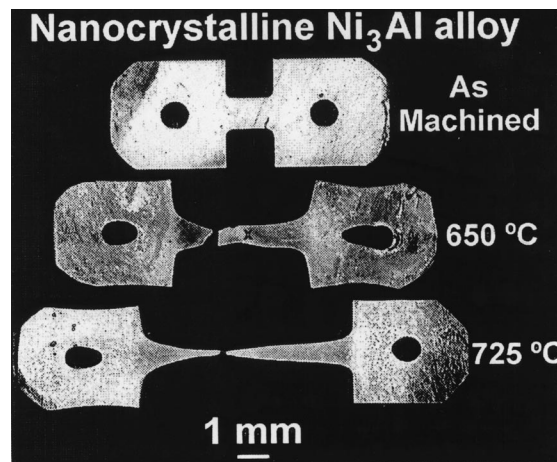

Fig. 43. Appearance of nanostructured Ni_3Al samples prior and after tension at temperature 650°C, 1×10^{-3}, elongation 390% (a cross indicates the place where the foil was cut out for HREM/TEM) and at temperature 725°C, 1×10^{-3}, elongation 560%.
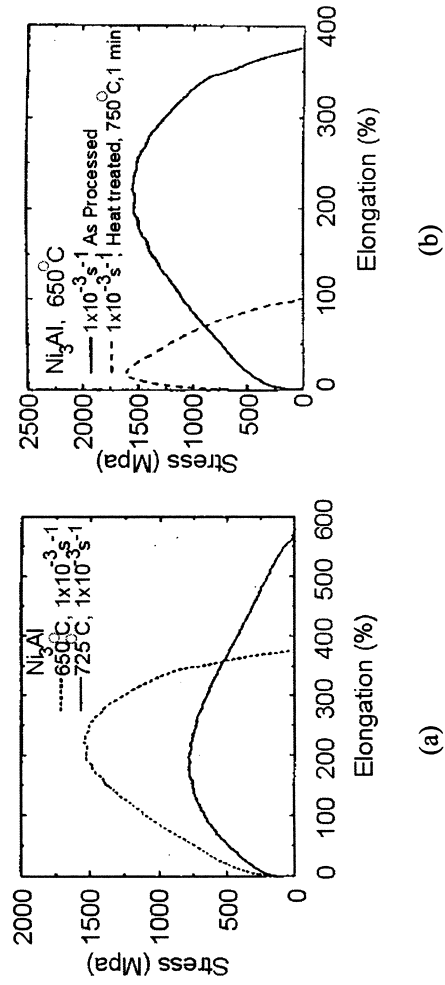
Fig. 44. The variation of true flow stress with elongation at 650 and 725°C and a strain rate of $1 \times 10^{-3} \, \text{s}^{-1}$.

conducted taking advantage of annealing twins (Fig. 45(b)). Such twin boundaries are known to trap and retain lattice dislocations easily [155]. However, we could not detect any dislocations at these interfaces. This experiment supports theoretical calculations demonstrating a difficulty of accommodation for grain boundary sliding through generation of lattice dislocations in nanograins during superplastic deformation [156]. Probably superplastic deformation of
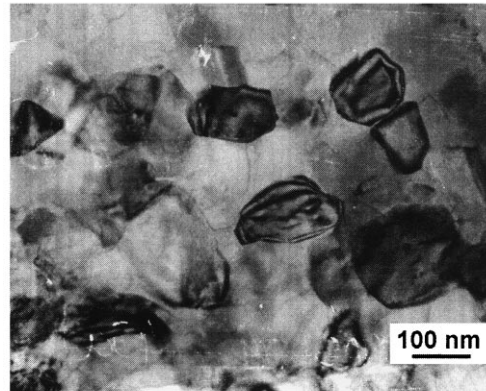
(a)
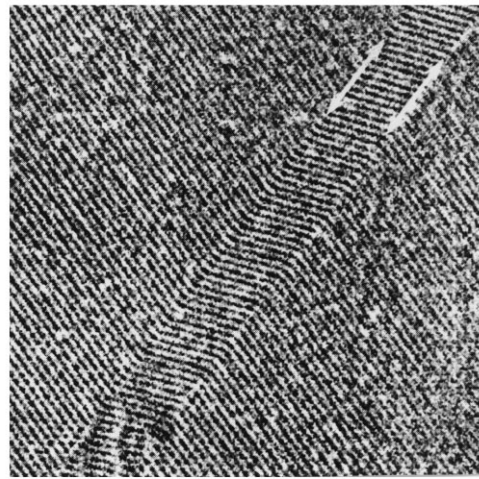
(b)

Fig. 45. Micrographs of nanostructured Ni₃Al: (a) TEM light field image after tension, (b) HREM image of twinning boundaries.

nanomaterials occurs as a result of grain boundary sliding and some diffusional accommodation without visible dislocation activity in the grains.

TEM micrographs of the nanostructured Al 1420 alloy produced by SPTS are shown in Fig. 39. The average grain size of the as-prepared alloy was less than 100 nm. The selected area diffraction pattern is shown as an inset and is consistent with the ultrafine grained microstructure. The grains have mostly equiaxed shape. After heating up 300°C there was some grain growth, but the mean grain size is still less than 300 nm.

The specimens before and after testing at various temperatures are shown in Fig. 46. The specimens show neck free elongation that is characteristic of superplastic flow. Another important feature is the shape of the flow curves, where a significant work hardening at all strain rates was observed and the work hardening rate was higher at higher strain rates [153]. Nevertheless, this alloy demonstrates superplasticity at very high strain rates, up to 5×10^{-1} s^{-1}, at a relatively low temperature of 300°C [153]. The high flow stresses and significant work hardening observed in Ni$_3$Al and Al 1420 have suggested that details of superplasticity are fundamentally different in nanostructured materials and this needs further investigations [156].

Submicrocrystalline alloys. Recent investigations have shown that the application of another SPD method, i.e. ECA pressing not only decreases significantly the temperature of superplastic flow but also produces high strain rate superplasticity in ultrafine grained alloys having a grain size of 0.5–1.0 μm as well [157,158] and it was shown [159] that the presence of mainly high angle grain boundaries is one of the most important requirements to obtain high strain rate superplasticity in cast aluminium alloys.

Further works on decreasing temperature of ECA pressing in alloy 1420 resulted in obtaining a grain size of 0.4 μm and a two-phase structure containing cagulated particles of the second-phase, 0.1–0.2 μm in size [160]. Using EDS
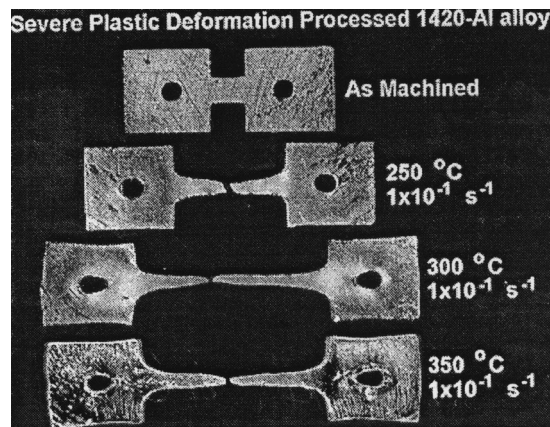

Fig. 46. View of the Al 1420 alloy samples after tensile tests.

analysis it was shown that these particles are T-Al$_2$LiMg phase which can be formed in Al–Li–Mg alloys at temperatures above 200°C [161]. This alloy is reasonably stable up to a high temperature of 400°C, since the grain size during heating remains less than 1 μm, though some relaxation of the structure occurs, attributed to some decrease in a level of internal stresses (Fig. 47). The alloy with the processed structure demonstrates very high strain rate superplastic properties. In particular, testing at 400°C and a strain rate of 10^{-1} s^{-1} showed an elongation to failure of 1240% (Fig. 48). At the same time, a low flow stress of less than 30 MPa was observed. Even at the high strain rate of 1 s^{-1} the alloy exhibits enhanced superplasticity. Under these conditions elongation to failure is about 1000%. The samples are shown in Fig. 48 and exhibit uniform elongation without necking during deformation. These results demonstrate the manifestation of superplasticity at the highest strain rates known in the literature for commercial cast alloys.

Note that an elongation to failure of more than 1000% was also observed in submicrocrystalline Ti alloy processed by multiple forging [162], but the strain rate did not exceed 10^{-3} s^{-1} in that case.

Thus the application of SPD techniques for processing of ultra fine-grained structures provided an opportunity to attain enhanced superplastic properties, namely low temperature and high strain rate superplasticity, in a number of alloys. Nanocrystalline alloys exhibit enhanced superplastic behavior, but this behavior is connected with significant strain hardening that is caused by a change in deformation mechanisms, probably due a difficulty of dislocation accommodation of grain boundary sliding in small grains [155]. High superplastic properties revealed in submicrocrystalline alloys depend not only on the small grain size, but also on the type of micro or nanostructure formed during processing.

The observations of superplasticity in ultra fine-grained materials at relatively

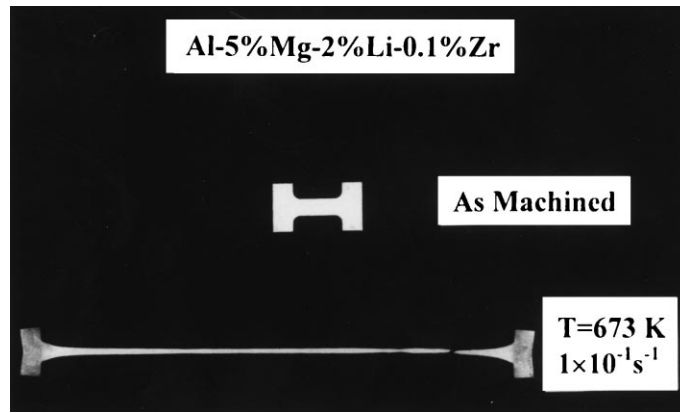Fig. 47. Microstructure of the A1 1420 alloy after ECA pressing.

Fig. 48. Appearance of the A1 1420 alloy processed by ECA pressing before and after tensile test at 400°C with a strain rate of 10^{-1}s^{-1}.

low temperatures and very high strain rates demonstrate the potential for developing different commercial alloys to extend the range of superplastic forming operations employed in current practice. However, to obtain outstanding superplastic properties in nanostructured alloys a precise control of their microstructure and phase composition is required.

4.3. Other physical and engineering properties

Formation of nanostructures from SPD methods results in changes of other properties of direct engineering interest. Such properties as magnetic hysteresis of magnetic materials, optical properties of semiconductors and corrosion properties of metals are considered below.

4.3.1. Magnetic hysteresis

A number of recent investigations show the strong influence of severe plastic deformation on magnetic hysteresis characteristics of soft magnetic metals (Ni [118,119], Co [163]) and hard magnetic alloys (Fe–Cr–Co [164] and Pr–Fe–B–Cu [165]).

A sharp increase in the coercive force was revealed in pure metals after SPD. The results of investigations of the coercive force dependence on temperature of annealing in nanostructured nickel [119] showed its close connection with mean grain size and the non-equilibrium state of the grain boundaries. For example, nanostructured samples exposed to annealing at 100 and 200°C have different values of coercive force H_c by almost 40%, though their grain sizes are almost the same. At the same time, at 200°C an intense recovery of non-equilibrium grain boundaries was observed. As the temperature of annealing increases, a further decrease in the value of H_c was correlated with increasing grain size. Thus, the sharp increase in the coercive force in the nanostructured nickel after SPD is

connected not only with the small grain size but also with the state of the grain boundaries. An analogous regularity was revealed in cobalt exposed to SPTS. TEM investigations of the domain structure of cobalt after SPTS with a grain size of about 100 nm used the Lorentz method [166]. It was established that the magnetic domain sizes were significantly larger than the grains sizes and remagnetization was conditioned by movement of domain walls, but at the same time this movement was hampered by grain boundaries with a high density of defects.

A significant increase in the coercive force H_c was also observed in hard magnetic alloys processed by SPD. This is very important for practical application
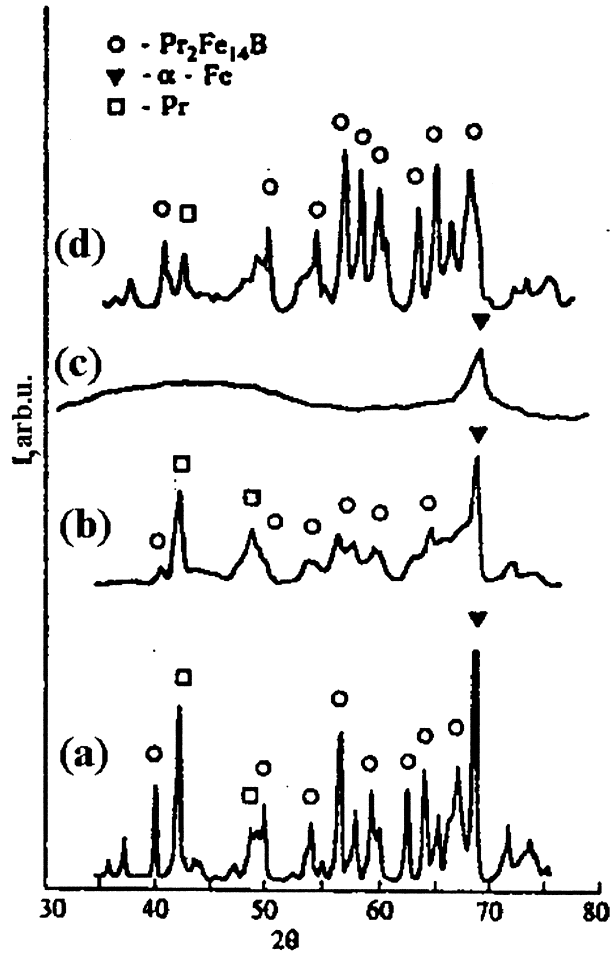

Fig. 49. X-ray diffraction patrtern of cast (a), deformed (b,c) and annealed at 600°C, for 0.5 h (d) of the $Pr_{20}Fe_{73.5}B_5Cu_{1.5}$ alloy.

and manufacture of permanent magnets. However, the origin of H_c changes in these alloys has a more complex character and it is caused not only by the formation of a nanostructure but also by changes in the phase composition. Let us consider more thoroughly all these points in R–Fe–B (R = Nd, Pr) system alloys which have attracted much research and practical interest in recent years. These alloys are used for fabrication of sintered [167] and hot deformed [168] permanent magnets with record values of magnetic force. The influence of SPTS at room temperature and subsequent annealing on magnetic properties and structural changes in the cast $Pr_{20}Fe_{73.5}B_5Cu_{1.5}$ alloy was studied in [165].

According to the data of metallographic and X-ray analyses (Fig. 49(a)), in addition to the basic tetragonal $R_2Fe_{14}B$ phase (2:14:1), bcc (α-Fe type) and hcp (Pr rich) phases were present in the initial cast alloy. The basic magnetic phase 2:14:1 was in the form of dendritic grains with average sizes of 14 μm in length and 3 μm in thickness, and α-Fe additions occupied about 8 vol.% and the non-ferrite hcp phase occupied 25 vol%.

At small strains the alloy is characterized by stable phase composition and broadening of X-ray diffraction lines and spots on diffraction patterns (Fig. 49(a) and (b)). The broadening of 2:14:1 phase lines is especially significant. The broadening is connected with the formation of a substructure with a mean subgrain size of less than 300 nm and a high density of dislocations.

With increasing strain the amount of the 2:14:1 phase relative to the amount of the bcc phase decreases, and in the alloy with the high strain (Fig. 49(c)) an amorphous phase is observed within the whole sample volume, while the 2:14:1 phase and other crystalline phases are not detected.

Severe plastic deformation exerts significant influence on the magnetic hysteresis properties of the cast $Pr_{20}Fe_{73.5}B_5Cu_{1.5}$ alloy. Fig. 50 shows H_c values of the
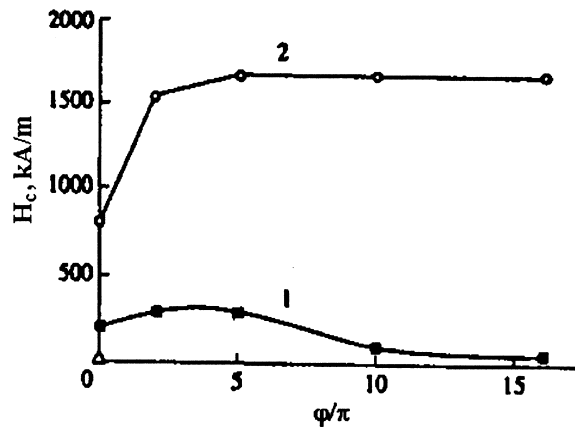

Fig. 50. Dependence of the coercive force H_c of the $Pr_{20}Fe_{73.5}B_5Cu_{1.5}$ alloy in as-deformed (1) and annealed at 600°C (b) states as function of the angle of rotation of anvils φ.

alloys processed at different angles of rotation of the anvils. In the initial state, H_c of the alloy is 20 kA/m (this value is marked by a triangle in Fig. 50). After upset straining H_c increases to 192 kA/m, rises further with increasing angle of rotation, and achieves its maximum over the angle range 2–5.

Annealing of the deformed samples restores the phase composition of the initial alloy, but the grain size of the 2:14:1 phase does not exceed 300 nm and the amount of the α-Fe phase decreases sharply. As a result, annealing leads to a significant increase in the H_c value (Fig. 50).

Thus, the application of the SPD method at room temperature with subsequent annealing resulted in a record value of $H_c > 1600$ kA/m for the $Pr_{20}Fe_{73.5}B_5Cu_{1.5}$ alloy. This value exceeds significantly H_c values in permanent magnets fabricated out of the same alloy via either sintering or hot deformation.

4.3.2. Optical properties of semiconductors

In Section 2.2 it was shown that SPD methods can be used for the formation of nanostructures not only in metals and alloys but also in semiconductors widely used in electronics. In recent years, optical properties of nanostructured silicon and germanium have attracted much interest due to luminescence observed in the visible area of spectrum. These effects were revealed in porous silicon processed by
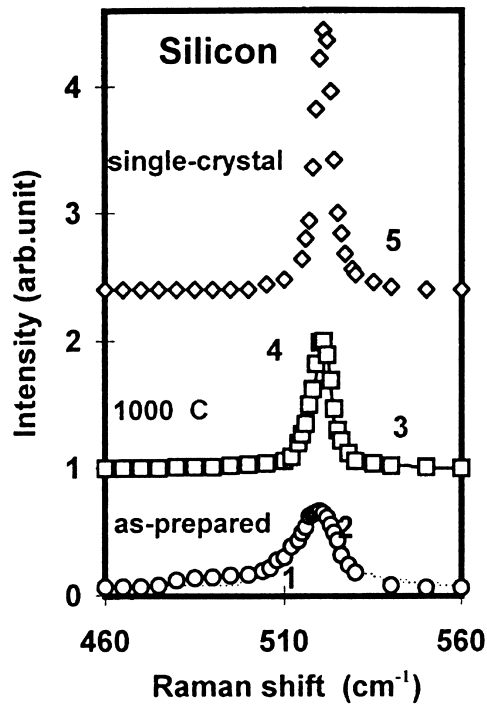

Fig. 51. Raman spectra of nanostructured silicon.

chemical etching [169,170], and in thin films of silicon [171] and germanium [172]. In this connection, it seems interesting to study optical properties of bulk nanostructured silicon and germanium processed by SPD methods. Raman scattering and photoluminescence spectra were studied in these samples [63,64].

Using SPTS, a sufficiently homogenous granular nanostructure was formed in germanium and silicon. The nanostructure was characterized by a log normal grain size distribution with a mean grain size of 24 nm in germanium and 17 nm in silicon (Section 2.2).

The Raman spectrum of single crystal silicon revealed a symmetrical profile with a maximum at 521 cm^{-1} and a full width at half maximum (FWHM) of about 5.0 cm^{-1} (Fig. 51) [64]. Significant changes were revealed in the spectrum of nanostructured silicon, in particular a decrease of peak intensity, an increase of FWHM to 14.2 cm^{-1}, an increase in peak asymmetry and a peak shift of about 2.5 cm^{-1} to low frequencies.

In single crystal germanium the Raman spectrum had the form of an asymmetric peak with a maximum at 301 cm^{-1} and FWHM of 5.1 cm (Fig. 52). Changes occurring in the spectrum of nanostructured germanium were similar to
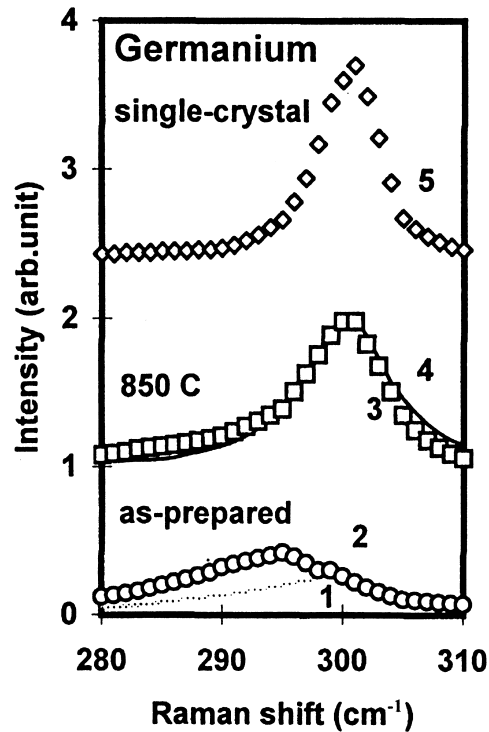

Fig. 52. Raman spectra of nanostructed germanium.

nanostructured silicon, namely a decrease in peak intensity, increase in FWHM to 14 cm^{-1}, increase in peak asymmetry and shift to low frequency [63].

The luminescence spectrum of nanostructured silicon revealed at room temperature had the form of an asymmetric peak disposed in the visible area of spectrum with a maximum at 650 nm and an FWHM of about 80 nm (Fig. 53). An analogous luminescence spectrum in the visible area of the spectrum was observed in porous silicon [170] as well as in thin films of silicon [171].

Notions of quantum confinement are often used to describe the luminescence spectrum observed in porous and thin film silicon and germanium [172]. This effect assumes the enlargement of the band gap in semiconductors due to their extremely small crystal size. As a result, the occurrence of additional levels of energy leads to some changes in the luminescence spectrum.

For realization of quantum confinement the mean grain size in nanostructured semiconductors should be less than some critical size. In the case of silicon this calculated value is equal to 5 nm [170] and for germanium it is 24 nm [172]. Moreover, the noticeable shift in the luminescence spectrum from infrared to visible is possible only when the mean grain size is less than 3 nm in silicon and 3.5 nm in germanium, i.e. the grain sizes should be significantly less than the ones observed by TEM. This gap can be explained if one accepts that only the perfect crystal interior of grains makes a major contribution to the photoluminescence spectrum in nanostructured semiconductors. In accordance with the structural model of NSM discussed in Section 2.2, undistorted areas in SPD materials are significantly smaller than the mean grain size.
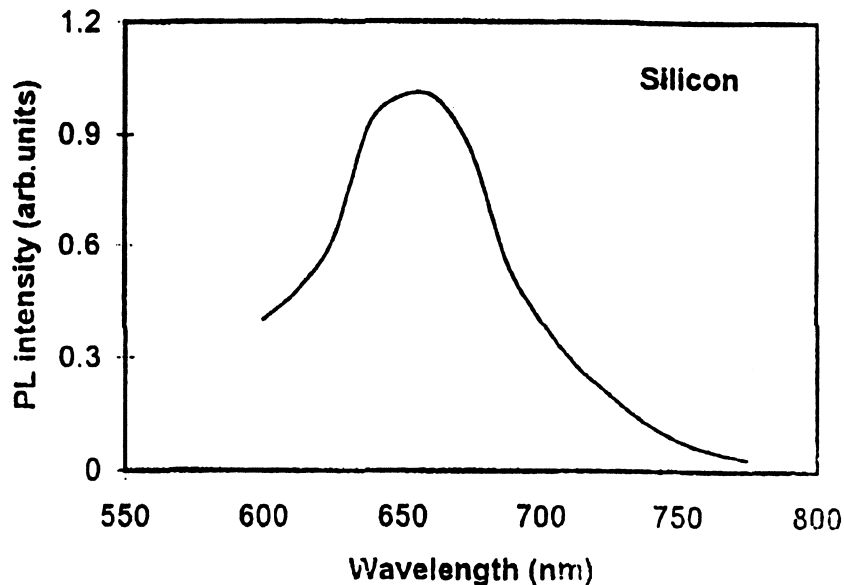

Fig. 53. Photoluminescence spectrum of nanostructured silicon.

4.3.3. Corrosion behavior

The corrosion behavior of nanostructured materials has been scarcely studied to date. Aust and co-authors have shown that this kind of material may possess enhanced corrosion properties in comparison with both their crystalline and amorphous counterparts [173]. On the other hand significant degradation of corrosion resistance in nanocrystalline Ni–P has also been reported for grain sizes of 8.4 and 44.6 nm [174]. Moreover, the same researches have shown that the good corrosion properties of pure nickel remain unchanged in the nanostructured state [175]. This ambiguity makes it difficult to predict the electrochemical behavior of nanomaterials from the known properties of their coarse-grained and amorphous analogs. One can reasonably suppose that the corrosion properties of NSM depend stongly on the processing technique, thermal history and material purity and they need futher investigations including SPD materials.
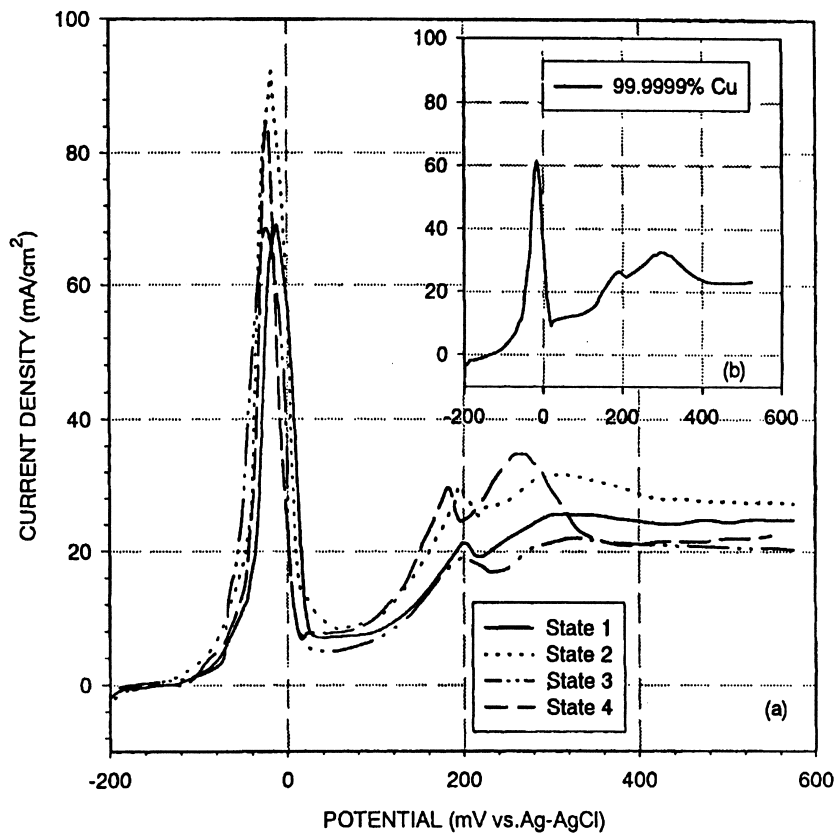

Fig. 54. Potentiodynamic anodic polarization curves measured in Livingston solution at 303 K for nanostructured copper subjected to different preliminary heat treatments (see text for details) (a) and for conventional polycrystalline high-purity copper (b).

There is one important report on the general corrosion behavior of ultra fine-grained Cu produced by severe plastic deformation via ECA pressing [176]. The samples were either left in the as-deformed state (State 1) or subjected to a short time isothermal annealing in a muffle furnance at 473 K for 3 min (State 2) or 10 min (State 3). For comparison coarse-grained reference specimens with a mean grain size of 50 μm were obtained from the as-received ECA pressed state by annealing at 823 K for 30 min in vacuum (State 4). Potentiodynamic electrochemical measurements were carried out in a standard cell containing a saturated calomel reference electrode. All tests were performed in the modified Livingston etchant [177] (HCl:30 ml + CH_3COOH:10 ml + H_2O:410 ml).

Fig. 54 shows typical potentiodynamic anodic polarization curves obtained at 303 K for ultra fine-grained and for annealed Cu. Two active-passive transitions are revealed from the polarization curves. High purity copper immersed into sulfuric acid or alkaline solutions usually shows a single passive region associated with cuprous oxide Cu_2O film formation on specimen surface. The presence of a secondary active-passive transition from 100 to 300 m V_{SCE} and passive region from about 300 m V_{SCE} for ultra fine-grained copper immersed into the Livingston electrolyte cannot be explained by the impurity content of this material because 99.9999% purity Cu shows similar polarization behavior, Fig. 54(b). Two stages of passivation can presumably be associated with two stages of protective film formation [178,179]. The steady-state anodic current is achieved at secondary passivation. Together with passivation potential this current density serves as a quantitative characteristic of general corrosion. One can see that the active-passive behavior of the ECA-pressed Cu (Fig. 54(a), curve 'State 1') is similar to that of conventional Cu (Fig. 54(a), curve 'State 4'). However, some differences can be noticed.

The shape of the polarization curve was not changed substantially with testing temperature and the open circuit corrosion potential, E_{corr}, was approximately the same for all the specimens tested (-200 ± 10 mV). All other characteristics of the polarization curves were sensitive to the structural state of material, changing uniformly with solution temperature. Lowering the electrolyte temperature necessarily shifts the passivation potential in the active direction and reduces the primary critical passivation current density for all state of marerial. This behavior is usually observed for passivating conventional metals. The differences between the ultra fine-grained and conventional polycrystals tend to diminish at high potentials (in the transpassive region). At all testing temperatures the secondary passive current density in copper in State 1 is higher in comparison with results on coarse-grained reference samples (State 4). This means that the steady-state rate of dissolution in State 1 is greater than in State 4. This demonstrates the decreased general corrosion resistance of ultra fine-grained copper in comparison with the relatively coarse-grained sample. This is consistent, in principle, with findings reported in [174,175] for nanostructured Ni and Ni–P alloy which possess poorer general corrosion properties than their coarse-grained counterparts.

Authors [176] also investigated the morphology of corrosion damage and the

effect of heat treatment on the corrosion behavior of ultra fine-grained copper, leading to three main conclusions:

First, the rate of dissolution at a given potential in the ultra fine-grained copper is 10% higher in comparison with relatively coarse-grained polycrystalline copper of the same purity. This rate depends strongly on the heat treatment applied to the initial ECA pressed material: short time (3 min) annealing at 473 K results in partial recovery of internal stresses and partial recrystallization but significantly reduces corrosion properties. Second, significant differences in the corrosion behavior of the as-received ECA pressed Cu and Cu subjected to preliminary annealing, is related to the degree of corrosion localization. Highly localized corrosion was observed also in relatively coarse-grained copper where the corrosion damage is almost entirely associated with grain boundaries. Although the total fraction of grain boundaries in the ECA pressed materials is much greater than that in conventional polycrystals, the surface relief in the nanostructured state is rather smooth and corrosion pits are distributed uniformly. Third, the homogeneity of corrosion damage makes the ECA pressed structure more attractive for practical applications in aggressive media in comparison with conventional polycrystals susceptible to localized intergranular corrosion.

4.4. The potential for practical applications

In this concluding section let us consider directions being most advantageous for practical applications of SPD nanostructured materials in the near future and some questions requiring further investigations. Many of the properties of nanostructured materials considered above are rather attractive for their practical application. Moreover, fabrication of large scale bulk billets by means of SPD
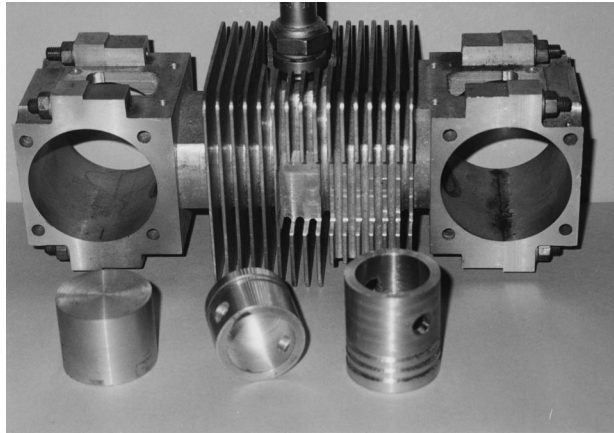

Fig. 55. View of the article of "Piston" type fabricated from the nanostructed Al 1420 alloy which is supposed to be used in small overall internal combustion engines (it is shown in the figure behind the piston).

methods provides an opportunity to manufacture pilot articels and their approbation. From this point of view one of the most important directions of practical use are engineering of new powerful permanent magnets on the basis of nanostructured ferromangets since severe plastic deformation results in a significant increase in the hysteresis properties of hard magnetic alloys (Section 4.3).

It is well known [147,148] that superplastic forming is a highly efficient method of processing of complex shape articles. In this connection, the manifestation of superplasticity in ultra fine-grained SPD materials at relatively low temperatures and/or high strain rates is rather advanced in terms of increasing the productivity of forming operations and the durability of die sets. The example of possible practical application of nanostructured Al alloys is shown in the Fig. 55. It presents a complex shape article of 'Piston' type which was fabricated from the nanostructured Al 1420 alloy by superplastic forming using the high strain rate superplasticity. This article can be used in small overall internal combustion engine presented in Fig. 55. The application of the nanostructured alloy allowed to conduct superplastic forming at temperature 350°C that is much lower than temperature of forming of the microcrystalline alloy (450°C).

Until recent years, the problem of practical application of nanostructured materials as structural materials has remained rather disputable. The most important demands which these materials should meet are states of high strength and ductility and elevated fatigue characteristics. Due to the formation of nanostructures with high angle grain boundaries predominating and an increase in homogeneity resulted from SPD methods, this problem of their structural use can be solved positively. The engineering of nanostructured titanium alloy [180] for manufacture of high strength threaded articles such as bolts which are widely used in automobile and aircraft industries [181] can be taken as an interesting example.

Processing of bulk nanostructured billets out of Russian alloy VT1–0 (commercial pure Ti) was realized via ECA pressing of rods, up to 30 mm in
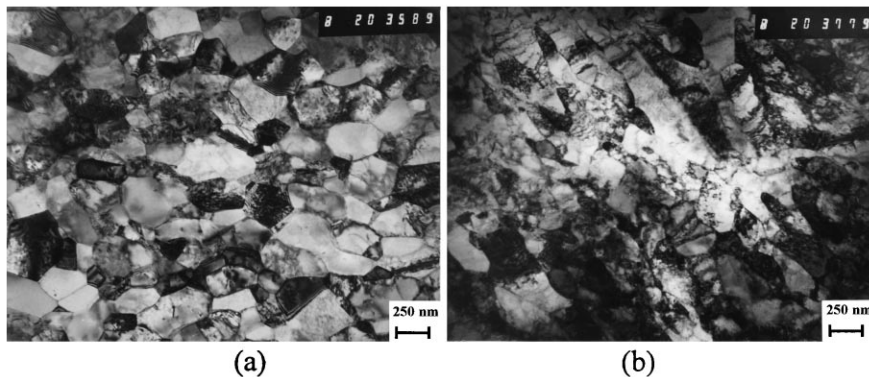

Fig. 56. Typical TEM microstructures of the alloy VT-1-0 after ECA pressing by different routes: (a) route 1, (b) route 2.

Table 5
Mechanical and fatigue properties of the processed billets and cyclic endurance of fasteners out of the VT1–0 alloy in the as-received state and after ECA pressing by two different routes

No	State	Tensile mechanical properties				Fatigue limit σ_{-1}, MPa	Cyclic endurance, N
		σ_s, MPA	$\sigma_{0,2}$ MPa	δ, %	ψ, %		
1.	As-received state	460	400	27	60	252	4.211
2.	After ECA pressing by route 1	816	800	15,5	60	403	34.504
3.	After ECA pressing by route 2	772	732	14	59	354	17.504

diameter and 120 mm in length. Two routes were studied. In the first case (route 1) the billet was rotated at an angle of 90° after each pass. In the second case (route 2) the angle of rotation was 180°. Structural investigations were conducted by TEM using thin foils cut out in parallel and perpendicular sections of the billets after ECA pressing. Mechanical tensile tests were conducted using standard samples (Russian standard 'GOST 1497-84'). A value of fatigue endurance was determined by Locati's method for accelerated testing [182].

Typical microstructures of the alloy VT1–0 after ECA pressing by route 1 and route 2 are shown in Fig. 56(a) and (b), respectively. It is seen that in the first case the homogeneity of the processed ultra fine-grained structure is much higher than in the second one. Moreover, analysis of electron diffraction patterns showed that ECA pressing by route 1 leads to formation of a mean grain size of 200–300 nm and granular structure with mostly high angle grain boundaries. ECA pressing by route 2 results in a similar mean grain size but a structure of a mixed type, which contains small and high angle grain boundaries. These results confirm the importance of applied route for structure formation via ECA pressing (see also Section 2.2).

The results of mechanical and fatigue tests of the ECA pressed billets of the VT1–0 alloy are presented in Table 5.

The tabular data show that formation of nanostructures by ECA pressing leads to a considerable increase of strength and satisfactory ductility. This effect is especially strong by ECA pressing using route 1. The fatigue limit of the VT1–0 alloy after ECA pressing is also increased considerably: 60% after ECA pressing by route 1 and 40% after ECA pressing by route 2. This difference is again due to the variation in ECA pressing regimes and the resulting nanostructures. Thus the type of nanostructure has a strong influence on the mechanical and fatigue properties of ultra fine-grained metals, even if the mean grain size is approximately the same. It was discussed above [109] how the defect structure of
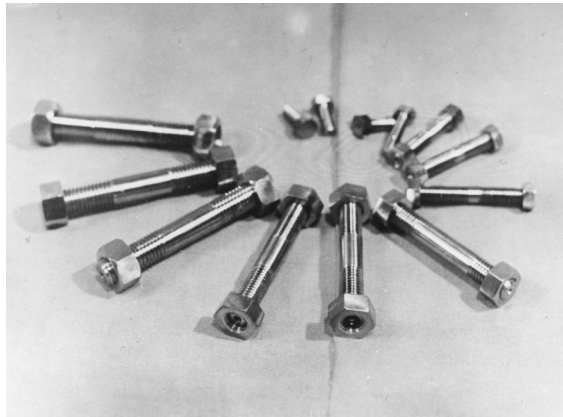

Fig. 57. High strength thread articles out of SPD Ti alloy.

the grain boundaries is a key factor influencing the mechanical behavior of nanostructured materials. The VT1–0 data show therefore the important role of uniform microstructure as well.

Now let us consider an interesting example of the application of processed nanostructured material. This is high strength threaded articles for application as fasteners widely used in the aircraft and automobile industries and in medical practice. (Fig. 57) shows the example of the threaded bolts, which were manufactured from billets out of the alloy VT1–0, in the initial as-received state, and processed by ECA pressing. This thread was formed by plastic forming using a rolling machine for this procedure [183]. The obtained stud-bolts were used as samples for low cyclic fatigue tests. These stud-bolts were tested on a special testing machine [183] with a loading scheme of: tension at pulsing cycle at $\sigma_{max} = 450$ MPa, $\sigma_{min} = 0$. Three samples of each state were tested. The results of testing are also shown in Table 5, too.

It is seen that formation of nanostructures in these articles provides an essential increase of cyclic endurance of thread in a low cyclic area, but it depends again from the processing route. The conducted investigations have demonstrated that the preliminary formation of nanostructure contributes to a significant increase in cyclic fatigue endurance of thread in fastener titanium articles.

References

[1] Valiev RZ, editor. Ultrafine-grained materials prepared by severe plastic deformation, vol. 21, Annales de Chimie. Science des Materiaux, 1996, p. 369, Special issue.

[2] Gleiter H. Progr Mat Sci 1989;33:223.

[3] Weertman JR. Mater Sci Eng 1993;A166:161.

[4] Koch CC, Cho YS. Nanostructured Mater 1992;1:207.

[5] Morris DG. In: Mechanical behavior of nanostructured materials. Switzerland: Trans Tech. Publ, 1998. p. 85.

[6] Pavlov VA. Phys Met and Metallogr 1989;67:924.

[7] Langford G, Cohen M. Trans ASM 1969;82:623.

[8] Rybin VV. Large plastic deformations and destruction of metals. Moscow: Metallurgia, 1987.

[9] Gil Sevillano J, Van Houtte P, Aernoudt E. Progr Mat Sci 1980;25:69.

[10] Valiev RZ, Korznikov AV, Mulyukov RR. Mater Sci Eng 1993;A168:141.

[11] Valiev RZ, Alexandrov IV, Islamgaliev RK. In: Chow GM, Noskova NI, editors. Nanocrystalline materials: science and technology. Nato ASI. Dordrecht: Kluwer Academic Publishers, 1998. p. 121.

[12] Valiev RZ, Kaibyshev OA, Kuznetsov RI, Musalimov RSh, Tsenev NK. DAN SSSR 1988;301(4):864.

[13] Valiev RZ, Krasilnikov NA, Tsenev NK. Mater Sci Eng 1991;A137:35.

[14] Valiev RZ, Islamgaliev RK. Superplasticity and superplastic forming. In: Ghosh AK, Bieler, TR, editors. The Minerals, Metals and Materials Society, 1998, p.117.

[15] Valiev RZ, Islamgaliev RK. Fiz Met Metalloved 1998;85:161.

[16] Valiev RZ. Nanostructured Mater 1995;6:73.

[17] Smirnova NA, Levit VI, Pilyugin VI, Kuznetsov RI, Davydova LS, Sazonova VA. Fiz Met Metalloved 1986;61:1170.

[18] Smirnova NA, Levit VI, Pilyugin VI, Kuznetsov RI, Degtyarov MV. Fiz Met Metalloved 1986;62:566.

[19] Smirnova NA, Levit VI, Degtyarov MV. Fiz Met Metalloved 1988;65:1027.

[20] Valiev RZ, Ivanisenko YuV, Rauch EF, Baudelet B. Acta Mater 1997;44:4705.

[21] Valiev RZ. Synthesis and processing of nanocrystalline powder. In: David L. Bourell, editors. The Minerals, Metals and Materials Society, 1996, p.153.

[22] Alexandrov IV, Zhu YT, Lowe TC, Islamgaliev RK, Valiev RZ. Nanostructured Mater 1998;10:49.

[23] Alexandrov IV, Zhu Y, Lowe T, Islamgaliev RK, Valiev RZ. Metall Mater Trans 1998;29A:2253.

[24] Segal VM, Reznikov VI, Drobyshevkij AE, Kopylov VI. Metally 1981;1:115.

[25] Iwahashi Y, Wang J, Horita Z, Nemoto M, Langdon TG. Scripta Mater 1996;35:143.

[26] Segal VM. Mater Sci Eng 1995;A197:157.

[27] Segal VM, Reznikov VI, Kopylov VI, Pavlik DA, Malyshev VF. In: Processes of plastic transformation of metals. Minsk: Navuka i Teknika, 1984. p. 295.

[28] Iwahashi Y, Horita Z, Nemoto M, Langdon TG. Acta Mater 1998;46:1589.

[29] Ferrase S, Segal VM, Hartwig KT, Goforth RE. Metall Mater Trans 1997;28A:1047.

[30] Iwahashi Y, Horita Z, Nemoto M, Langdon TG. Acta Mater 1997;45:4733.

[31] Ahmadeev NH, Valiev RZ, Kopylov VI, Mulyukov RR. Russian Metally 1992;5:96.

[32] Valiahmetov OR, Galeyev RM, Salishchev GA. Fiz Metall Metalloved 1990;10:204.

[33] Galeev RM, Valiahmetov OR, Salishchev GA. Russian Metally 1990;4:97.

[34] Imayev RM, Imayev VM, Salishchev GA. J Mater Sci 1992;27:4465.

[35] Salishchev GA, Valiakhmetov OR, Galeyev RM. J Mater Sci 1993;28:2898.

[36] Kaibyshev O, Kaibyshev R, Salishchev G. Mater Sci Forum 1993;113-115:423.

[37] Valitov VA, Salishchev GA, Muhtarov Sh H. Russian Metally 1994;3:127.

[38] Salishchev GA, Valiakhmetov OR, Valitov VA, Muktarov SK. Mater Sci Forum 1994;170-172:121.

[39] Salishchev GA, Valiahmetov OR, Galeev RM, Malysheva SP. Russian Metally 1996;4:86.

[40] Zhorin VA, Shashkin DP, Yenikoponyan NS. DAN SSSR 1984;278:144.

[41] Kuznetsov RI, Bykov VI, Chernyshov VP, Pilyugin VP, Yefremov NA, Posheyev VV. Plastic deformation of solid bodies under pressure, Sverdlovsk, IFM UNTS RAN, 1985, Preprint 4/85 (in Russian).

[42] Bridgmen J. In: Processing of metals under high pressure conditions. Techizdat M, 1936, Moscow: p. 230, (Russian translation).

[43] Mishin OV, Gertsman VYu, Valiev RZ, Gottstein G. Scripta Mater 1996;35:873.

[44] Valiev RZ, Mishra RS, Grosa J, Mukherjee AK. Scripta Mater 1996;34:1443.

[45] Shen H, Li Z, Gunther B, Korznikov AV, Valiev RZ. Nanostructured Mater 1995;6:385.

[46] Mazurskiy MI, Murzinova MA, Salischev GA, Afonichev DD. Russian Metally 1995;6:83.

[47] Islamgaliev RK, Chmelik F, Kuzel R. Mater Sci Eng 1997;A237:43.

[48] Gertsman VYu, Birringer R, Valiev RZ, Gleiter H. Scr Metall Mater 1994;30:2294.

[49] Islamgaliev RK, Chmelik F, Kuzel R. Mater Sci Eng 1997;A234-236:335.

[50] Popov AA, Pyshmintsev IY, Demakov SL, Illarionov AG, Lowe TC, Sergeeva AV, Valiev RZ. Scripta Mater 1997;37:1089.

[51] Kozlov EV, Popova NA, Ivanov YuF, Ignatenko LN, Koneva NA, Pekarskaya EE. Ann Chim Science des Materiaux Fr 1996;21:427.

[52] Valiev RZ, Kozlov EV, Ivanov YuF, Lian J, Nazarov AA, Baudelet B. Acta Metall Mater 1994;42:2467.

[53] Utyashev FZ, Enikeev FU, Latysh VV. Ann Chim Science des Materiaux Fr 1996;21:379.

[54] Stolyarov VV, Latysh VV, Shundalov VA, Salimonenko DA, Islamgaliev RK, Valiev RZ. Mater Sci Eng 1997;A234-236:339.

[55] Islamgaliev RK, Salimonenko DA, Shestakova LO, Valiev RZ. Izv Vuzov, Tsvetnaja Metallurgia 1997;6:52.

[56] Furukawa M, Ma Y, Horita Z, Nemoto M, Valiev RZ, Langdon TG. In: Chandra T, Sakai T, editors. Proc. Int. Conf. On Thermomechanical Processing of Steels and Other Materials, 1997, p. 1875.

[57] Korznikov AV, Ivanisenko YuV, Laptionok DV, Safarov IM, Pilyugin VP, Valiev RZ. Nanostructured Mater 1994;4:159.
[58] Senkov ON, Froes FH, Stolyarov VV, Valiev RZ, Liu J. Scripta Mater 1998;38:1511.
[59] Abdulov RZ, Valiev RZ, Krasilnikov NA. J Mater Sci Lett 1990;9:1445.
[60] Languillaume J, Chmelik F, Kapelski G, Bordeaux F, Nazarov AA, Canova G, Esling C, Valiev RZ, Baudelet B. Acta Metall Mater 1993;41:2953.
[61] Korznikov A, Dimitrov O, Quivy A, Korznikova G, Devaud J, Valiev R. J Physique IV 1995;5:C7–271.
[62] Korznikov A, Dimitrov O, Korznikova G. Ann Chim Science des Materiaux 1996;21:443.
[63] Islamgaliev RK, Kuzel R, Obraztsova ED, Burianek J, Chmelik F, Valiev RZ. Mater Sci Eng 1998;A249:152.
[64] Islamgaliev RK, Kuzel R, Mikov SN, Igo AV, Burianek J, Chmelik F, Valiev RZ. Mater Sci Eng A 1998;266:205.
[65] PDF-2, Database of X-ray powder diffraction data, International Centre for Diffraction Data, PA, USA, 1995.
[66] Valiev RZ, Islamgaliev RK, Kuzmina NF, Li Y, Langdon TG. Scripta Mater 1998;40:117.
[67] Mishra RS, Valiev RZ, McFadden SX, Islamgaliev RK, Mukherjee AK. Scripta Mater 1999;40(10):1151.
[68] Essmann U, Mughrabi H. Phil Mag (a) 1979;40(6):731.
[69] Grabski MW. J Physique 1985;46(C4/4):567.
[70] Valiev RZ, Gertsman VYu, Kaibyshev OA. Phys Stat Sol (a) 1986;97(11):11.
[71] Musalimov Sh R, Valiev RZ. Scr Metall Mater 1992;27:1685.
[72] Hirsh P, Hovy A, Nickolson R, Peshly D, Welan M. In: Electron microscopy of fine crystals. Moscow: Mir, 1968. p. 574.
[73] Utevskyi LM. In: Diffraction electron microscopy in material science. Moscow: Metallurgy, 1973. p. 584.
[74] Williams DB, Carter CB. In: Transmission electron microscopy. New York: Plenum Press, 1996. p. 729.
[75] Islamgaliev RK, Valiev RZ. Solid State Phys 1995;37:3597.
[76] Islamgaliev RK, Valiev RZ. Fiz Met Metalloved 1999;87(3):46.
[77] Zhang K, Alexandrov IV, Lu K, Valiev RZ. J Appl Phys 1996;80:5617.
[78] Alexandrov IV, Zhang K, Lu K. Ann Chim Science des Materiaux 1996;21:407.
[79] Hirth JP, Lothe J. Theory of dislocations. New York: McGraw-Hill, 1983.
[80] Nazarov AA, Romanov AE, Valiev RZ. Acta Metall Mater 1993;41:1033.
[81] Tyumentsev AN, Pintzin YuP, Korotaev AD, Islamgaliev RK, Valiev RZ. Fiz Met Metalloved 1998;86:6.
[82] Dahmen Y, Hetherington CJD, Westmacott KH. In: Proc. XII Int. Congr. for Electron Microscopy. 1990. p. 338.
[83] Valiev RZ, Musalimov R Sh. Fiz Metal Metalloved 1994;78:114.
[84] Horita Z, Smith DJ, Furukawa M, Nemoto M, Valiev RZ, Langdon TG. Mater Sci Forum 1996;204-206:437.
[85] Horita Z, Smith DJ, Nemoto M, Valiev RZ, Langdon TG. J Mater Res 1998;13:446.
[86] Warren BE. X-ray diffraction. New York: Dover Publisher, 1990.
[87] Krill CE, Birringer R. Phil Mag 1998;A77(3):621.
[88] Averbach BI, Warren BE. J Appl Phys 1949;20:885.
[89] Williamson GK, Hall WH. Acta Metal 1953;1:22.
[90] Jang JSC, Koch CC. J Mater Res 1990;5:498.
[91] Alexandrov IV, Valiev RZ. Fiz Met Metalloved 1994;77:77.
[92] van Berkum JGM, Vermeulen AC, Delhez R, de Keijser ThH, Mittemeijer EJ. J Appl Cryst 1994;27:345.
[93] Nieman GW, Weertman JR, Siegel RW. Mat Res Soc Proc 1991;206:493.
[94] Zhang K, Alexandrov IV, Valiev RZ, Lu K. J Appl Phys 1998;84(4):1924.
[95] Alexandrov IV, Wang YD, Zhang K, Lu K, Valiev RZ. In: Liang Z, Zuo L, Chu Y, editors.

Textures of materials. Proceedings Int. Conf. ICOTOM-11. International Academic Publisher, 1996. p. 929.

[96] Xu SS. X-ray diffraction in metals. Ithaca, Shanghai: Science Technical Publication Press, 1962.

[97] James RW. The optical principles of the diffraction of X-ray. Ithaca: Cornell University Press, 1965.

[98] Valiev RZ, Mulyukov RR, Ovchinnikov VV, Shabashov VA. Scr Metall Mater 1991;12:25.

[99] Valiev RZ, Mulyukov RR, Ovchinnikov VV. Phil Mag Lett 1990;62:253.

[100] Lian J, Valiev RZ, Baudelet B. Acta Metal Mater 1995;43:4165.

[101] Amirkhanov NA, Islamgaliev RK, Valiev RZ. Fiz Met Metalloved 1998;86(3):99.

[102] Amirkhanov NA, Bucki JJ, Islamgaliev RK, Valiev RZ, Kurzydlowski KJ, Mat Sci Eng, to be published.

[103] Nazarov AA, Romanov AE, Valiev RZ. Nanostructured Mater 1994;4:93.

[104] Nazarov AA. Scripta Mater 1997;37:1155.

[105] Nazarov AA, Romanov AE, Valiev RZ. Scripta Mater 1996;34:729.

[106] Seeger A, Haasen P. Phil Mag 1958;3:470.

[107] Chmelik F. Private communication.

[108] Weertman JR. Mater Sci Eng 1993;A166:161.

[109] Valiev RZ. Mater Sci Eng 1997;A234-236:59.

[110] Chokshi AH, Mukherjee AK, Langdon TG. Mater Sci Eng 1993;R10:237.

[111] Valiev RZ. Mater Sci Forum 1997;243-245:207.

[112] Gryaznov VG, Trusov LI. Prog Mater Sci 1993;37:289.

[113] Chokshi AH, Rosen A, Karch J, Gleiter H. Scr Metal Mater 1989;23:1679.

[114] Christman T, Jain M. Scr Metal Mater 1991;25:767.

[115] Nieman GW, Weertman JR, Siegal RW. Scr Metal Mater 1989;23:2013.

[116] El-Sherik AM, Erb U, Palumbo G, Aust KT. Scr Metal Mater 1992;27:1185.

[117] Korolev AV, Deryagin AI, Zavalishin VA, Kuznetsov RI. Fiz Metall Metalloved 1989;68(4):672.

[118] Mulyukov KhYa, Khaphisov SB, Valiev RZ. Phys Stat Sol (a) 1992;133:447.

[119] Valiev RZ, Korznikova GF, Mulyukov Kh Ya, Mishra RS, Mukherjee AK. Phil Mag B 1997;75(6):803.

[120] Handrich K, Kobe S. Amorphe ferro- and ferrimagnetica. Berlin: Academie-Verlag, 1980.

[121] Richter J, Handrich K, Schreider. J Phys Stat Sol (b) 1975;68:K61.

[122] Eastman JA, Fitzsimmons MR. J Appl Phys 1995;77:522.

[123] Birringer R, Gleiter H. In: Encyclopedia of material science, vol. 1. Oxford: Pergamon Press, 1988.

[124] Mutschele T, Kirchheim R. Scr Metall Mater 1987;21:135.

[125] Horvath J. Defect and Diffusion Forum 1989;66/69:207.

[126] Kolobov YuR, Grabovetskaya GR, Ratochka IV, Kabanova ER, Naidenkin EV, Lowe T. Ann Chim Science des Materiaux 1996;21:483.

[127] Valiev RZ, Razumovskii IM, Sergeev VI. Phys Stat Sol (a) 1993;139:321.

[128] Wurschum R, Kubler A, Gruss S, Acharwaechter P, Frank W, Valiev RZ, Mulyukov RR, Schaeffer HE. Ann Chim Science des Materiaux 1996;21:471.

[129] Mishin YuM, Razumovskii IM. Scripta Metall 1991;25(6):1375.

[130] Akhmadeev NA, Kobelev NP, Mulyukov RR, Soifer Ya M, Valiev RZ. Acta Metall Mater 1993;41:1041.

[131] Lebedev AB, Burenkov Yu, Pulnev SA, Vetrov VV, Kopylov VI. Journale de Physique IV 1996;C8:365.

[132] Lebedev AB, Pulnev SA, Kopylov VI, Burenkov Yu, Vetrov VV. Scripta Mater 1996;35:1077.

[133] Mulyukov R, Weller M, Valiev RZ, Gessmann Th, Schaefer HE. Nanostructured Mater 1995;6:577.

[134] Lebedev AB, Burenkov YuA, Kopylov VI, Romanov AE, Gryaznov VG. Phil Mag Lett 1996;73(5):241.

[135] Favstov YuK, Shulga YuN, Rachshtad AG. In: Metal science of high damping alloys. Moscow: Metallurgy, 1980. p. 272.

[136] Mulyukov RR. MiTOM 1998;8:34.

[137] Gertsman VY, Valiev RZ, Akhmadeev NA, Mishin OV. Mater Sci Forum 1996;233:80.
[138] Loikowski W. Acta Metall Mater 1991;39:1891.
[139] Nazarov AA, Romanov AE, Valiev RZ. Scr Metall Mater 1990;24:1929.
[140] Milman VYu. Acta Metall Mater 1994;42:1349.
[141] Islamgaliev RK, Salimonenko D, Shestakova LO, Valiev RZ. Izv Vuzov Tsvetnaja Metallurgia 1997;6:52.
[142] Senkov ON, Froes FH, Stolyarov VV, Valiev RZ, Liu J. Scripta Mater 1998;38:1511.
[143] Witney AB, Sanders PG, Weertmann JR, Eastman JA. Scr Metall 1998;33:2025.
[144] Agnew SR, Weertmann JR. Mater Sci Eng 1998;A244:145.
[145] Vinogradov A, Kaneko Y, Kitagawa K, Hashimoto S, Stolyarov VV, Valiev RZ. Scripta Mater 1997;36:1345.
[146] S. Hashimoto, Y. Kaneko, K. Kitagawa, A. Vinogradov and R. Z. Valiev, Proceedings Int. Conf. ISMANAM 10, Sydney, 1998, [to be published].
[147] Nieh TG, Wadsworth J, Sherby OD. In: Superplasticity in metals and ceramics. Cambridge: Cambridge University Press, 1997. p. 290.
[148] Kaibyshev OA. Superplasticity in metals, intermetallics and ceramics. Frankfurt: Springer, 1992.
[149] Langdon TG. Metall Trans 1982;13A:689.
[150] Mishra RS, Bieler TR, Mukherjee AK. Acta Met Mater 1995;43:877.
[151] Mishra RS, Valiev RZ, McFadden SX, Mukherjee AK. Mater Sci Eng 1998;A252:174.
[152] Valiev RZ, Islamgaliev RK, Stolyarov VV, Mishra RS, Mukherjee AK. Mater Sci Forum 1998;269-272:969.
[153] Mishra RS, Valiev RZ, McFadden SX, Islamgaliev RK, Mukherjee AK. Phil Mag, to be published.
[154] Valiev RZ, Gayanov RM, Yang HS, Mukherjee AK. Scr Metall Mater 1991;25:1945.
[155] Sutton AP, Balluffi RW. In: Interfaces in crystalline materials. Oxford: Claredon Press, 1995. p. 728.
[156] Mishra RS, Mukherjee AK. Superplasticity and superplastic forming. In: Ghosh AK, Bieler TR, editors. TMS Publisher, 1998, p.109.
[157] Valiev RZ, Salimonenko AD, Tsenev NK, Berbon PB, Langdon TG. Scripta Mater 1997;37:724.
[158] Komura S, Berbon PB, Furukawa M, Horita Z, Nemoto M, Langdon TG. Scripta Mater 1998;38:1851.
[159] Berbon PB, Furukawa M, Horita Z, Nemoto M, Tsenev NK, Valiev RZ, Langdon TG. Phil Mag Lett, 1998;78(4):313.
[160] Valiev RZ, Islamgaliev RK. Mat Sci Forum 1999;304-306:39.
[161] Papazin JM, Sigli C, Sanchez JM. Scr Metall Mater 1986;20:201.
[162] Salischev GA, Valiakhmetov OR, Valitov VA, Muktarov SK. Mater Sci Forum 1994;170-172:121.
[163] Mulyukov KhYa, Korznikova GF, Abdulov RZ, Valiev RZ. Phys Stat Sol 1991;125:609.
[164] Stolyarov VV, Salimgareev ShCh, Valiev RZ, Kloadas J, Chrost K. Phys Stat Sol (a) 1992;129:529.
[165] Stolyarov VV, Popov AG, Gundarev DV, Gaviko BS, Korznikova GF, Ermolenko AS, Valiev RZ. Fiz Met Metalloved 1997;2:100.
[166] Mulyukov KhYa, Korznikova GF, Sagdatkireyeva MB, Timofeyev VN, Valiev RZ. J Magn Magn Mater 1992;110:73.
[167] Sagawa M, Fujimura S, Yamamoto H, Matsuura Y, Hiraga K. IEEE Trans Magn 1984;20(5):1584.
[168] Shimoda T, Akioka K, Kobayashi O, Yamagami T, Ohki T, Miayagawa M, Yuri T. IEEE Trans Magn 1989;25(5):4099.
[169] Cullis AG, Canham LT, Calcott PDJ. J Appl Phys 1997;82:909.
[170] Canham LT. Appl Phys Lett 1990;57:1046.
[171] Zhao X, Schoenfeld O, Aoagi Y, Sugano T. J Phys D: Appl Phys 1994;27:1575.
[172] Maeda Y, Tsukamoto N, Yazawa Y, Kanemitsu Y, Masumoto Y. Appl Phys Lett 1991;59:3168.
[173] Thorpe SJ, Ramaswami B, Aust AT. J Electrochemical Soc 1988;135:2162.
[174] Rofagha R, Erb U, Ostander D, Lalumbo G, Aust KT. Nanostructured Mater 1993;2:1.

[175] Rofagha R, Langer R, El-Sherik AM, Erb U, Palumbo G, Aust KT. Scripta Metall 1991;25:2867.
[176] Vinogradov A, Mimaki T, Hashimoto S, Valiev R. Scripta Mater 1999;41:319.
[177] Livingston JD. J Appl Phys 1960;31:1071.
[178] Leckie HP. J Electrochem Soc 1970;117:1478.
[179] Ives DJG, Rawson AE. J Electrochemical Soc 1962;109:447.
[180] Zhernakov VS, Latysh VV, Stolyarov VV, Zharikov AI, Valiev RZ. In: Proceedings Int. Conf. NANO-98. Stokholm. 1998. p. 609.
[181] Mavlyutov RR. In: The stress concentration in construction elements. Moscow: Nauka, 1996. p. 240.
[182] Locati L. Met Ital 1995;47:832.
[183] Zhernakov VS, Yakupov RG. In: Calculation of bolt and rivet type connections at high temperatures and dynamic loads. Moscow: MAI Publisher, 1997. p. 218.